UNIVERSITY OF JYVÄSKYLÄ

Analysis of 5 MW hydrogen power system with thermal energy storage

Master's thesis

Rafael Cuellar

26/11/13

Master's Degree Program in Renewable Energy

Department of Physics, University of Jyväskylä

Advisors: Maria Puig Arnavat (DTU), Allan Schrøder Pedersen (DTU), Peter Vang Hendriksen (DTU)

Supervisor: Jussi Maunuksela

Preface

This work is in partial fulfilment of the Master Degree in Renewable Energy. The thesis was carried out at The Department of Energy Conversion and Storage, Technical University of Denmark (DTU), campus Risø.

I would like to express my sincerely gratitude to my advisors at DTU, Maria Puig Arnavat, Peter Vang Hendriksen and Allan Schrøder Pedersen and to my supervisor at Jyväskylä University, Jussi Maunuksela.

I would like to thank Linda Pollari for all her help to understand Finnish culture. I would like to thank many friends in Jyväskylä and Risø for their support.

I really would like to thank my parents and my siblings who always supported me because without their support I could not have accomplished this work.

Jyväskylä, 26th of November 2013

Rafael Cuellar

Abstract

Energy storage for further energy production has become a feasible option to deal with energy fluctuation, energy over production and energy shortcomings caused by the penetration of renewable energies. Hydrogen storage has been studied through mathematical model and simulation to predict its performance and technological feasibility. This thesis presents a model where a 5 MW electrolysis plant is simulated. The power plant consists on an electric input from renewable sources like wind turbines or photovoltaic panels. Electrolysis is done by a solid oxide cell that also produces electric power working as fuel cell. Thermal energy storage is added in order to recover heat released by the cell.

The main objective of the present work is to analyse the advantages of implementing thermal energy storage in order to store heat released by the fuel cell, determine the best configurations of the system to achieve high efficiencies and identify those parameter that contribute to significant losses.

In general, the model shows an efficiency value between 0.54 and 0.84 against 0.28 and 0.44 in similar models. Electrolysis process is validated with high temperature electrolysis models, which consider solid oxide cells as the electrolyser with heat recovery systems. Power generation process is validated against solid oxide fuel cell models, which use the heat produced by the fuel cell in different applications.

Using phase change materials (PCM) as thermal energy storage (TES) can increase the round cycle efficiency of the system from 0.44 without TES up to 84% with the application of TES at high and low temperatures. Efficiencies can increase up to 10% when liquid water is pressurized at the initial stage instead of compressing hydrogen at the final stage. Periods of operation are another parameters that could be modified in order to raise the efficiency. The same system working 12 hours as electrolysis at 1.2 V and 12 h as fuel cell has a power ratio of 0.6886, whereas working 5 hours as electrolysis at 1.2 V and 19 h as fuel cell has a power ratio of 0.7838, showing better heat management.

Effective utilization of by-product oxygen is an added value to the system. Energy savings around 70% are achieved respect common technologies of oxygen production, which could justify a new cell design in order to keep oxygen purity.

List of symbols

A_s	Exchange Area [m^2]
ASR	Area specific resistance [Ω cm^2]
Cp	Specific heat [kJ/kg K)
E	Energy [J]
E_N	Nernst voltage [V]
E_o	Equilibrium overpotential [V]
E_{OCV}	Open circuit voltage [V]
F	Faraday's constant [96485 s*A/mol]
G	Gibbs free energy difference [J/mol]
$\dot{H}$	Enthalpy flow [W]
H	Enthalpy [J/mol]
H_{lh}	Latent heat of fusion [kJ/kg]
H_2	Hydrogen
H_2O	Water or steam
h_a	Heat transfer coefficient [W/(m^2 K)]
HE	Heater
HHV	Higher heating value [kJ/mol]
i	Current density [A/cm^2]
k	Specific heat ratio
$k_{insulation}$	Thermal conductivity of the insulation material [W/(m K)]
m	Mass [kg]
$\dot{m}$	Mass flow [kg/s]
n	Mole [mol]
$\dot{n}$	Mole flow [mol/s]
Ncell	Number of cells
O_2	Oxygen
P	Electric Power [W]
$P_{H_2O}, P_{H_2}, P_{O_2}$	Partial pressures
Q	Heat (kJ)
$\dot{Q}$	Heat flow [W]
$\dot{Q}_{loss}$	Heat losses
R	Universal gas constant [8.31 J/mol K]
r	Power ratio
R_{air}	Air ratio
R_i, R_2 and R_T	Thermal Resistance [K/W]
S	Entropy [J/mol K]
S_a	Cell active surface area [cm^2]
SR	Hydrogen steam ratio
SU	Steam utilization factor
T	Temperature [K]
t	Time [h]
T_f	Final Temperature [K]
th	Thickness [m]
T_i	Initial temperature [K]
T_m	Melting Temperature [K]
T_o	Final temperature [K]
U	Overall heat transfer coefficient [W/(m^2K)]

UF	Fuel utilization factor
V_{act}	Activation overpotential [V]
V_{con}	Concentration overpotential [V]
V_{ec}	Electrolysis cell voltage [V]
V_{fc}	Fuel cell voltage [V]
V_{ohm}	Ohmic overpotential [V]
V_{op}	Operating Voltage [V]
w	Work [kJ/kg]
X	Molar fractions
z	Number of electrons

List of Subscripts

am	Ambient
c	Rankine cycle
ca	Compressed air
con	conduction
comp	Compressor
cs	Cold stream
ec	Electrolysis
eh	Electric heater
fc	Fuel cell
hs	Hot stream
i	Chemical species
in	Input
l	Liquid
lh	Latent heat
lm	Log mean
out	output
m	mean
mec	Mechanical
p	produced
q	heat
r	required
pcm	Phase change material
s	Isentropic
so	Solid
t	Total

Greek Characters

Δ	Difference
η	Efficiency
ρ	Density

Contents

1 Introduction

The increase of the renewable energy penetration has raised the interest on multiple energy storage and power production technologies in order to deal with energy fluctuation, energy over production and energy shortcomings. Implementing energy storage and power production allows storing the excess of energy produced by renewable resources and using it to produced energy when it is needed. For that reason, implementation of energy storage technologies has become an essential technology. Different energy storage technologies have been developed and others are under development to be applied in combination with solar and wind energy production facilities. Each technology has advantages and drawbacks and some are more suitable for specific applications than others [1]. The main technologies are: pumped hydroelectric, batteries, compressed air, superconducting magnetics materials, hydrogen production and storage, flywheels and capacitors and super capacitors. Cycle efficiencies can vary between 40% for hydrogen storage to 95% for flywheels and super capacitors [2]. For previously mentioned technologies, the observed capital costs can be estimated between $2 to $80,000/kW being compressed air technology and pumped hydroelectric the cheapest and super capacitors the most expensive followed by the superconducting magnetic materials [3,4]. Hydrogen storage is in the range of $425 to $10,000/kW [3,4]. The number of cycles varies between 200 and 500,000. Super capacitors technology can last up to 500,000 cycles while fuel cells 1,000 cycles [3]. However, in an overall analysis, hydrogen produced by electrolysis and its storage for further energy generation has been considered as the best energy carrier to balance energy production by renewable sources and the demand of final users [5,6,7].

Hydrogen storage offers multiple advantages over other energy storage technologies. One of these advantages is energy diversification. Hydrogen can be used as fuel for internal combustion engines [7], as well as syngas and methane production, through co-electrolysis by mixing hydrogen with carbon dioxide. In addition, Fischer-Tropsch method offers the possibility to generate liquid fuels with efficiencies about 54% [8].

Hydrogen storage can be powered using High Temperature Electrolysis (HTE). At higher temperatures, the required electric power is lower than at ambient temperature and it decreases as the temperature increases. Thermal energy supplies the required energy to compensate the endothermic electrolysis reaction. HTE is a very convenient option when thermal energy is available as energy waste or it is very cheap to get it. There are several studies that focus on HTE using waste heat from nuclear reactors reporting efficiencies between 32% and 48% [9]. Another option is the use of geothermal energy that reaches efficiencies around 50% [10]. Both techniques use solid oxide cells (SOC) as the electrolysis module. It has been shown that using an effective heat recovering system in SOC systems, electrolysis efficiency can increase up to 90% [11].

Solid oxide cells have shown good performance when operating as fuel cells to produce electricity as well as operating as electrolyser cells. The possibility to operate a solid oxide cell either as fuel cell or electrolyser makes them more attractive in a matter of cost and space requirements. Solid oxide cells are operated at high temperatures (600C - 1000C). When a SOC is operated to produce electricity, some of the energy is lost as heat and efficiency decreases; however, the efficiency of the system can be increased if thermal energy can be reutilized or stored for further use.

Several thermal energy storage technologies exist and they can be coupled with renewable sources. The increment of thermal solar plants has boosted the research and development of thermal energy storage [12]. Sensible, phase change materials (PCM) and thermochemical technologies are the most common ones. Sensible and phase change material technologies have been studied for long time and they are in the commercialization stage. It is possible to find many systems running with sensible and phase change materials as energy storage [12]. Thermochemical technology has been studied for long time. They represent a very good option for thermal energy storage because energy losses are minimal and without energy degradation [13], they have higher storage density and very long storage periods. Unfortunately, this technology is not commercially available, it is more complex than sensible and PCM storage, moreover the capital cost of thermochemical storage is higher [14].

1.1 High Temperature Electrolysis

Electrolysis dissociates water molecules into hydrogen and oxygen atoms. Water electrolysis is represented by the reaction 1, which is an endothermic reaction i.e. it absorbs thermal energy from the surroundings. Electrolysis can take place at ambient temperature with liquid water or at higher temperatures where water is at vapour stage.

$$H_2O \rightarrow H_2 + \tfrac{1}{2}O_2 \qquad (1)$$

Figure 1 shows the relation between the electric energy and thermal energy to split water molecules. At 300 K the electric energy required for electrolysis is 236.88 kJ/mol of H_2 and thermal energy is 48.75 kJ/mol of H_2, at 1000 K the electric energy required is 192.65 kJ/mol of H_2 and thermal energy is 55.19 kJ/mol of H_2.

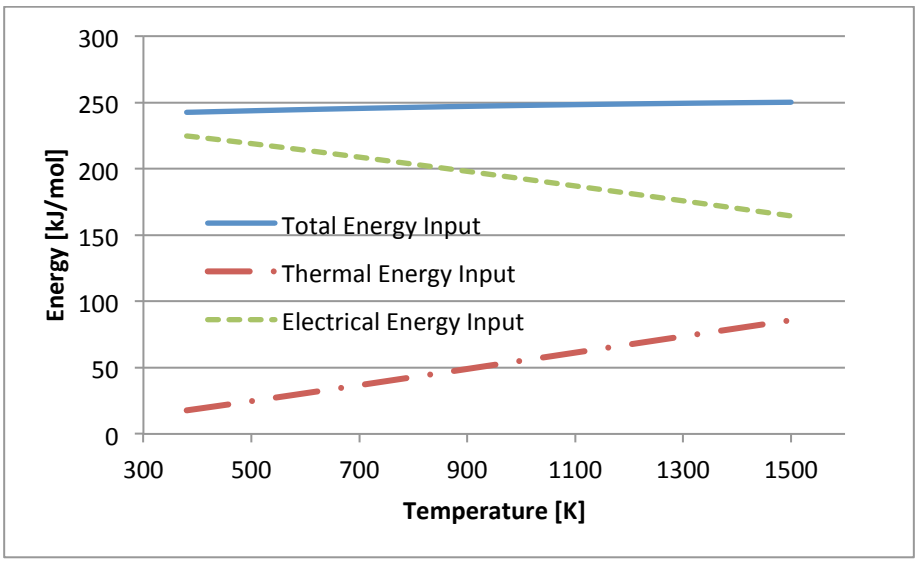

Fig. 1. Energy supply to electrolysis process

Electrolysis process can be endothermic, thermoneutral or exothermic. An endothermic electrolysis process is when the electric energy supplied to the system is just enough to perform the electrolysis but it is not enough to heat the system, therefore extra thermal energy is required for an isothermal process, otherwise the temperature drops. In a thermoneutral process, electric energy performs the electrolysis process and heats the system. In this process, extra thermal energy is replaced by electric energy by Joule effect in the electrolyser material that heats the system. At 300 K the thermoneutral voltage is 1.48 V and 1.2843 V at 1000 K. Figure 2 shows the thermoneutral voltage between 1000 K and 1500K. At this temperature range, thermoneutral voltage increases when temperature increases but the variation is less than 0.02 V. The process becomes exothermic when the electric input supplies thermal and electric energy for electrolysis and there is still an excess of energy; as a consequence, the system temperature increases.

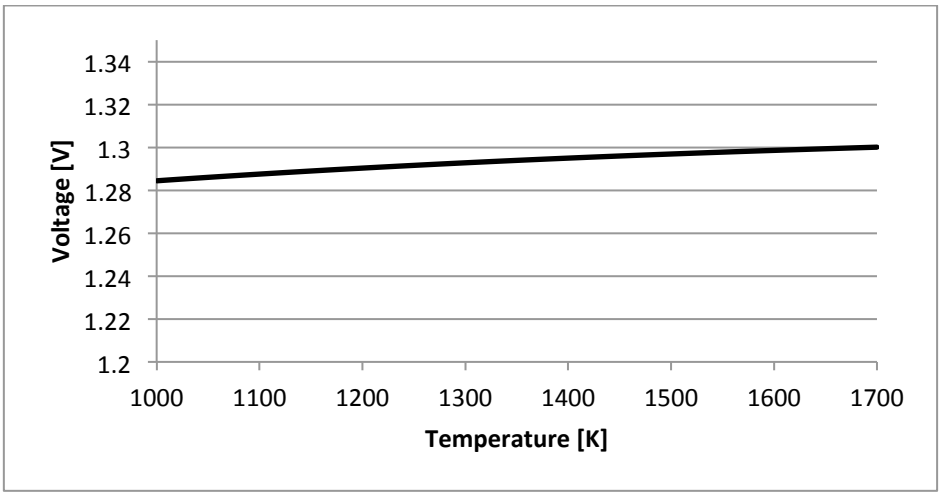

Fig. 2. Thermoneutral voltage between 1000 K and 1700 K

High temperature electrolysis or steam electrolysis can be performed using solid oxide cells (SOC) as the electrolyser when the operating temperature is above 773K [11]. SOC can be coupled with renewable energy systems to produce carbon-free hydrogen [11].

1.2 State of the art

Numerous studies have been done in electrolysis at low temperatures and high temperatures. In the recent years, the use of fuel cells as electrolysis cells has been investigated. However, it has not been possible to find published studies analysing the use of the same cell for electrolysis and fuel cell. However, several studies have been reviewed dealing with the use of electric power from renewable energies to run electrolysis in proton exchange membrane cells or SOC and where electric power is generated by fuel cells.

Considering only electric power from wind and solar sources reduces significantly the references found in open literature. When electric power and heat sources are not restricted, the list of references increases because several studies couple SOC technology with geothermal plants and nuclear reactors. However these systems are not similar to the system studied in the present work.

Table 1 summary of studies found with the criteria specified.

Reference	Electric power source	Electrolysis temperature[°C]	Electrolysis technology	η_{ec} [%]	Heat source	Fuel cell technology	Capacity [kW]	P_r
Agbossou et al. [15]	WT PV	23-55	NS	55-75	NA	PEMFC	5	0.42
Escobar et al. [16]	WT PV	23	PEWE	NS	NA	PEMFC	1	0.28
Karellas et al. [17]	WT	NS	Alkaline	84	NA	PEMFC	450-600	0.29
Iora et al. [18]	SOFC and EX	750	SOEC	NS	SOFC	SOFC	NS	0.93
Iora et al. [19]	SOFC and EX	750	SOEC	NS	SOFC	SOFC	NS	1.04

Wind Turbine (WT), Photo Voltaic [PV], Solid Oxide Fuel Cell (SOFC), External source (EX), Not specified (NS), Proton exchange water electrolysis (PEWE), Not applicable (NA), Proton exchange membrane fuel cell (PEMFC), Solid oxide Fuel Cell (SOFC).

The studies presented by Iora et al. [18,19] are the most similar to the present work. They describe a model to produce oxygen by high temperature electrolysis using solid oxide cells as electrolyser and fuel cell but the system considers two different cells in order to perform electrolysis and power generation at the same time.

The study done by Karellas et al. [17] describes a hydrogen storage system with an alkaline electrolyser, PEMFC and wind energy as the main source of electric power. It is aimed for standalone system located at the island of Karpathos Greece. The systems proposed by Agbossou [15] and Escobar [16] are standalone system coupled with a wind turbine and photovoltaic panels. The capacity of both systems is small, just enough to meet domestic requirements for a single house.

Even though the difference between the studies in table 1 and the present work are considerably, they can be used as a good reference to compare the performance of the present work. Moreover, the literature reviewed justifies the present work because none of the studies presented in this section come with a system like the one described in the present study.

1.3 Justification and objectives

As mentioned before, penetration of renewable energy sources increases energy fluctuation, energy over production and energy shortcomings, thus storage technologies are required to deal with these problems. All of the storage technologies have advantages and drawback in specific conditions [1]. Many research works have analysed these technologies and compared. However, hydrogen produced by electrolysis and its storage for further energy generation has been considered as the best energy carrier to balance energy production by renewable sources and the demand of final users [5,6,7].

Hydrogen storage and high temperature electrolysis have been studied for years. Literature shows satisfactory results coming from the combination of these two technologies. However, results and efficiencies can be improved using new technologies in HTE like solid oxide cell as electrolyser and fuel cells combined with thermal energy storage technologies. Moreover, efficiencies can be increased when the system runs at propitious conditions.

After revision of the literature, it can be concluded that few published studies analyse the same solid oxide cell use as electrolysis cell and fuel cell. Furthermore, fuel cell systems with heat storage for further use in electrolysis have not been studied.

For those reasons, this thesis proposes a system based on SOC for electrolysis and power generation. The system is intended to store the excess of energy produced by renewable sources, such as wind power or photovoltaic facilities, with higher round cycle efficiencies than the efficiencies of the current systems. In order to increase cycle efficiency, a thermal storage is added to store heat released, which could be considered as waste, at the power generation process for further use in electrolysis process.

The objectives of this work are: to model a power plant that uses the same solid oxide cell as electrolyser and fuel cell (SOEC/SOFC), analyse the system performance when a thermal energy storage (TES) is added and analyse different scenarios in order to determine the best configuration and conditions to operate the system.

The model is developed in Aspen plus^{TM} and it is able to simulate the energy flow through the different components of the plant. Mathematical models for the SOEC, SOFC and thermal storage are developed in FORTRAN to be used in the model done in Aspen plus^{TM}. The mathematical model for the SOEC/SOFC and the thermal storage are zero-dimensional.

Different scenarios are simulated. Thermal storage at different working temperature is a parameter to be studied; therefore, different materials for the thermal storage are evaluated. Different electric loads and different steam conversions are simulated in order to see their consequences in the cycle efficiency of the system and its operational performance.

1.4 Thesis structure

This thesis is divided in four chapters. First chapter describes different energy storage systems, their efficiencies, cost and current market status. It explains hydrogen storage as energy storage and the different applications of hydrogen. It also gives an introduction to high temperature electrolysis, available technologies, the introduction of solid oxide cells as electrolysers and the advantages compared to liquid water electrolysis. At the end of this chapter, justification and objectives are presented.

In the second chapter, a system description, assumptions and equations used to model mathematically of every component are given. Validation results and sensitivity analysis are described in this chapter. Validation is done comparing results of electrolysis process of the present study with previous studies that analyse electrolysis performed with SOC. Power generation process is compared with systems using SOFC

couple with heat recovery systems. The present work evaluates the effects of the power input in operating voltage, current density and heat recovered and they are presented in the sensitivity section.

Chapter three presents the results for the different scenarios modelled in the present work. The first scenario to be presented is the reference system and operates 12 hours as electrolysis cell and 12 hours as fuel cell and it considers only polarization losses. After that, different irreversibilities are added to the reference system to analyse their effects on the system performance. Then, changes in the configuration of the reference system are presented and compared to evaluate different scenarios.

Finally, in the last chapter, conclusions and further work are presented.

2 Development and Validation

2.1 General system description

From the previous section, hydrogen electrolysis and storage was mentioned as the best energy carrier to deal with power generation problems due by the penetration of renewable energy technologies. Following, a power plant based on SOC capable of producing hydrogen, storing and using it for power generation is presented. Basically, the plant uses electric power and thermal energy to produce hydrogen via steam electrolysis and stores the hydrogen produced. The electrolysis process takes place in the SOC unit. Electric power is supplied by renewable sources and the heat required by the system is produced within the system by electric power (electric heaters) or is obtained from the thermal storage. Then, hydrogen is used at the same cell (working as fuel cell) to produce electric power and heat. Electric power is sent to the grid and the heat produced by the fuel cell is used to preheat the input gases. Then, the excess of heat is stored in a thermal storage. Figure 3 shows the sketch of the plant.

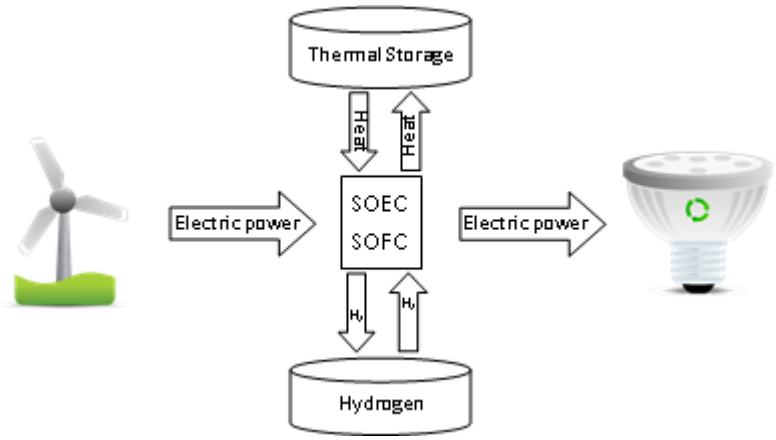

Fig. 3. Basic plant description

2.1.1 Solid oxide cells

A solid oxide cell (SOC) consists of two electrodes separated by a solid electrolyte, usually the electrolyte is Y_2O_3-stablilized ZrO_2 and the electrodes are Ni-ZrO_2 and Sr-doped $LaMnO_3$ [20]. The operating temperatures are between 500 ^{o}C and 1000 ^{o}C.

SOC's have been widely studied as energy producers. When a SOC is operated as energy producer is commonly called solid oxide fuel cell [SOFC]. SOFC produces electricity combining fuel and oxidant gases across an ionic conducting material [21]. Fuel is fed to the anode; an oxidation reaction takes place releasing electrons through the electrodes. The flow of electrons (from the anode to the cathode) produces direct current [21]. At present, SOFC technology is able to produce electricity from different fuels like hydrogen, methane, etc. Actually, any gas capable of being oxidise and reduced can be used as a fuel [21]. Air is the most common oxidant gas because its oxygen content and its availability. The reaction in the cell is an exothermic reaction i.e. it releases heat [21].

When the solid oxide cell is operated to produce hydrogen is commonly called solid oxide electrolysis cell (SOEC). It operates in a reverse way of a SOFC. The cell produces hydrogen and oxygen by steam electrolysis applying electricity to the cell, which shares the same physical characteristics as the cell used to produce electricity. Several studies have analysed the possibility of coupling SOFC modules and SOEC modules [18,19,21,22,23]. However, none of this studies use the same SOC module for both ways of operation. The idea of using the same cell to produce electricity and hydrogen is going to be analysed in this work.

For a better understanding of this work, it is relevant to explain what a cell, a cell stack and a module are. A cell is the basic unit of the system. Electrochemical and thermodynamic model are done at cell scale. Then, these results are scale to stack or module size. A cell stack is the array of many individual cells and a module is the array of cell stacks. Figure 4 shows a cell, stack and module.

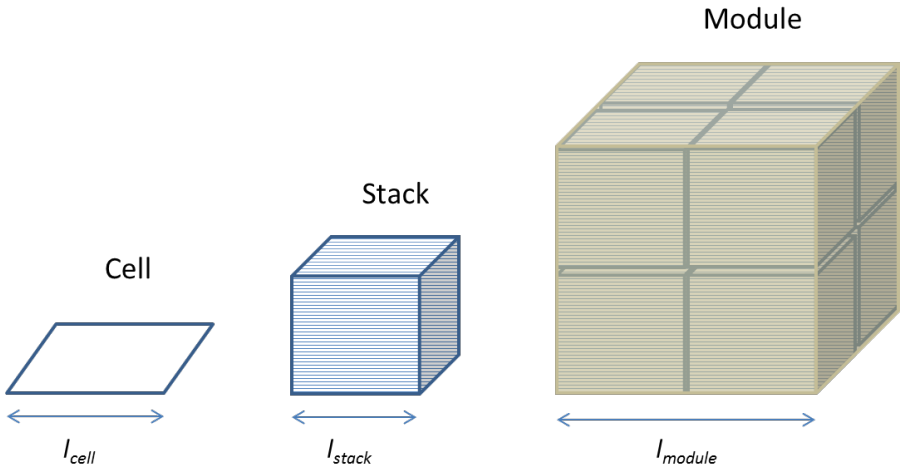

Fig. 4. Cell, stack and module figures

Cell dimensions consider the electrolyte layer, electrode layers, supports and interconnects. The thickness of a single cell is considered 2 mm, the initial value of l_{cell} is assumed to be 0.22 m, the dimension of the stack, l_{stack}, considers the air and fuel manifolds, a distance of 0.02 m around the cell length is added, l_{module} considers insulation thickness and supports between stacks. The final dimensions of the module will be described later on this work.

2.1.1.1 Energy balance

As it was mentioned before, SOEC and SOFC operate similarly but in reverse direction, for a cell working as a fuel cell the energy balance is given by equation 2

$$\dot{H}_{in} = \dot{H}_{out} + P_{fc} + \dot{Q}_{loss} \quad (2)$$

Where $\dot{H}_{in}$ [W] is the enthalpy flow rate sum of the reactants at the inlet of the cell, $\dot{H}_{out}$ [W] is the enthalpy flow rate sum of the products at the outlet of the cell, P_{fc} [W] is the electric power generated by the cell and $\dot{Q}_{loss}$ [W] is the heat loss from the surface of the stack. In this work no radiation losses are considered, only thermal losses by conduction and convection are considered.

When the cell is operated as electrolyser the energy balance is given by equation 3

$$\dot{H}_{in} + P_{ec} = \dot{H}_{out} + \dot{Q}_{loss} \quad (3)$$

Where P_{ec} is the electric power supplied to the cell, given by the operating voltage and the current in the cell.

$$\Delta\dot{H} = \dot{H}_{out} - \dot{H}_{in} \quad (4)$$

$$P_{fc} = -\Delta\dot{H} - \dot{Q}_{loss} \quad (5)$$

$$P_{ec} = \Delta\dot{H} + \dot{Q}_{loss} \quad (6)$$

Substituting $\Delta\dot{H}$ in equation 2 and 3, it is possible to observe that in ideal conditions, P_{ec} is equal to P_{fc} but with different direction as long $\Delta\dot{H}$ is the same in both equations.

We can define the total energy required for electrolysis as ΔH. In the previous section, the total energy required was defined as the thermal and electric energy required for electrolysis.

$$\Delta H = \Delta G + T\Delta S \quad (7)$$

Where, ΔG [J/mol] is the free Gibbs energy difference between the products and reactants and it can be seen as the electric energy required, T [K] is the temperature of operation, ΔS is the change of the entropy between the products and reactants, $T\Delta S$ is the total heat in the reaction. When the cell is operated as fuel cell and irreversibilities are not involved, ΔG is the electric energy produced and $T\Delta S$ is the total heat produced by the cell.

The equilibrium overpotential of the electrolysis reaction is the Gibbs free energy resulting from the reaction between hydrogen and oxygen and it is given by equation 8,

$$E_o = -\frac{\Delta G}{zF} \quad (8)$$

Where E_o [V] is the equilibrium overpotential also called the reversible potential, F is the Faradays Constant [96485 s*A/mol] and *z* is the number of electrons acting in the reaction. For steam electrolysis, *z* is equal to two electrons. At 1000 K E_o is equal to 0.998 V.

The open circuit voltage is the maximum theoretical potential of the cell and it depends on the gas concentration and pressure. It can be determined by Nernst equation

$$E_{OCV} = E_o + \frac{RT}{zF}\ln\left(\frac{Partial\ pressure\ Products}{Partial\ pressure\ Reactants}\right) \quad (9)$$

E_{OCV} is the open circuit voltage, R is the Universal gas constant 8.31[J/mol K]. Open circuit voltage for a fuel cell working at atmospheric pressure with hydrogen as fuel is [24].

$$E_{OCV} = E_o + \frac{RT_{fc}}{zF}\ln\left(\frac{P_{H_2}P_{O_2}^{0.5}}{P_{H_2O}}\right) \quad (10)$$

While for a cell working as electrolyser is

$$E_{OCV} = E_o + \frac{RT}{zF}\ln\left(\frac{P_{H_2O}}{P_{H_2}P_{O_2}^{0.5}}\right) \quad (11)$$

P_{H_2O}, P_{H_2} and P_{O_2} are the partial pressure of each gas. It can be assumed that partial pressures across the cell are equal to the mean molar fraction across the cell. The mean molar fraction can be assumed as the average molar fraction of the gasses between the inlet and outlet of cell [25].

$$X_{im} = \frac{X_{in,i} + X_{out,i}}{2} \quad (12)$$

Nernst equation is valid when no current crosses the electrolyte, i.e. no hydrogen is produced or consumed. As soon as current circulates in the electrolyte, some irreversibilities occur [26]. There are three main irreversibilities that affect the cell voltage, the activation overpotential, ohmic overpotential and concentration overpotential. The activation overpotential is the energy required to activate electrochemical reactions at the electrodes. Ohmic overpotential is the energy lost due the ohmic effect at the electrodes and electrolyte. The concentration overpotential is the energy lost due the mass transfer limitations of the cell. Figure 5 [20], shows the effect of the irreversibilities in the cell voltage for fuel cell working at low temperature.

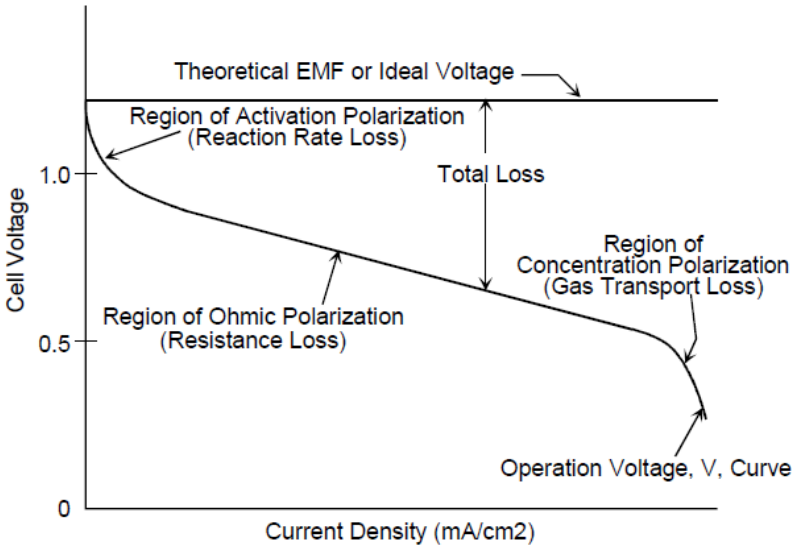

Fig. 5. Ideal and Actual Fuel Cell Voltage/Current Characteristic

Ohmic losses represent the most significant losses, activation losses and concentration losses are easy to identify. At higher temperature the effect of activation losses are less significant and less obvious to identify. Concentration overpotential becomes more significant [20].

The total cell voltage is calculated considering the losses by the activation overpotential, ohmic overpotential and concentration overpotential.

$$V_{fc} = E_{OCV} - V_{act} - V_{ohm} - V_{con} \quad (13)$$

$$V_{ec} = E_{OCV} + V_{act} + V_{ohm} + V_{con} \quad (14)$$

Where $V_{fc}$is the fuel cell voltage, V_{ec} is the electrolysis cell voltage, V_{act} is the activation overpotential, V_{ohm} is the ohmic overpotential and V_{con} is the concentration overpotential. Figure 6 shows the theoretical voltage of a cell operating in both ways electrolyser and fuel cell. When the current density is equal to zero, the cell voltage approximates to the open circuit voltage value.

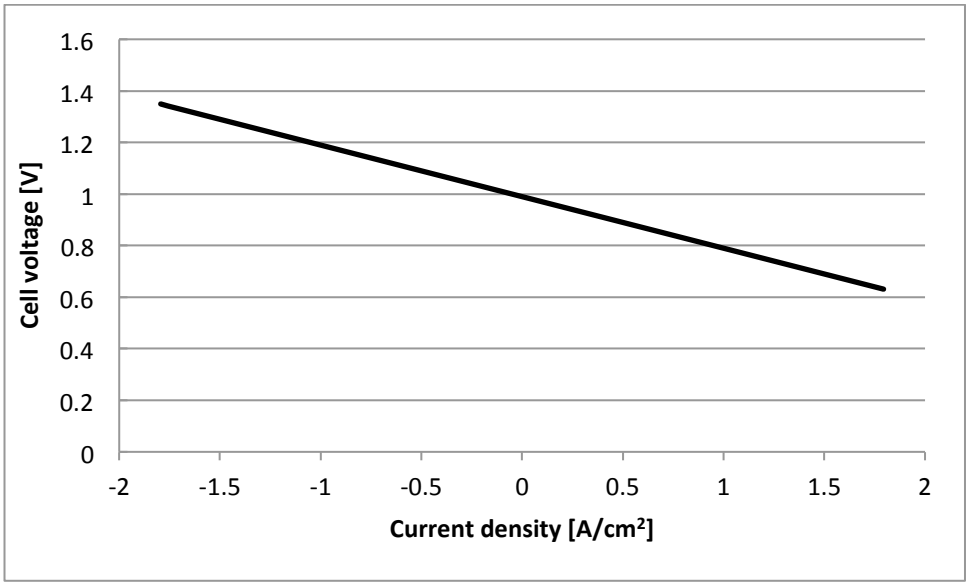

Fig. 6. Cell voltage in function of current density

The three different losses previously mentioned can be considered as a unique specific resistance. In some literature this resistance is defined as the Area Specific Resistance ASR. Applying this concept, the ASR is given by [27]

$$ASR = \frac{V_{act} + V_{ohm} + V_{con}}{i} \quad (15)$$

Where i [A/cm^2] is the current density. It is assumed a constant value of 0.2 [Ω cm^2] for the ASR, which is a reasonable approximation value to experimental values in different studies [26,27,28]. Substituting equation 15 in equations 13 and 14, the cell voltages are given by

$$V_{fc} = E_{OCV} - i * ASR \quad (13)$$

$$V_{ec} = E_{OCV} + i * ASR \quad (14)$$

2.1.1.2 Gas composition

The open circuit voltage of the cell is strongly related to the gas composition, it can be seen from equations 10 -12 that the changes in the concentration of fuel or steam at the input of the cell will modify the open circuit voltage. Therefore, figure 6 is only valid when the gas composition used for fuel cell mode is the same as electrolysis mode.

In this work, the gas composition in fuel cell mode at the anode is 100% hydrogen and at the cathode is 100% oxygen. Air is used to cool down the fuel cell, it is assumed that air has a different channel and does not mix with the oxygen flow. At these conditions the open circuit voltage is equal to 1.0027 V at 1073 K.

In the electrolysis mode, the gas composition at the cathode input is 90% steam and 10% hydrogen; the presence of hydrogen is necessary to prevent the oxidation of the nickel-based electrode [8,9]. At the anode input, oxygen flow is zero and the air in the system is considered only as thermal energy carrier in the cell. Air is fed into the system in a different channel, a mix between the oxygen and air is not considered; therefore the oxygen in the air does not contribute to calculate the open circuit voltage. The

open circuit voltage at these conditions calculated with equation 11 is 1.012 V at 1000 K. Figure 7, shows the open circuit voltage in function of the percentage of steam conversion.

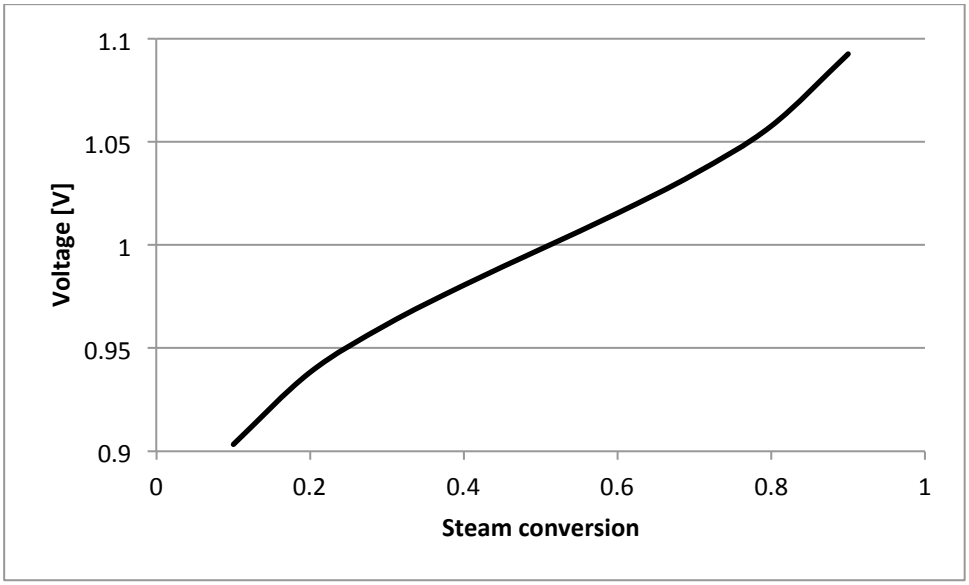

Fig. 7. Open circuit voltage in function of the steam conversion

2.1.1.3 Mass Balance

Electric current in the cell is proportional to the amount of hydrogen produced in electrolysis or consumed in fuel cell mode. Knowing the power input and the Nernst voltage (electrolysis mode), the current density can be found by equation 16 [11].

$$i = \frac{-E_N}{2*ASR_{cell}} + \sqrt{\frac{P_{cell}}{S_a*ASR_{cell}} + \left(\frac{E_N}{2*ASR_{cell}}\right)^2} \quad (16)$$

Where S_a [m^2] is the total active surface area of the cell and P_{cell} [W] is the total power input divided by the total number of cells.

It is assumed mass conservation exists in the cell, therefore all the mass enters the system, exits the system. Mass conservation through the cell is described by the following equations [11].

$$\dot{n}_{H_2,p} = \frac{i*S_a}{2*F} \quad (17)$$

$$\dot{n}_{H_2O,in} = \frac{\dot{n}_{H_2,p}}{SU} \quad (18)$$

$$\dot{n}_{H_2O,out} = \dot{n}_{H_2O,in} - \dot{n}_{H_2,p} \quad (19)$$

$$SR = \frac{\dot{n}_{H_2,in}}{\dot{n}_{H_2,in}+\dot{n}_{H_2O,in}} \quad (20)$$

$$\dot{n}_{H_2,out} = \dot{n}_{H_2,in} + \dot{n}_{H_2,p} \quad (21)$$

$$\dot{n}_{O_2,in} = 0.5 * \dot{n}_{H_2,p} * R_{air} \quad (22)$$

$$\dot{n}_{O_2,out} = \dot{n}_{O_2,in} + 0.5 * \dot{n}_{H_2,p} \quad (23)$$

$$\dot{n}_{air,in} = \dot{n}_{air,out} \quad (24)$$

In similar way, mass balance in fuel cell mode can be obtained. Hydrogen input is the hydrogen output from the electrolysis.

$$\dot{n}_{H_2O,out} = UF * \dot{n}_{H_2,in} \quad (25)$$

$$\dot{n}_{H_2,out} = \dot{n}_{H_2,in}(1 - UF) \quad (26)$$

$$\dot{n}_{O_2,in} = 0.5 * \dot{n}_{H_2,in} \quad (27)$$

$$\dot{n}_{O_2,out} = \dot{n}_{O_2,in}(1 - UF) \quad (28)$$

$$\dot{n}_{air,in} = \dot{n}_{air,out} \quad (29)$$

It is worth noting that air input can be obtained from the energy balance in equations 2 and 3. Another important aspect to mention is that air is not mixed with the oxygen produced or consumed.

2.1.1.4 Extra air channel

As it was mentioned before, air is used as energy carrier in the cell and the oxygen in air does not take part in the reaction. An air channel has to be added in the cell in order to avoid air and oxygen mixing. Figure 7(a) shows the sketch of a current solid oxide cell and figure 7(b) shows the cell with the extra air channels.

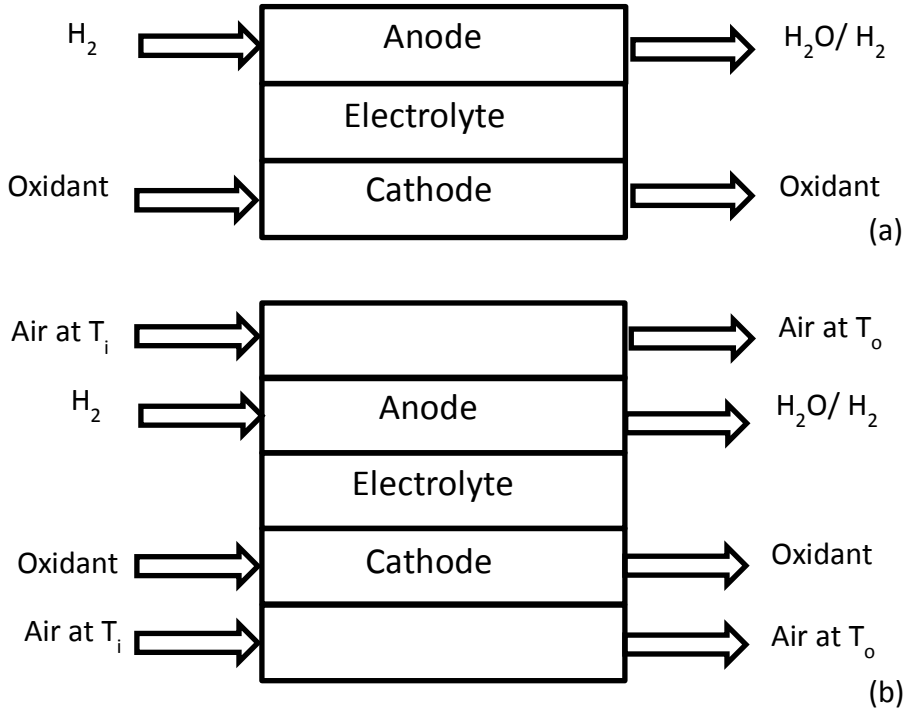

Fig. 7(a). Sketch of a current solid oxide cell. **7(b).** Solid Oxide cell sketch with extra air channels

In fuel cell mode, heat transfer is from the central part of the cell to the air channels. In electrolysis, heat transfer is from the hot air in the channels to the centre of the cell, where heat is required to perform the electrolysis process.

2.1.2 Electric power input

Aspen plus™ simulates steady state systems; consequently, the electric power input is constant in all the different scenarios. It is considered to be supplied by renewable energy sources like wind energy or photovoltaic energy. The different configurations are designed to operate a constant input of 5 MWe. Nevertheless, system's configurations are sensitive to different electric power inputs. It is worth mentioning that the electric power here mentioned is only used to perform the electrolysis process and extra power input to run compressors, blower and electric heaters will be added to this electric power input.

2.1.3 Aspen plus™ system description

The extra energy used to run the system beside the electric energy used for the electrolysis process is described in this section. In this work, compressors, electric heaters and heat exchangers are detailed enough to give a good approximation of their performance within the system. Compressors are required to increase the hydrogen pressure from 0.1 MPa to 2 MPa. Heat exchangers are used to recover heat from the gases at the output and preheat the input from ambient temperature (298 K) to operational temperatures between 1000 K and 1030 K. Electric heaters are used in the system to supply the energy to complete the preheat stage in case the recovered energy is not enough to complete this process.

2.1.3.1 Electric heaters

As a first instance, electric heater performance is described with equations 30 and 31

$$\dot{Q}_{eh} = \dot{n}_i(H_{i,out-}H_{i,in}) \quad (30)$$

$$\dot{W}_{eh} = \eta_{eh} * \dot{Q}_{eh} \quad (31)$$

Where $\dot{Q}_{eh}$ [W] is the thermal power to increase the temperature, $\dot{n}_i$ [mol/s] is the molar flow of the different species, $\dot{W}_{eh}$ [W] is the electric work required by the heater and η_{eh} is the heater efficiency that has a constant value of 95%.

2.1.3.2 Compressors

Hydrogen compression from 0.1 MPa to 2 MPa is done by two stages compression system. The system consists of two isentropic compressors and intercooling between the compression stages. Intercooling is used in order to approach the process to an isothermal process. The work done by the compressors is given by the next equation [29]

$$w_{comp} = w_{comp1} + w_{comp2} = \left(\frac{kR}{\eta_s \eta_{mec}}\right)\left(\frac{T_1}{k-1}\left[\left(\frac{P_x}{P_1}\right)^{\frac{(k-1)}{k}} - 1\right] + \frac{T_2}{k-1}\left[\left(\frac{P_2}{P_x}\right)^{\frac{(k-1)}{k}} - 1\right]\right) \quad (32)$$

Where w_{comp}, w_{comp1} and w_{comp2} [kJ/kg] are the total electric work of the compressors, electric work of the compressor at stage 1 and the electric work of the compressor at stage 2, respectively, k is the specific heat ratio, $\eta_s$and η_{mec} are the isentropic and mechanical efficiencies, respectively, of the compressors.

From equation 32, it can be seen when T_1 is equal to T_2 the only variable is P_x and the function can be minimized. After differentiating respect with P_x and setting to zero the minimum work is obtained when [29]

$$P_x = (P_1 P_2)^{\frac{1}{2}} \tag{33}$$

Figure 8 shows the Hydrogen compression subsystem used in this work. Intercooling and final cooling are model as heat exchange processes between cold air and hydrogen after the compression stages. After the compression process hydrogen is stored at ambient temperature at 2 MPa.

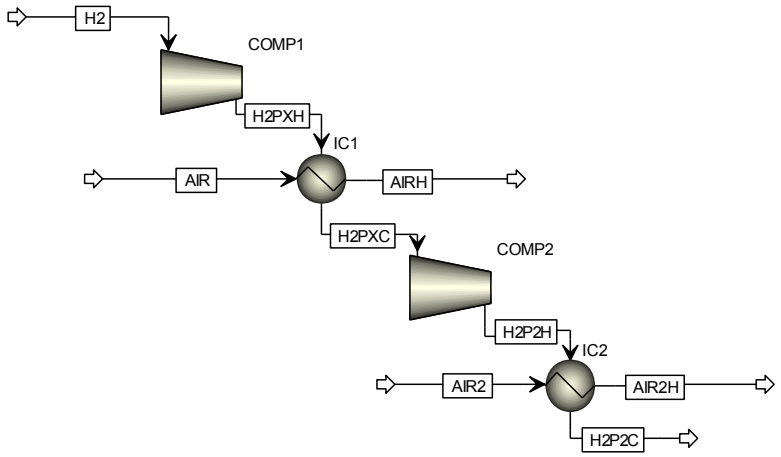

Fig. 8. Illustration of the H_2 compression subsystem in Aspen plus™

Another method to store hydrogen at high pressure is running the system at the desired pressure. This leads to a different configuration system, where the compression process takes place at the beginning. In this configuration, water is compressed at liquid state instead of compressing hydrogen at the end of the electrolysis process.

2.1.3.3 Heat exchangers

Heat exchangers are used to transfer heat from hot fluids to cold fluids. In this work, they are mainly used to transfer heat from hot gases from the output of the cell to cold gases at the input of the cell. As first instance, the output temperature calculations of cold and hot streams were made solving the energy balance between the two streams in the heat exchanger. It is assumed that the heat exchangers are well insulated and all the heat from the hot stream is transferred to the cold stream.

$$\dot{m}_{cs} Cp_{cs} \left(T_{o,cs} - T_{i,cs}\right) = -\dot{m}_{hs} Cp_{hs} (T_{o,hs} - T_{i,hs}) \tag{34}$$

Equation 34 has two variables $T_{o,cs}$ and $T_{o,hs}$, in some heat exchangers , the output temperature of the cold stream is already known because it is the desired temperature, thus the number of variables in equation 34 reduces to one. However, for other heat exchangers the output temperature of the cold side and the hot side are unknown; therefore, an infinite number of solutions can be obtained. In this work, all the heat exchangers are treated as counter flow heat exchangers and the minimum temperature difference is setting at 10 K, i.e. the hot side output temperature cannot be lower than 10 K above the cold side inlet

temperature or the cold side output temperature cannot be higher than 10 K below the hot side input temperature. Having this restriction, calculations of the output temperatures are done considering the minimum temperature difference.

The heat exchanger network was design using the pinch analysis method. The pinch analysis is a method to reduce the energy consumption of a process. This method evaluates feasible heat transfer between hot and cold streams, optimizes the heat recovery system and reduces to the minimum energy consumption of cooling and heating facilities. The pinch point was set after analysing the composites curves. The curves show that the system constrains at 25 ^{o}C and 100 ^{o}C, showing the highest constraint at 25 ^{o}C, thus the pinch point was set at 25 ^{o}C. Figure 9 shows one of the heat exchanger network arrangements.

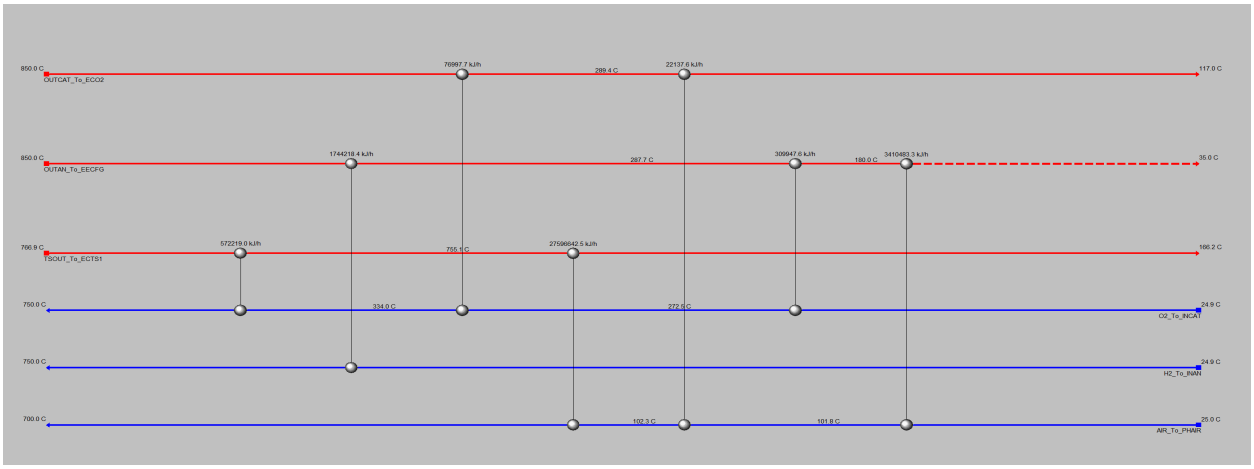

Fig. 9. Heat exchanger network to recover heat from the exhaust gases from the cell

Once the heat duty of the heat exchanger has been calculated the exchange area can be calculated. To calculate the area, the log mean temperature difference (LMTD) method is used. This method is useful to size heat exchangers when the input and output temperatures are known.

$$\dot{Q}_{he} = U A_s \Delta T_{lm} \quad (35)$$

$$\Delta T_{lm} = \frac{\Delta T_1 - \Delta T_2}{\ln\left(\frac{\Delta T_1}{\Delta T_2}\right)} \quad (36)$$

Where $\dot{Q}_{he}$ [J/s] is the heat transfer, U [W/(m^{2}K)] is the overall heat transfer coefficient, which is given by Aspen plus^{TM} based on the heat transfer properties of the heat exchanger material, cold stream and hot stream, ΔT_{lm} is the log mean temperature difference and A_s [m^2] is the exchange area.

It is important to mention that pressure drops are neglected.

2.1.3.4 Thermal energy storage

One of the aims of this study focuses on the thermal energy recovered from the fuel cell and store it in thermal energy storage (TES), thus the analysis of this component becomes essential for this study. The type of TES chosen in this study was a phase change material (PCM) for many reasons. Solar plants work in a wide range of temperatures, depending on the plant application. Different studies have shown the

performance and feasibility of TES coupled with solar plants [12,30,31,32], thus they offer a good alternative to be implemented with fuel cells systems. Thermal energy can be stored at very high temperature (600 – 1000 ^{o}C), medium temperature (200 – 300 ^{o}C) and low temperature (lower than 200 ^{o}C). PCMs, unlike thermochemical storage, are commercially available and they are easier to model. Simple models of PCM give a good approximation to the real performance.

A phase change material energy storage is the storage which changes its phase while energy is supplied. It can change from solid to solid, solid to liquid, liquid to liquid and liquid to gas. It is always preferably to have solid to solid or liquid because the expansion and volume change of the material are closely negligible; while in materials with liquid to gas, the volume change is considerable. A material changes its phase when the optimal temperature is reached and keeps that temperature until the total mass has changed of phase. Heat transfer at the phase changing stage can be considered as an isothermal heat transfer.

The energy storage chosen for this work (figure 10) is based on the model described by Sharma [12]. In charging mode, thermal energy is collected and transferred to the energy storage tank that is filled with encapsulated PCM, and heat transfer fluid flows parallel to them. In discharging mode, cold fluid flows parallel to it but absorbing energy from the PCM. In this case, the heat transfer fluid (HTF) is air. The Heat storage can be then treated as a heat exchanger (figure 11(a) and(b)) [33].

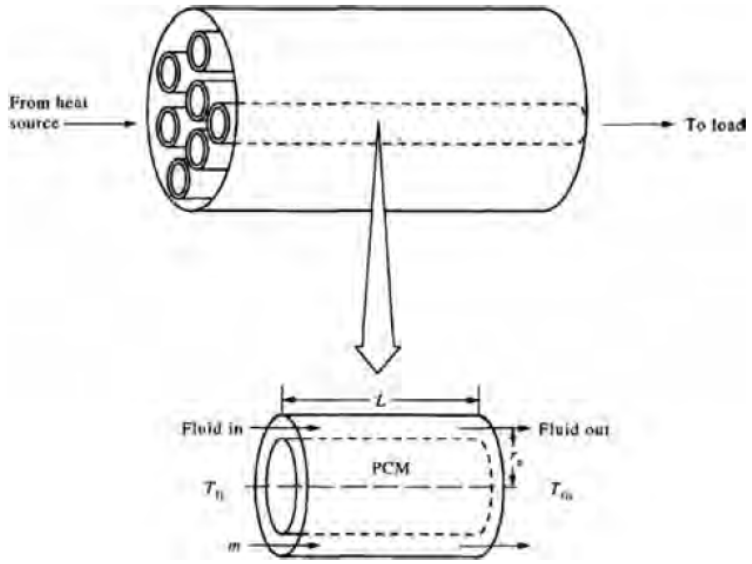

Fig. 10. Schematic configuration of phase change material storage tank [33].

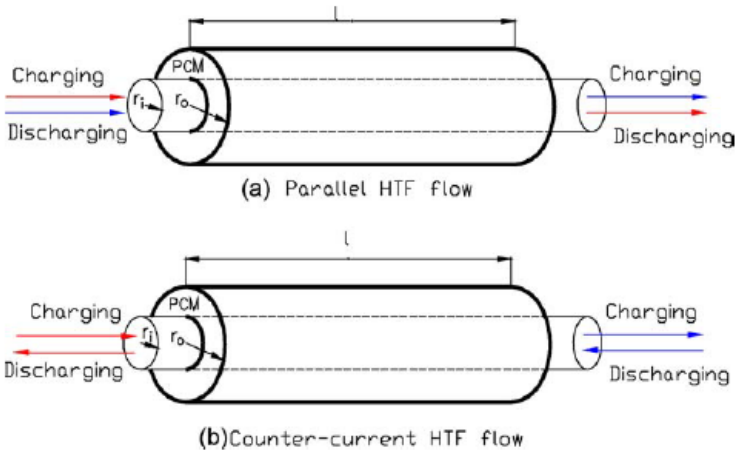

Fig. 11. The physical model illustrating parallel and counter-current HTF flow in a shell and tube system [33].

The TES can be then treated as a heat exchanger, where all the heat transferred from the air to the PCM storage tank is given by equations 36 and 37 [12,33].

$$Q = \frac{n_{air*}(H_i - H_o)}{1000} \quad (37)$$

$$Q = m_{pcm} * Cp_{so} * (T_m - T_i) + m_{pcm} * H_{lh} + m_{pcm} * Cp_l * (T_f - T_m) \quad (38)$$

Where m_{pcm} [kg] is the PCM mass packed in the TES, Cp_{so} [kJ/(kg K)] is the specific heat at solid phase, T_m [K] is the melting temperature, T_i and T_f[K] are the initial and final temperature respectively, H_{lh} [kJ/kg] is the latent heat of fusion. The first and third terms of the right part of equation 37 are the energy required to heat the TES when phase changing is not present. At these stages, TES can be treated as a sensible energy storage material.

Figure 12 [34] and 13 show the enthalpy in function of temperature, figure 12 shows the enthalpy measured in laboratory and the parametrized curve, while figure 13 shows the enthalpy curve by the thermal storage model done in the present work.

In order to decrease the difference between the model of the TES and the real performance, the TES was designed to operate close to the middle point of the latent heat, where the difference between real performance and modelled performance is minimum. In figures 12 and 13, this point is at 300 K.

To store thermal energy at different temperatures, it is necessary to have different thermal storage with different PCM. To store heat at low temperature, the material chosen was the molten salt $MgCl_2$-$6H_2O$, at medium temperature Na/K/NO_3 (0.5/0.5) and for high temperatures LiF-CaF_2. Table 2 [33,35,36] shows the properties of the materials used in this work.

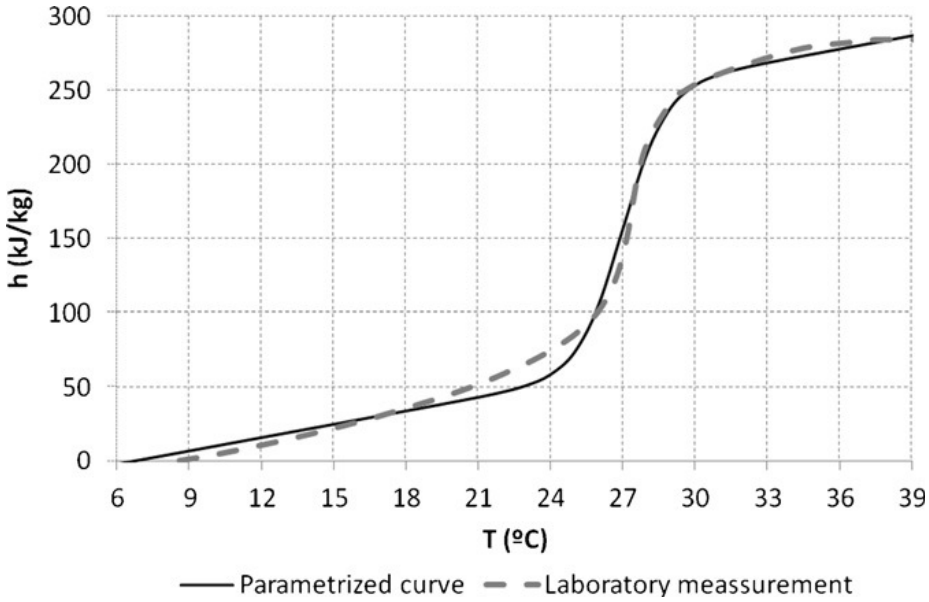

Fig. 12. Fit degree with the PCM h–T curve obtained in the laboratory and parametrized [34].

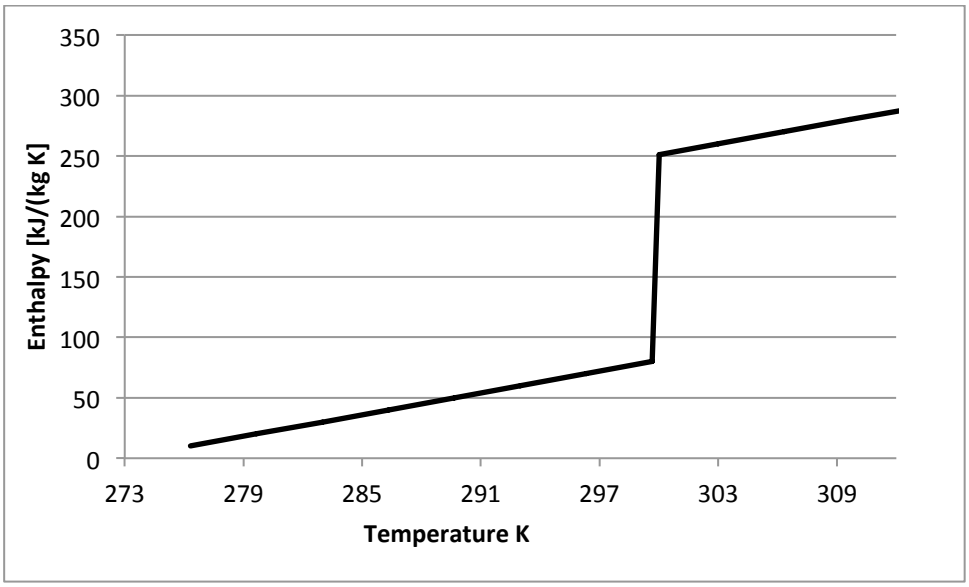

Fig. 13. Fit degree with the PCM h–T curve obtained with TES model.

Table 2. Thermo physical Properties of used PCM.

Compound	T_m (°C)	ΔH_l [kJ/kg]	Cp_{so} [kJ/(kg K)]	Cp_l [kJ/(kg K)]	k_{so} [W/(m K)]	k_l [W/(m K)]	P_{so} [kg/m3]	P_l [kg/m3]
$MgCl_2$-6H_2O	116.7	168.6	2.25	2.61	0.704	0.57	1570	1450
Na/K/NO_3 (0.5/0.5)	220	100.7	1.35	1.35	0.733	0.326	1920	1920
LiF-CaF_2	767	816	1.77	1.77	3.8	1.7	2390	2390

2.1.3.5 Heat losses and thermal insulation

Some of the thermal energy released by the fuel cell is released to the environment as heat losses [37,38]. Conductive, convective and radiation heat transfer take place inside the stack between cells. Even between components of each cell, heat transfer exists. Different studies have analysed the heat distribution along the cell, for the purpose of this work this analysis is beyond the scope; therefore, a uniform temperature distribution inside the stack is considered, thus the only heat transfer is from the stack to the environment.

As it was mentioned before, the three mechanism of heat transfer take place inside the stack between the cells and the stack surface. It is assumed that the temperature at the outside face of the stack is at the cell operating temperature. When an insulation layer is applied to the stack surface it is possible to assume that the only heat transfer mechanism is by conduction. Assuming that the outside face of the insulation layer is at ambient temperature, we have the maximum heat loss through conduction and heat transfer by convection and radiation mechanisms to the environment can be neglected.

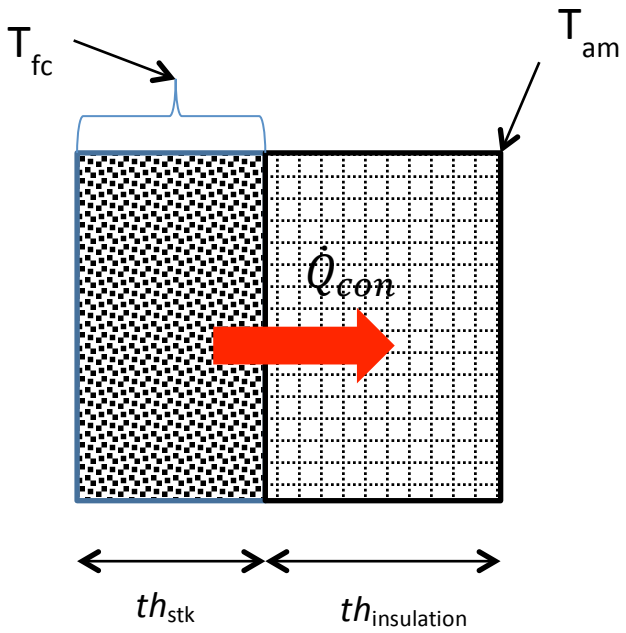

Fig. 14. Heat transfer illustration across the stack cover and the insulation layer.

Form figure 14, it is possible to see that the application of the simple equation of thermal conductivity satisfy the diagram, thus the heat loss ratio by the fuel cell can be described by the following equations.

$$R_i = \frac{l_{insulation}}{k_{insulation} * A_{stk}} \quad (39)$$

$$R_2 = \frac{1}{h_a * A_{stk}} \quad (40)$$

$$R_T = R_i + R_2 \quad (41)$$

$$\dot{Q}_{loss} = \frac{(T_{fc} - T_{am})}{R_T} \quad (42)$$

Where $\dot{Q}_{loss}$ [W] is the heat loss, $k_{insulation}$ [W/(m K)] is the thermal conductivity of the insulation material, A_{stk} is the total surface area of the stack [m^2], T_{fc} and T_{am} [K] are the operational temperature of the cell and ambient temperature, respectively, R_i, R_2 and R_T [K/W] are the thermal resistances and h_a [W/(m^2 K)] is the heat transfer coefficient.

On the same way, heat losses in the TES can be obtained. Assuming that the thermal energy storage is well insulated, equation 41 can be used to obtain the heat losses in the thermal storage. As it was assumed in the cell stack, a uniform temperature distribution is considered inside the thermal storage and the only mechanism of heat transfer is thermal conduction.

Different materials for insulation are considered because the different heat storage temperatures. Table 3 [39,40] shows the properties of the insulation materials considered in this work.

Table 3. Thermal Conductivity for hot insulation [W/(m K)]

Mean temperature [°C]	Resin bonded Mineral wool	Ceramic Fiber Blankets
100	0.04	-
200	0.06	0.06
300	0.08	0.07
400	0.11	0.09
700	-	0.17
1000	-	0.26

2.1.3.6 Plant description

Figure 15, shows the basic plant layout in electrolysis mode. A mix of 90% water and 10% hydrogen enters the system in stream 1 at ambient temperature and atmospheric pressure. It is preheated in the heat exchangers 1 and 2 by the recovered heat of hot streams 11 and 12. The water is vaporized in the heater 1. Once the water has been converted to steam, the mix of steam and hydrogen is preheated to 1000 K to enter the cell stack. At the same time, air enters the system at ambient temperature (stream 6) and it is preheated in the heat exchanger by hot air coming from the cell stack at temperature above 1000 K. Inside the cell stack, steam is split into hydrogen and oxygen. The maximum steam conversion is set to 90%. The mix of hydrogen and steam goes out from the cell stack (stream 11) through the cathode while oxygen goes out through the anode (stream 12). Hydrogen-steam mixture and oxygen enter the heat exchangers 1 and 2, respectively, to be cooled down and preheat the water-hydrogen mixture. Air at cell operation temperature exits the cell stack in stream 13 and enters heat exchanger 3 to drop its temperature and heat the entering air. Once, the hydrogen-steam mixture has cooled down, enters to a flash separator where hydrogen will be separated from the steam by condensation. It is assumed that a perfect separation of hydrogen from water occurs at the flash separator. Stream 17 contains pure hydrogen at ambient temperature and atmospheric pressure and enters the first compressor to be compressed at a partial pressure. In order to increase compression efficiency hydrogen is cooled down in heat exchanger 4 and compressed to the final pressure in compressor 2. After compressing hydrogen to the desire pressure, it is sent to a storage tank where it will be kept until it is used in the fuel cell. Oxygen can be stored, recycled or release to the ambient, in this work a further analysis of oxygen storing and recirculation will be covered.

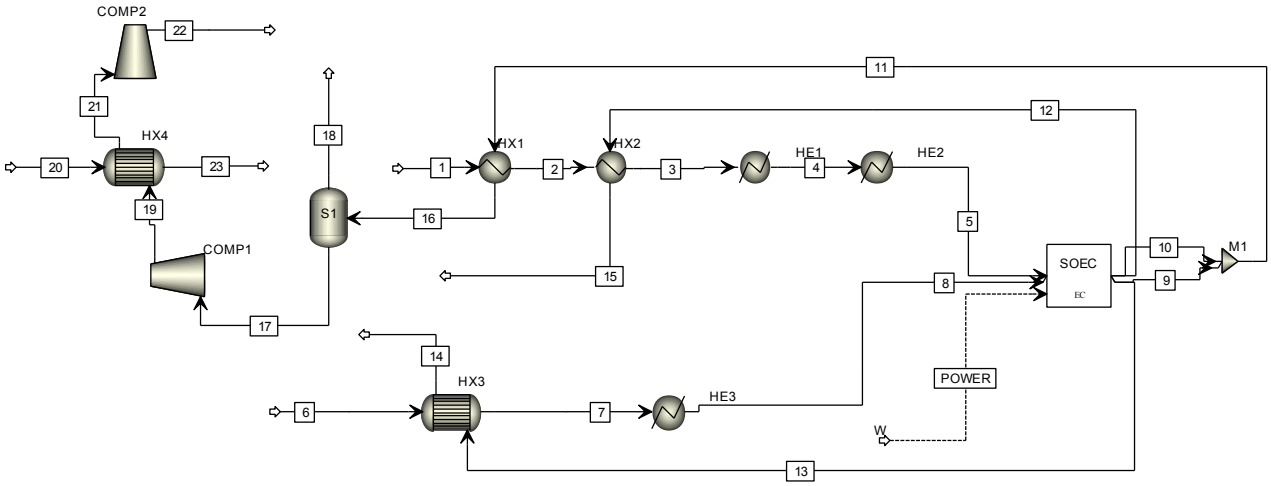

Fig. 15. Electrolysis plant layout in Aspen plus™

Figure 16 shows the plant layout to produce electric power. Hydrogen enters the system at ambient temperature and atmospheric pressure. Then, it is preheated in heat exchanger 1 to the operating cell temperature and enters the cell stack through the anode inlet (stream 3). Stream 3 contains oxygen at ambient temperature and atmospheric pressure. Oxygen is preheated to the operating cell temperature by crossing a series of heat exchangers. After oxygen was preheated to the desired temperature, it enters the cell stack through the cathode inlet (stream 6). Air enters the system at ambient temperature and it is preheated to the desired temperature by crossing a series of heat exchangers. Preheated temperature of air will be described later in this work because it is an important factor in the recovered heat by the thermal energy storage system. Figure 16 shows the base layout of the plant on fuel cell mode. In this configuration, air enters the cell stack through a different channel to the cathode channel. Inside the fuel cell, hydrogen oxidation occurs releasing thermal and electric energy and producing steam. The maximum hydrogen conversion rate is set at 90%. Thermal energy is dissipated by the air flow that is used to keep the desired working temperature; part of the thermal energy is dissipated as heat losses. The electric power output is sent to the electric power control device for further use in the electric network. The mix of steam generated in the cell and hydrogen that was not converted is used to preheat the hydrogen in heat exchanger 1, to preheat the oxygen in heat exchanger 2 and finally, preheat the air in heat exchanger 14. After being cooled down, the water-hydrogen mixture is sent to a system to recuperate the hydrogen for further use in electrolysis. At the same time, mix of steam and hydrogen is cooled down to ambient temperature. In the same way, oxygen that was not used in the reaction exits the cell stack through stream 15 and it is used to preheat the entering oxygen and air while its temperature decreases. Hot air exits the cell stack through stream 18. Air is directed to the first TES at high temperatures, above 1000 K, to heat the TES. After heating the first thermal storage, air is directed to raise the temperature of the entering oxygen and air. At stream 21, part of the thermal energy carried by the air has been transferred to the first TES, oxygen and air. However, there is still thermal energy in the air that can be stored; therefore, air is directed to a second TES where it will transferred all the energy left and be cooled down to ambient temperature.

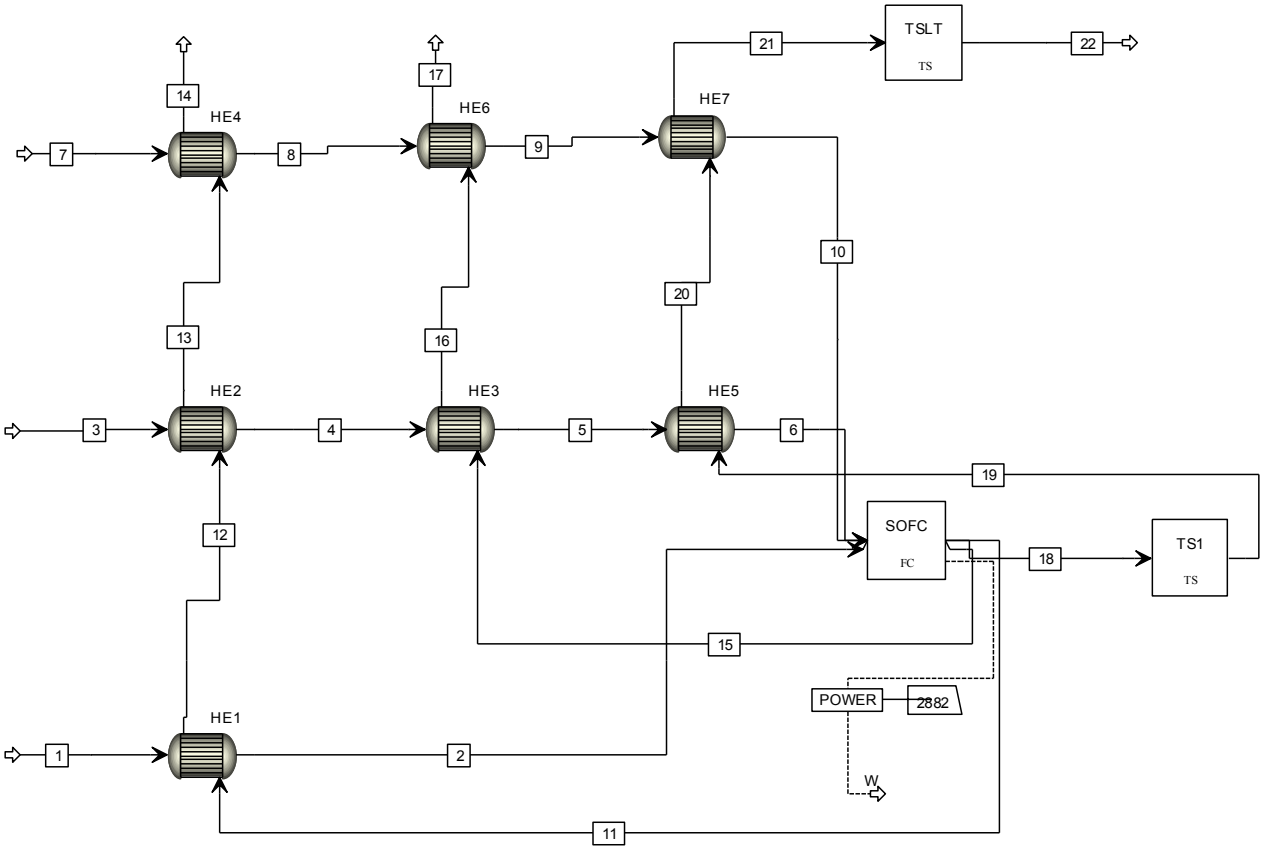

Fig. 16. Fuel cell plant layout in Aspen plus™

2.1.4 Performance Parameters

In this study, different power ratios are defined i.e., delivered power and supplied power for electrolysis, delivered power and the total power for electrolysis. Additionally, electric fuel cell efficiency, electrolysis efficiency and heat ratio are defined.

Power ratios are given by the following equations:

$$r_p = \frac{P_{fc}*t}{P_{ec}*t} \quad (43)$$

$$r_t = \frac{P_{fc}*t}{P_t*t} \quad (44)$$

Where

$$P_t = P_{ec} + W_{comp} + W_{eh} \quad (45)$$

$$r_c = \frac{(P_{fc}+P_{rc})*t}{P_{ec}*t} \quad (46)$$

Where P_{rc} [W] is the delivered power by the Rankine cycle.

$$r_{ct} = \frac{(P_{fc}+P_{rc})*t}{P_t*t} \quad (47)$$

$$r_{ca} = \frac{(P_{fc}+P_{ca})*t}{P_t*t} \quad (48)$$

$$r_q = \frac{W_{eh}*t}{Q_{TES}} \quad (49)$$

Where P_{ca} [W] is the power delivered by the expansion of hydrogen in turbines. P_{ca} and P_{rc} are explained in detailed in results chapter. r_q is the heat ratio, t [h] is the time of operation and Q_{TES} [kJ] is the heat stored in the TES.

Electrolysis efficiency [11]and electric fuel cell efficiency are given by the following equations

$$\eta_{ec} = \frac{\dot{n}_{H_2,p}*HHV}{P_t+\dot{Q}_{ec}} \quad (50)$$

$$\eta_{fc} = \frac{P_{fc}}{\dot{n}_{H_2,in}*HHV} \quad (51)$$

Where η_{ec} and η_{fc} are the electrolysis and electric fuel cell efficiencies, HHV [kJ/mol] is the higher heating value of H_2 (286 kJ/mol) and $\dot{Q}_{ec}$ is the required thermal power to compensate the heat absorbed by the reaction.

2.1.5 Model assumptions

General assumptions are considered along the system in order to simplify the model. Some components could have particular assumptions, which are mentioned in the component description. The following simplifications are done:

- Air composition is 79% N_2 and 21% O_2;
- All the gases in the system behave like ideal gases;
- Water is considered to be incompressible;
- Pipes are well insulated and there are not heat losses through them;
- Calculations are performed only for steady-state conditions;
- Pressure drops are neglected [24]

Extra assumptions could be done and they will depend on the scenario to model. These assumptions are mentioned on the scenario description.

2.2 Model validation

Validation process of a model is done with the aim to prove the reliability of the model. Validation can be done comparing results with similar studies or previous experiments. The system proposed in this work is a novel system; therefore, there is a lack of literature studying the same system. However, the described system in the present work collects different subsystems that can be compared with previous studies. The system is validated comparing two main processes, electrolysis and power production. Electrolysis is compared with previous electrolysis studies with heat recovery systems [11,41] and power production is compared with fuel cell simulations with heat recovery systems and hybrid fuel cell systems [24,42].

2.2.1 Electrolysis validation

At first instance, electrolysis model behaviour was compared with the study made by Gopalan et al. [41], which describes the utilization of the thermal energy of the exhaust gases of the solid oxide electrolysis cell (SOEC) to preheat the input gases. It also describes the effect of voltage and steam utilization in the temperature of the exhaust gases.

The study done by Gopalan et al. [41] defines thermoneutral voltage as:

$$V_{Tn} = \frac{\Delta H_{comp}}{zF} \quad (52)$$

Where ΔH_{comp} [kJ/mol] is the net enthalpy change of the system, z is the number of electrons transferred and *F* is Faraday's constant. The net enthalpy change is given by:

$$\Delta H_{comp} = H_{(H2/H2O/N2)} + H_{(Sweepair+O2)} - H_{(H2O/H2/N2)} - H_{(Sweepair)} \quad (53)$$

The study considers extra heat required and electric energy consumed by the fan to calculate efficiency, which calculation is given by

$$\eta_{actual} = \frac{LHV}{V_{op}I + Q_{extra} + FanPower} \quad (54)$$

Where η_{actual} is the real efficiency of the system, LHV is the low heating value of hydrogen, V_{op} [V] is the operating voltage and I [A] is the current.

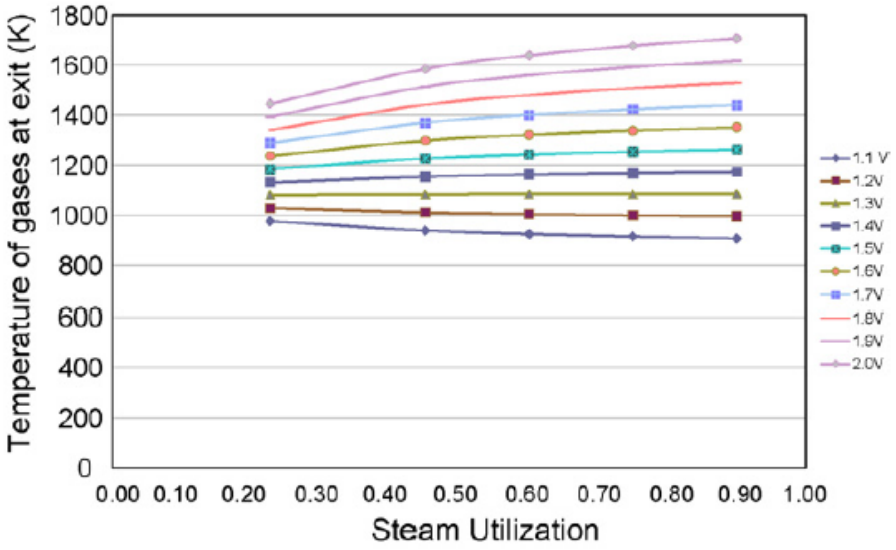

Fig. 17. Temperature of gases at exit versus steam utilization for various operating voltages [41].

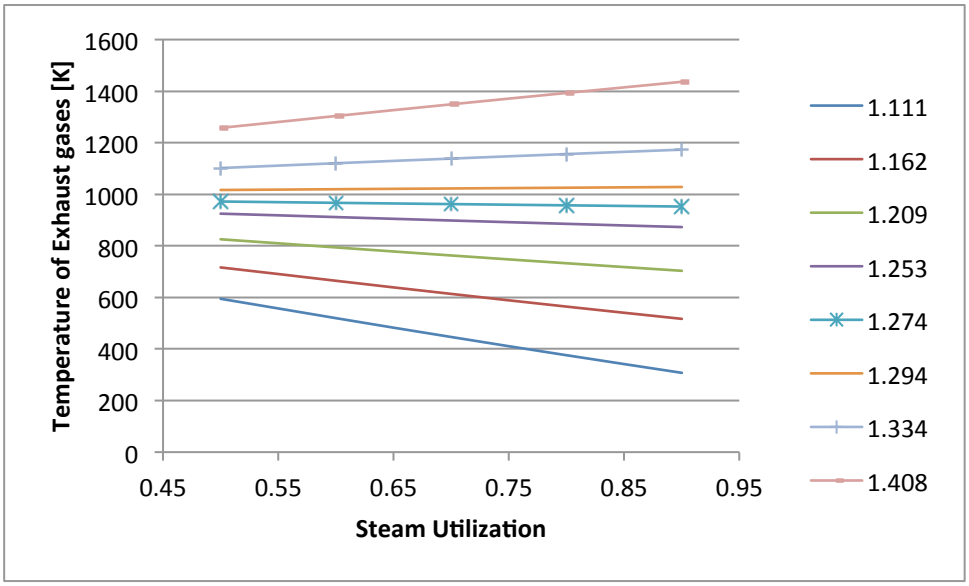

Fig. 18. Temperature of exhaust gases versus steam utilization for various operating voltages for the present model.

From figures 17 and 18, it can be observed in both plots the effect of steam utilization at different voltages. When the operating voltage is lower than the thermoneutral voltage, exhaust gases temperature decreases as the steam utilization factor increases. When operating voltage is close to thermoneutral voltage temperature variations are minimum. Temperature increases drastically when the operating voltage is higher than the thermoneutral voltage. However, there is a big difference between the values in figure 17 and figure 18, the reason for the difference in the values is the air input. Gopalan et al. [41] considered an air input in the cathode that is mixed with oxygen produced by electrolysis, the mass flow is determined by certain oxygen-air ratio. In the present model air at the input is not considered; therefore air is not contributing to heat or cool the system, thus the changes in temperatures are more drastically than the study by Gopalan.

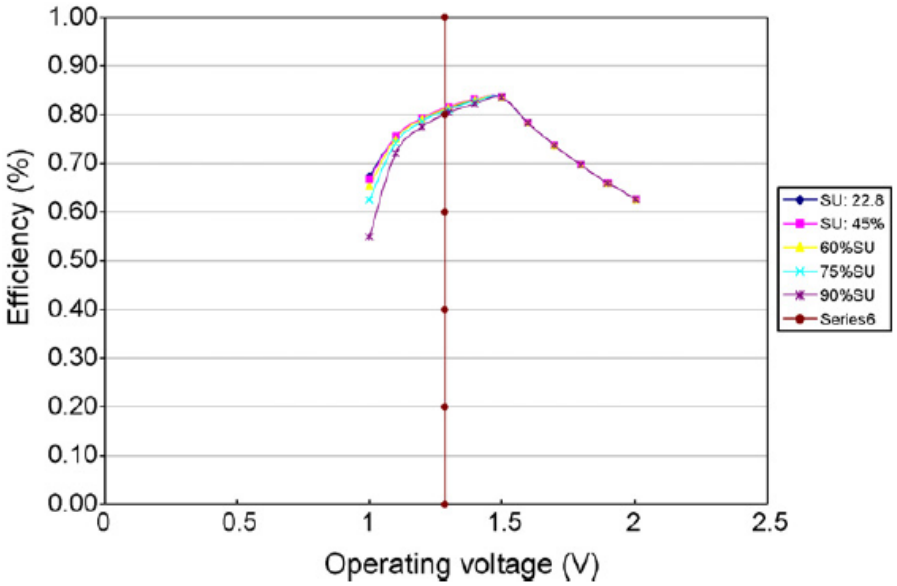

Fig. 19. Efficiency versus steam utilization for various operating voltages for a stack size of 50 cells [41].

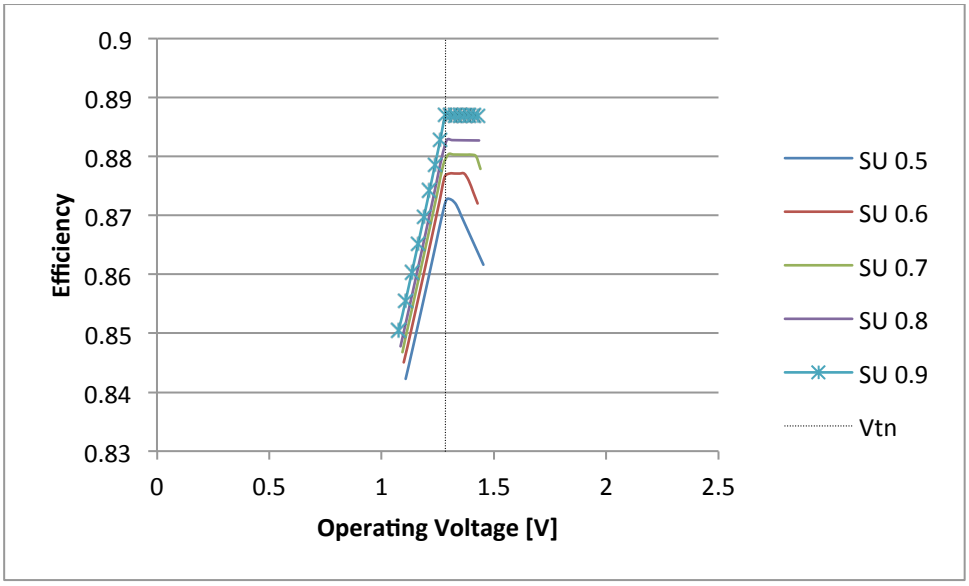

Fig. 20. Efficiency versus steam utilization for various operating voltages in the present model.

Figure 19 and figure 20 show the efficiency in function of the operating voltage. Efficiency increases when the operating voltage increases to the thermoneutral voltage. After thermoneutral voltage, efficiency starts decreasing. There are two reasons in the difference between the values of the study of Gopalan and the values of the present study. One of the reasons is the heating value of hydrogen. Gopalan et al, used the LHV to calculate the efficiency while in this work the HHV is considered to calculate the efficiency. Air input and the heat recovery system is another reason. In the study presented by Gopalan, it is assumed an air input to the system and the heat recovery system transfer thermal energy from hot air to cold inlet streams. In this work, in order to save energy of the air blower and air preheating, air input is considered only when the operating voltage is lower than thermoneutral voltage, thus air heats the system. Once the

operating voltage is higher than the thermoneutral voltage, air is not supplied to the system; therefore there is not air to heat and blow and there is not thermal energy to transfer from the air to the cold streams. Despite these differences, the system in this work shows a congruent efficiency behaviour compared with the study done by Gopalan et al. [41].

Once the behaviour of the electrolysis process was validated, it was compared with a study done by Petipas et al. [11]. The study describes a steady state SOEC system operated at different power loads without any external heat source and producing compressed hydrogen at 3MPa. Table 4 shows the principal parameters used by Petipas et al. and the parameters used in this work. In order to make an accurate comparison both studies share the same value for Number of cells, active cell area, gas composition inlet, electric power input and steam utilization.

Table 4. Electrolysis input parameters

Parameter	Petipas et al. [11]	Present model (1)	Present model (2)
$ASR_{@Tin}$ [Ω cm^2]	0.5	0.2	0.2
Ncell	10,000	10,000	5,800
SA [cm^2]	100	100	100
pH2O_in	100%	100%	100%
pH2_in	0%	0%	0%
pO2_in	100%	100%	100%
SC	75%	75%	75%
Tin [K]	1073	1000	1000
ΔT [T]	100	0	0
ηBoP_heater	95%	95%	95%
ηBoP_pump	75%	90%	90%
ηisentropic	75%	90%	90%
ηmechanical	90%	90%	90%

The results of the simulation compared with the results in [11] are shown in table 5.

Table 5. Comparison of the result with the results presented in reference [11].

	Petipas et al. [11]	Present model (1)	Present model (2)
Cell voltage [V]	1.32	1.22	1.32
Operating pressure [MPa]	0.1	0.1	0.1
Total electrical power [kWe]	1360	1558.95	1443.3
Electrical power [kWe]	1184	1184	1260
Heating power [kWth]	167	300.21	174.5
Heater power [kWe]	176	316.01	183.7
Hydrogen production rate [kg/h]	31.4	34.01	33.1
System efficiency [vs. HHV]	91.00%	90.30%	91.7%

The efficiency in the present work in case 1 is less, mainly, because the system is designed to operate a voltages lower than the thermoneutral voltage, consequently, it requires more thermal energy from the electric heaters and less energy from the exhaust gases can be recovered. The system presented in reference [11] operates above thermal neutral voltage; thus the thermal energy required is less. Exhaust gases have a temperature 100 K higher than gases at the input; therefore more thermal energy is recovered. These results are congruent with figures 19 and 20 that show the increase of efficiency is directly proportional to the increase of the operating voltage until it reaches the thermoneutral voltage, after that, efficiency keeps the maximum value and then decreases while operating voltage increases. Case 2 for the present model also shows the system working at thermoneutral voltage and it can be observed that efficiencies of both reference study and the present model are similar.

2.2.2 Fuel cell performance validation

Validation of energy production process is the second part to validate. The validation compares two systems previously simulated [24,42], which use thermal energy produced in the fuel cell to run parallel systems. Reference [24] operates the fuel cell as a micro combined heat and power system (mCPH) and the second reference [42] simulates a fuel cell system combined with a gas turbine. Table 6 shows electrical efficiency, thermal efficiency and total efficiency.

Table 6. Fuel cell performance

Parameter	mCHP (LHV methane) [24]	SOFC-GT (LHV methane) [42]	Present study (HHV H_2)
Electrical efficiency	38.50%	51.40%	49.63%
Thermal efficiency	41.90%	30.31%	27.10%
Total efficiency	80.40%	81.71%	76.73%

Reference [24]and [42] measure the efficiency using the LHV of methane. This is mainly because it is highly preferably to use methane instead of hydrogen in cogeneration systems, due availability and cost [24,25]. However, the present study shows reasonable results in all of the efficiencies mentioned before.

The validation of the present model exposes its reliability. The two main processes, electrolysis and power production, have shown reasonable hydrogen production, electrolysis, electric, thermal and total efficiencies. Therefore, the present study can be used to predict the behaviour of the SOEC/SOFC stack for electrolysis and power generation.

2.3 Sensitivity analysis

2.3.1 Input power effects

The present model predicts hydrogen production, thermal energy recovered, electric power generation and round efficiency of a SOEC-SOFC system. When the number of cells, active area and the ASR have been fixed, electric power input becomes a parameter to set current density and operating voltage. Regularly, electric power is shown in function of current density but figure 21 shows current density in function of electric power. The effects of the power input in other parameters like cell voltage can be related directly

with the effects of the power input in the current density. Thus, it is possible to represent the effects of the power input by presenting the current density values, which describe in more general way the system and make it easy to compare with similar systems.

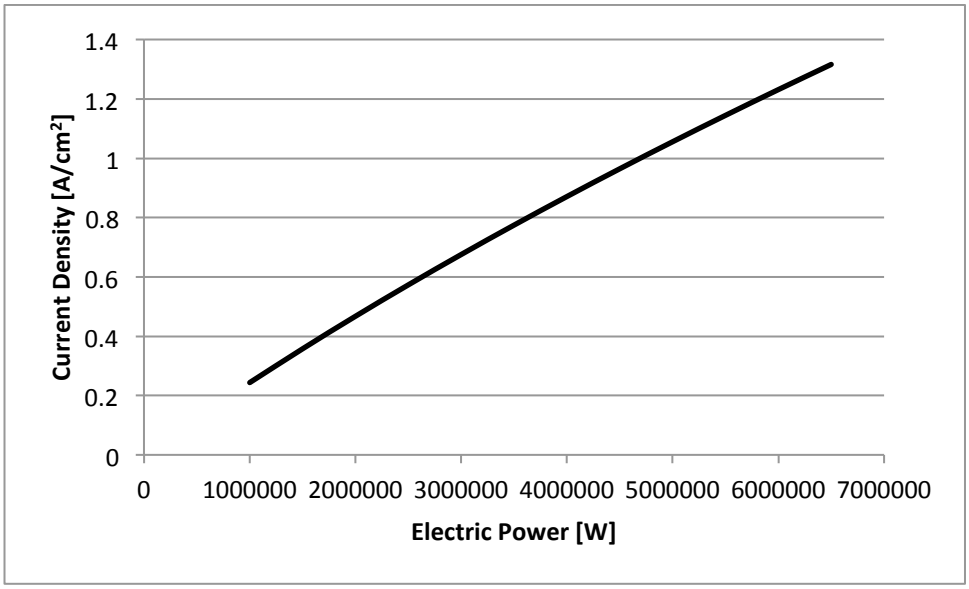

Fig. 21. Current density in function of Electric power input

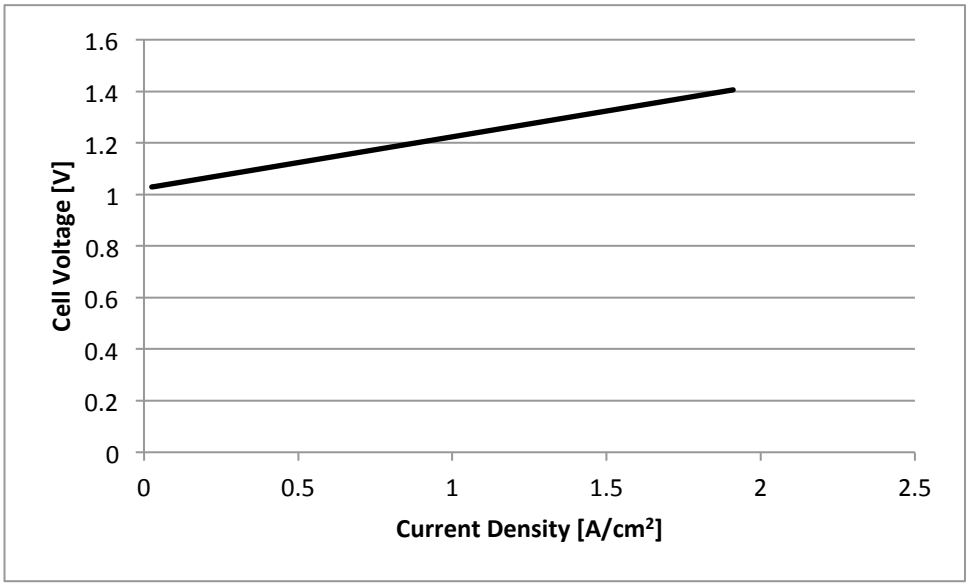

Fig. 22. Cell Voltage in function of current density

Electric power input affects the amount of thermal energy recovered from the fuel cell. Figure 23 shows the influence of the power input in the ratio between the heat recovered from the fuel cell and the heat required by electrolysis. It is worth noting that figure 21 assumes a symmetrical operation between the SOFC and SOEC i.e. hydrogen in the fuel cell is used at the same ratio it was produced.

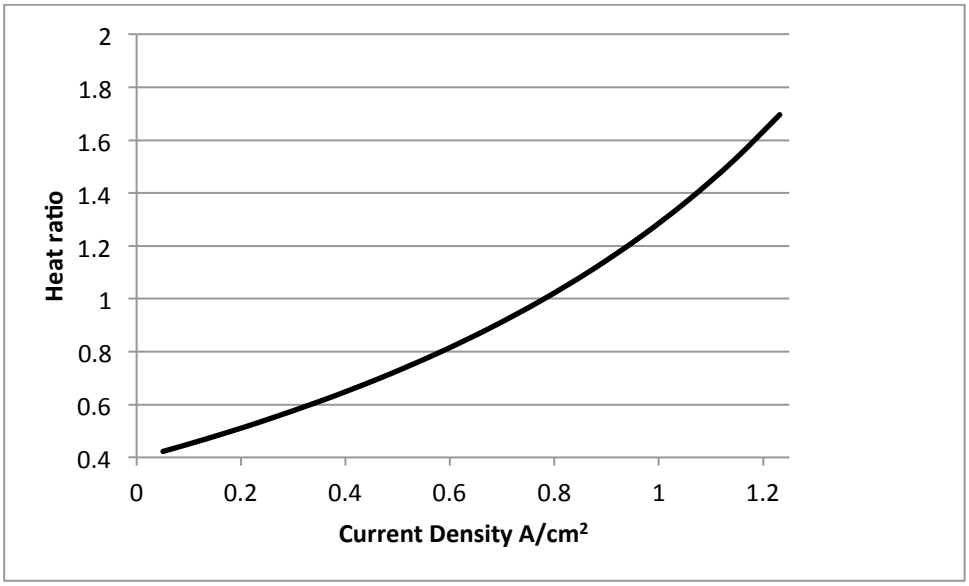

Fig. 23. Heat ratio in function of the current density

As long as current density increases, heat required in electrolysis decreases because the increment in cell voltage, in the other side, heat delivered by fuel cell increases, as a consequence of this opposite behaviour, heat ratio increases at higher polarization.

2.3.2 Influence of air temperature at the fuel cell input

Air is used in the system as energy carrier. Hot air supplies heat to electrolysis and thermal energy storage and cold air cools down the fuel cell. Cold air enters the fuel cell and exits as hot air, without any temperature drop, enters the High Temperature TES (HT-TES) and provides it with thermal energy. After preheating cold gases, air is directed to the low temperature thermal energy storage (LT-TES). Airflow depends on the air temperature at the fuel cell inlet. As long as the difference between air temperature at the input and the average temperature of the fuel cell decreases, a higher air flow is needed to remove heat. Figure 24 shows the relation between the air flow and the temperature difference between the anode input temperature in the fuel cell and the input temperature of air.

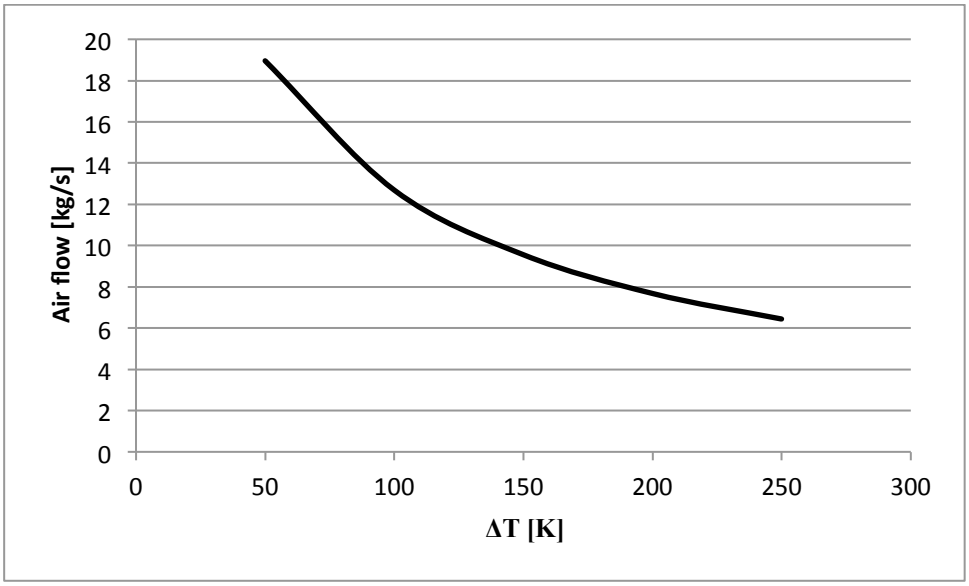

Fig. 24. Relation of air flow and the temperature difference between the mean temperature in the fuel cell and the air temperature at the fuel cell input

Air input temperature does not affect the heat produced at the fuel cell. Therefore, variations of temperature will not affect the amount of heat that is removed from the fuel cell by air. However, variations of air input temperature will change the distribution of heat stored in thermal energy storage. From figure 25, it is possible to observe heat storage distribution in the TES. Air input at low temperature allows the system to store more energy at lower temperatures, on the other hand; high air temperatures make the system to store energy at higher temperatures. The same trend is present at different H_2 flow rates, the difference is the amount of heat produced and the point of intersection of the two curves that moves slightly to the left.

Air temperature at the outlet of the fuel cell does not change with the variations of air temperature at the inlet and only mass flow of air increases or decreases according to temperature of the air at the inlet. From equations 37 and 38, it can be deduced that a bigger quantity of mass will increase the heat stored, as long the temperatures remain constant.

$$Q = n_{air} * \frac{H_i - H_f}{1000} \quad (37)$$

$$Q = m_{pcm} * Cp_{so} * (T_m - T_i) + m_{pcm} * H_{lh} + m_{pcm} * Cp_l * (T_f - T_m) \quad (38)$$

Where H_i and H_f are the enthalpy values of air at the inlet and outlet of the TES, respectively.

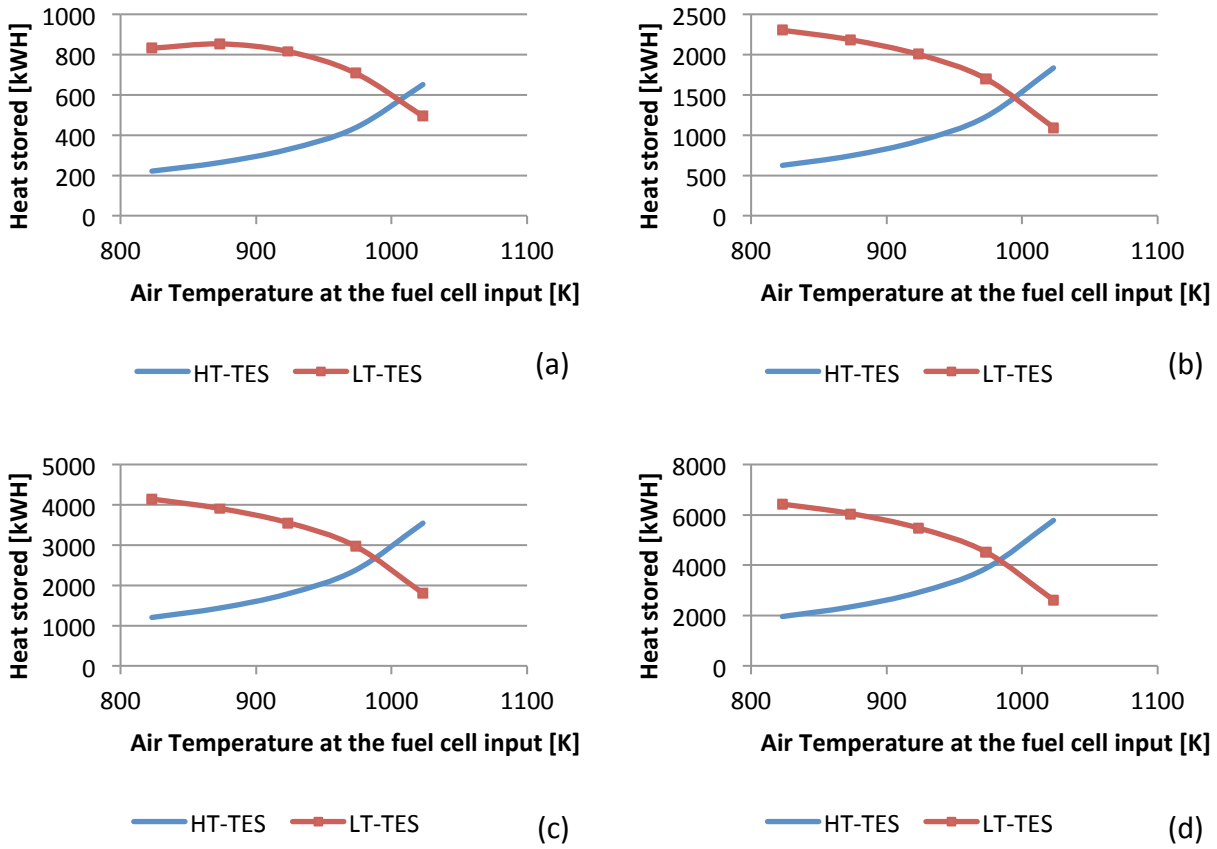

Fig. 25. Influence of air temperature at the fuel cell input at different H_2 flow rates in thermal energy storage distribution (a) 0.01 kmol/s, (b) 0.02 kmol/s, (c) 0.03 kmol/s, (d) 0.04 kmol/s.

Unlike the temperature of air at the output of the fuel cell, the temperature of air at the end of the heat recovery system varies with the changes in the temperature of air at the fuel cell input. Exhaust temperature is very important because determines the temperature at which heat is stored in the LT-TES. Figure 26 shows the different exhaust temperatures. The aim to have a low temperature thermal storage (390 K) is to generate steam, so temperatures lower than vaporization temperature are not appropriate for the system, even though the amount of heat stored is higher.

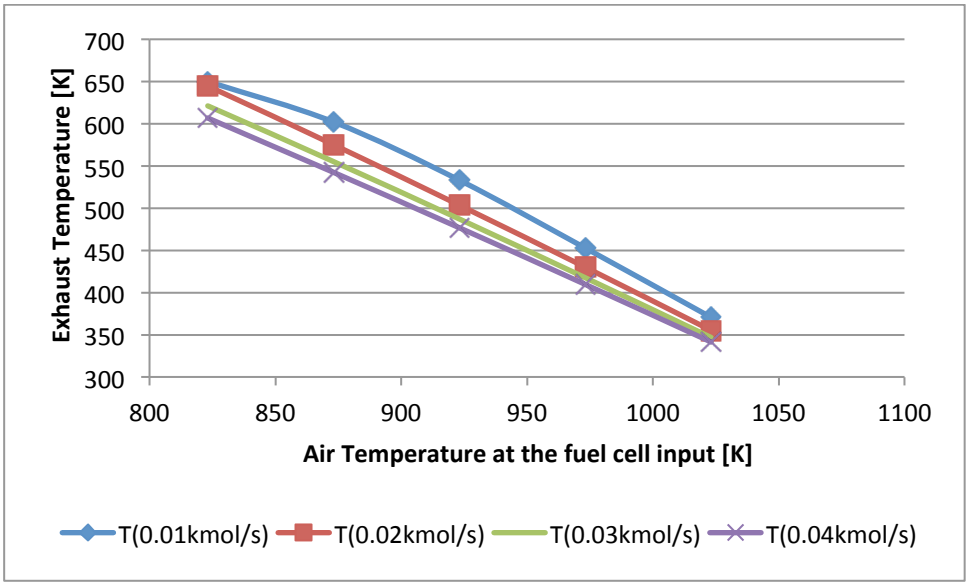

Fig. 26. Influence of air temperature at the fuel cell input at different H_2 flow rates in the exhaust air temperature.

2.3.3 Effects of the TES operational temperatures

TES based on phase change material behave as sensible heat storage when heat transfer takes place at temperatures different to the melting temperature. Therefore, thermal energy stored can be increased or decreased changing the operational temperatures. Figure 27 shows the different heat ratios at different operating temperatures of the LT-TES. The curve at 298.15 K is the theoretical curve when it is assumed that exhaust air can be cooled down to ambient temperature inside the heat storage.

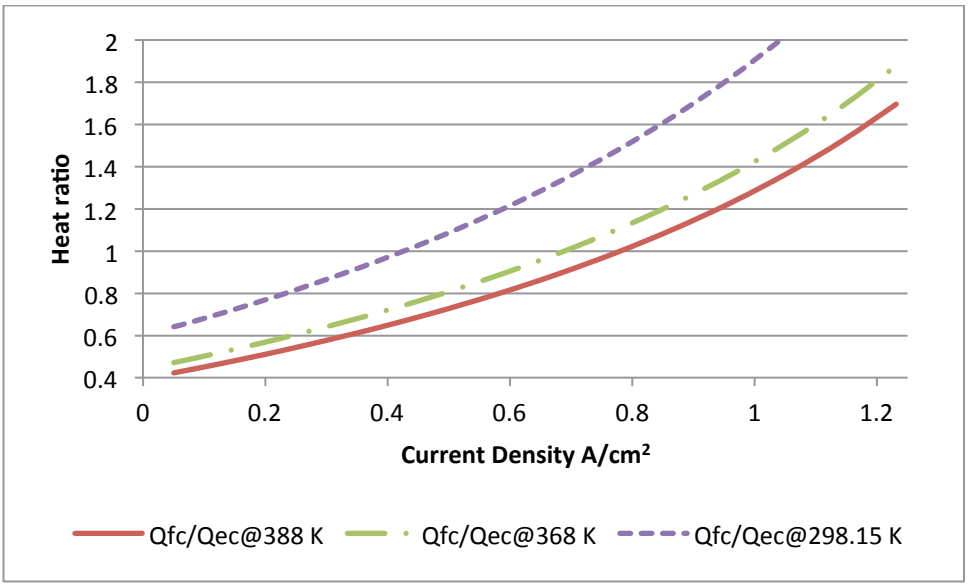

Fig. 27. Effects of operating temperature of the LT-TES on the heat ratio

With the information presented in this section, it is possible to set an operating point, where current density is between 0.8 and 1.3 A/cm^2 to have an electrolysis voltage between 1.1 V and thermoneutral

voltage. Temperatures of air at the fuel cell input higher than 973.15 K are not beneficial to store energy at low temperature. 973.15 K represents the point where the maximum amount of heat can be stored at temperatures higher than vaporization temperature.

3 Results and discussion

For a better comprehension of the parameters affecting the efficiency of the system, results are presented in an evolutionary way i.e. simple and ideal systems will be presented first, then systems more complex are presented.

Different scenarios operated at different cell voltages will be presented in order to determine the best operating voltage for a given configuration. Four different voltages are considered from 1.1 to 1.284 V. In order to prevent heat generation within the cell, the maximum operating voltage is set at the thermoneutral voltage (1.284 V).

3.1 Stack size

Electric power is considered to be a constant input of 5 MWe for all the cases. In order to have different operating voltages, the total resistance of the stack must be different. The total resistance of the cell stack can be modified by changing quality of the cell, active area of the cell or number of cells in the stack.

The first parameter to be fixed is cell quality, based on previous studies [11,26,27,28] values of ASR can be between 0.18 and 1.37 Ω cm^2. In presence of clean gases, the ASR can be 0.19 Ω cm^2 for steam electrolysis and 0.18 Ω cm^2 for H_2 oxidation [43]. The value assumed in the present work is 0.2 Ω cm^2 for both electrolysis and oxidation. Due the constant temperatures in the cell, effects of temperature on the ASR are not considered in the present model.

Once the quality of the cell has been specified, the second parameter to be fixed is the cell active area. The cell is a square cell that has a length of 25 cm and 484 cm^2 of active area, 96% of the total area. The values are based on data from reference [44].

Using the electrolysis cell voltage and current density equations (equation 14 and 15) it is possible to determine the number of cells for a specific cell voltage. Table 7 shows the number of cells for the four different voltages to analyse. The number of cell is rounded to the closest hundred number to have a more realistic value.

Table 7. Number of cell for different operating voltages

V_{ec}	Number of cells	round number
1.10	21361.16	21400
1.15	13025.61	13000
1.20	9161.73	9200
1.28	5910.31	5900

Each value of V_{ec} corresponds to a different system; results are going to be referenced to the voltage system.

3.2 Scenario 1: Ideal case

The first scenario presented is the model described in figures 15 and 16. Four different systems are evaluated in this scenario where each system operates at different V_{ec}. Table 8 presents a summary of the general operating conditions and general characteristics of the systems.

Table 8. General conditions, and general characteristics of the systems

System characteristics	
ASR [Ω cm^2]	0.2
Active Surface [cm^2}	484
HT-TES Material	LiF-CaF_2
LT-TES Material	$MgCl_2$-$6H_2O$
Electrolysis operating conditions	
$T_{in\ anode}$ [K]	1000
$T_{in\ cathode}$ [K]	1000
$T_{out\ anode}$ [K]	1000
$T_{out\ cathode}$ [K]	1000
$T_{in\ air}$ [K]	1030
$T_{out\ air}$ [K]	1000
Steam utilization	0.9
HSR	0.1
Time of operation [h]	12
Fuel cell operating conditions	
$T_{in\ anode}$ [K]	1023
$T_{in\ cathode}$ [K]	1023
$T_{out\ anode}$ [K]	1123
$T_{out\ cathode}$ [K]	1123
$T_{in\ air}$ [K]	973
$T_{out\ air}$ [K]	1123
Fuel Utilisation	0.9
Time of operation [h]	12

Particular assumptions are done in this scenario:

- Heat losses in the module and thermal storage are not considered;
- Energy quality is not considered;
- The minimum temperature difference in the heat exchangers is 1 K

Table 9 shows electrolysis mode results; table 10 shows fuel cell mode results and table 11 shows thermal energy storage values of the simulation for the different systems.

Table 9. Electrolysis results for the reference scenario

V_{ec} [V]	i [A/cm^2]	Cmp1 [W]	Cmp2 [W]	HE1 [W]	HE2 [W]	HE3 [W]	H_{2P} [mol/s]	η_{ec}
1.28	1.36	3.36E+05	2.48E+05	3.21E+05	5.75E+05	1.90E+02	20.18	0.8904
1.20	0.94	3.60E+05	2.65E+05	3.44E+05	6.15E+05	3.51E+05	21.59	0.8475
1.15	0.69	3.75E+05	2.77E+05	3.59E+05	6.42E+05	5.84E+05	22.53	0.8239
1.10	0.44	3.92E+05	2.89E+05	3.75E+05	6.71E+05	8.38E+05	23.56	0.8016

Columns Cmp1 and Cmp2 are the electric work from the compressors to increase the pressure from 0.1 MPa to 20 Mpa. Columns HE1 and HE2 are the electric work of the heaters to generate steam and preheat it to 1000 K. Column HE3 is the electric work of the air preheater to increase the air temperature to 1000 K.

Electrolysis efficiency varies considerably at different voltages. At thermoneutral voltage, the cell produces enough heat to keep the temperature at the same level, but at lower voltages, the heat required to keep the process isothermally is higher. This can be seen in column HE3, where the power at thermoneutral voltage is 190 W and the power at 1.1 V is 838 kW.

For the same electric power input, when the voltage decreases the current increases, thus H_2 production increases. From another perspective, at voltages lower than thermoneutral voltage, more electric power is used to produce H_2 instead of heating the system. The highest hydrogen production, shown in column H_{2P} in table 9, occurs at 1.1 V.

Electric work used to compress hydrogen represents more than 10% of the total electric energy input. Electrolysis efficiencies could increase if the power utilised to compress hydrogen decreases. Figure 28 shows the distribution of the energy consumption by the electrolysis process. Where Cmp1 and Cmp2 are the energy consumed by the compressors and blowers, HE1 is the required energy to generate steam, HE2 is the required energy to preheat steam to 1000 K and HE3 is the required energy to preheat air to 1030 K.

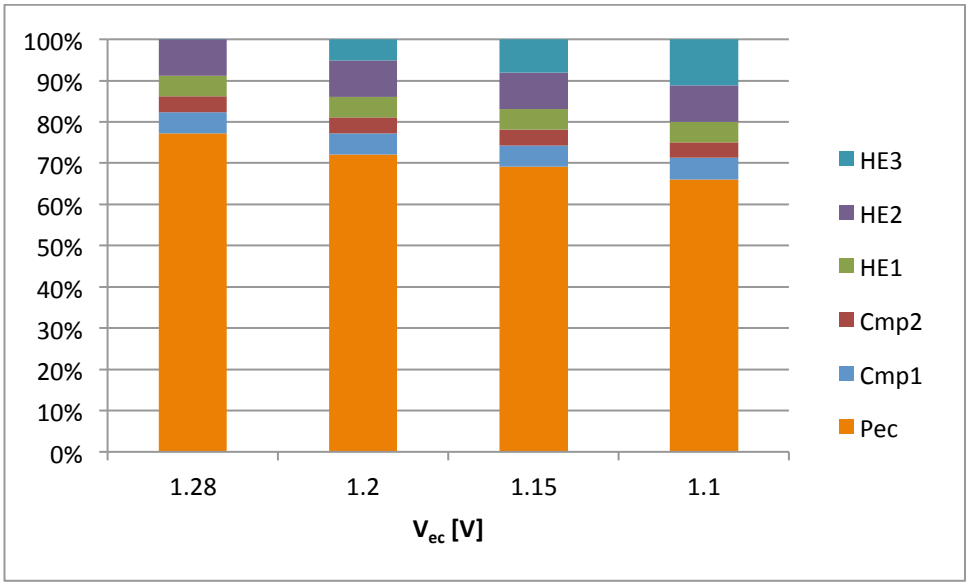

Fig. 28. Energy input distribution for electrolysis process at different V_{ec}

Table 10. Fuel cells results for the reference scenario

H_{2i} [mol/s]	$P_{fc\ [W]}$	V_{fc} [V]	i [A/cm^2]	η_{fc}
22.7	2.88E+06	0.7321	1.3761	0.4445
24.3	3.44E+06	0.8173	0.9501	0.4963
25.3	3.82E+06	0.8678	0.6973	0.5270
26.5	4.22E+06	0.9184	0.4445	0.5577

Electric fuel cell efficiency increases when the current density decreases. Table 10 shows the fuel cell electric power (P_{fc}), fuel cell voltage V_{fc}, current density and the efficiency for a given hydrogen flow, which corresponds to the total hydrogen flow in the electrolysis. Comparing the electric currents between table 9 and table 10, it is possible to observe that the amount of hydrogen reacted and produced is similar. In fact, in fuel cell mode the system used all the hydrogen produced in electrolysis at the same rate. The hydrogen flow in table 10 shows the hydrogen produced plus the hydrogen that was mixed with water for electrolysis. Each hydrogen flow corresponds to a certain voltage in table 7, i.e. 22.7 mol/s correspond to the total flow for voltage 1.28 in table 7, in this way fuel cell results can be related with electrolysis results and know which results correspond to the same system.

Thermal energy storage results after 12 h of fuel cell operation are described in table 11. Operating voltage influences thermal energy storage at high temperatures more drastically than lower temperatures. It is also possible to observe that operating the fuel cell with a higher current density, the heat generated will be higher and if the fuel cell is operated at lower current density heat generation will be lower.

Table 11. Thermal energy stored in 12 h and TES dimensions

LT-TES V_{ec} [V]	Heat [kJ]	Mass [kg]	Volume [m^3]	Length [m]	Area [m^2]	Heat Losses [W]
1.28	9.22E+08	5.47E+06	3772.176	15.567	1453.938	2.81E+04
1.20	9.04E+08	5.36E+06	3698.830	15.465	1435.029	2.77E+04
1.15	8.92E+08	5.29E+06	3649.966	15.397	1422.363	2.75E+04
1.10	8.79E+08	5.21E+06	3596.341	15.321	1408.397	2.72E+04
HT-TES V_{ec} [V]	**HT-TES Heat [kJ]**	**Mass [kg]**	**Volume [m^3]**	**Length [m]**	**Area [m^2]**	**Heat Losses [W]**
1.28	6.01E+08	7.36E+05	308.104	6.754	273.705	2.03E+05
1.20	5.39E+08	6.61E+05	276.567	6.515	254.694	1.89E+05
1.15	4.99E+08	6.11E+05	255.671	6.347	241.698	1.79E+05
1.10	4.54E+08	5.57E+05	232.875	6.152	227.108	1.68E+05

For a better understanding of the energy flow through the operation time, figure 29 and 30 show the electric power input and output, thermal power input and output and the stored heat in the TES. It is

assumed that the heat reservoir is totally full and when electrolysis starts, discharge mode of the TES starts and when fuel cell mode starts, charging mode of the TES starts.

Electric power and thermal power output are considered to be positive values, while electric power and thermal power input are considered negative. Electric power input is 5 MWe for electrolysis; electric power output considers the electric power of the fuel cell. Thermal power input considers the heat required to vaporize water and preheat steam and air to the operating temperature; thermal power output is the heat stored in both HT-TES and LT-TES.

At 1.1 V, thermal power required for electrolysis is less than the thermal power released by the fuel cell. Thermal energy values are around 2000 kW and the ratio between the heat released and the required is 1.37. At 1.28 thermal power required is still less than thermal power released by the fuel cell. However, at 1.284 V the ratio between the heat released and required is 3.26. At 1.284 V most of the heat released by the fuel stored will be impossible to use it for electrolysis and it will be wasted if it is not used in other processes. In the other side, at 1.1 V the use of heat stored is more efficient because most of this heat is used for electrolysis.

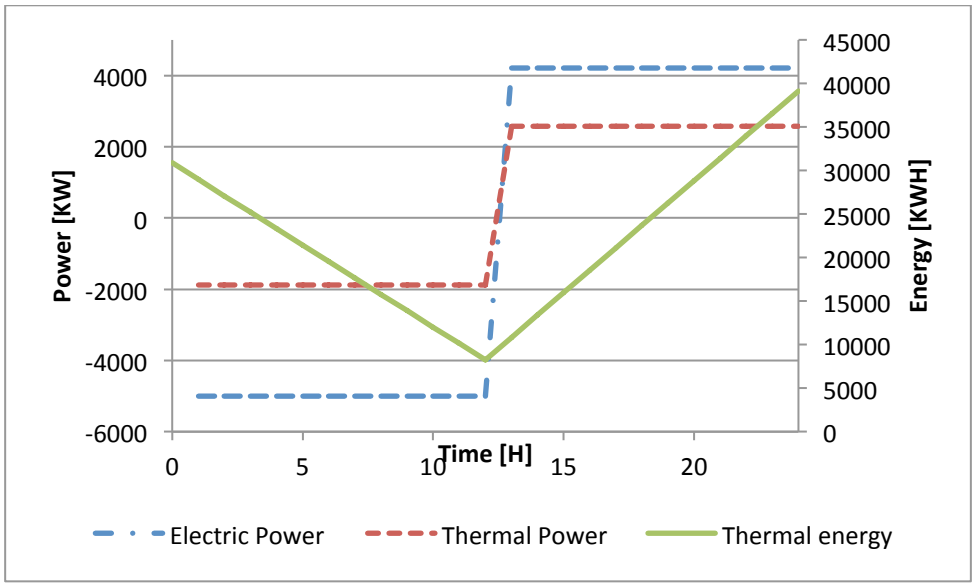

Fig.29. Power and energy in 12 h electrolysis at 1.1 V and 12 h fuel cell

In both operating voltages, electric power input is higher than the electric power output. However, the ratio of electric power output and the electric power input is 0.84 at 1.1 V and 0.57 at 1.284 V.

The system operating at 1.1 V shows a better management of thermal and electric power and thermal energy than the system operating at thermoneutral voltage.

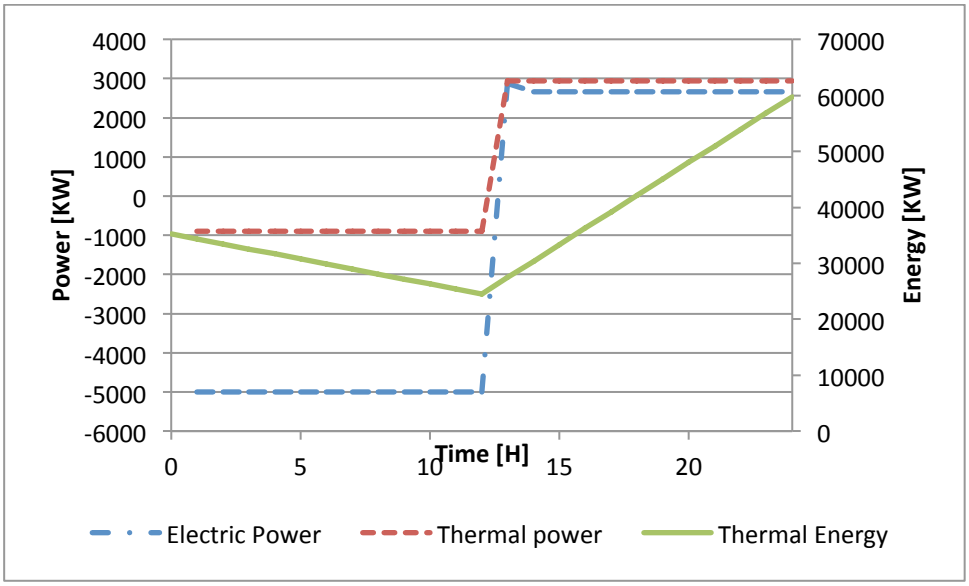

Fig.30. Power and energy in 12 h electrolysis at 1.2843 V (thermoneutral voltage) and 12 h fuel cell

Hydrogen production affects the volume of the storage tank. Figure 31 shows the evolution of the tank volume respect with the operating voltage of the system for 12 hours of electrolysis. At lower voltages the system requires a bigger storage tank because hydrogen production is higher than at higher voltages.

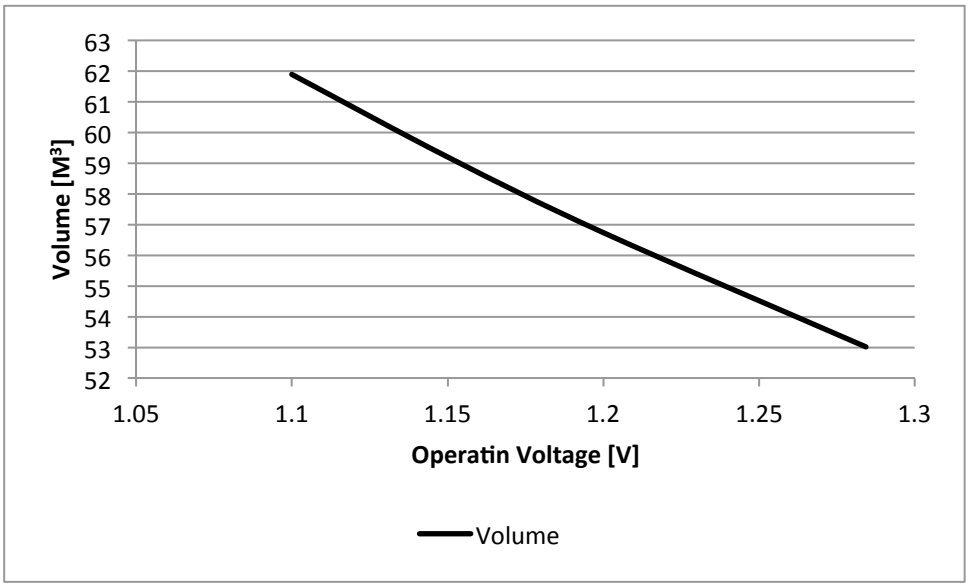

Fig.31. Hydrogen tank volume required for 12 h of H_2 production at different voltages

Table 12 shows a summary of the electric and thermal power ratios and the efficiency of electrolysis and fuel cell for the different systems. It is worth mentioning the increase on the ratio between the power released by the fuel cell and the total power required when thermal energy storage is used. At thermoneutral voltage, the ratio increases from 0.445 to 0.516 and at 1.1 V increases from 0.558 to 0.7429. Therefore, the use of thermal energy storage helps to increase the round cycle efficiency of the systems. Advantages of using TES are higher when electrolysis-operating voltages are lower than thermoneutral voltages.

Table 12. Power ratios, heat ratio and electrolysis and fuel cell efficiency for the reference system

V_{ec}	r_p	r_c	r_t	r_t no HT-TES	r_t no TES	r_q	η_{ec}	η_{fc}
1.2843	0.5764	0.6989	0.5161	0.4674	0.4447	3.2786	0.8904	0.4445
1.2000	0.6886	0.7771	0.6121	0.5217	0.4965	2.1252	0.8475	0.4963
1.1500	0.7630	0.8289	0.6750	0.5538	0.5272	1.6930	0.8239	0.5270
1.1000	0.8442	0.8854	0.7429	0.5857	0.5579	1.3650	0.8016	0.5577

It is worth noting that power ratios do not increase considerably only by the application of LT-TES. As it can be seen from figure 28, the required energy to generate steam represents less than the 10 per cent of the total required energy by the electrolysis process.

Round cycle efficiency can be increased if the excess of heat is used to run parallel system like gas or steam turbines. Hybrid systems were mentioned before in references [23,42]. In the present model, it is assumed that the excess of heat is used in a Rankine cycle with an overall efficiency of 30% [42]. Power supplied by the Rankine cycle is calculated with equation 55

$$P_{rc} = \dot{Q}_{ex} * \eta_{rc} \quad (55)$$

Where P_{rc} [W] is the power generated by the Rankine cycle, $\dot{Q}_{ex}$ [W] is the excess of heat stored in the thermal energy storage and η_{rc} is the overall Rankine cycle efficiency. At thermoneutral voltage, the benefits of including a Rankine cycle in the system are higher than the system operating at 1.1 V.

3.2.1 Effects of heat losses in the cell stack

Table 13 shows the result of the simulation previously described but considering heat losses in the module. Heat losses represent a very small portion of the total energy and their values are around 2 to 3% of the total energy output.

Table 13. Power ratios, heat ratio and electrolysis and fuel cell efficiency considering heat losses in the module

V_{ec}	r_p	r_c	r_t	r_t no HT-TES	r_t no TES	r_q	η_{ec}	η_{fc}
1.284	0.5764	0.6980	0.5161	0.4674	0.4442	3.2462	0.8886	0.4445
1.200	0.6886	0.7760	0.6121	0.5217	0.4958	2.1035	0.8454	0.4963
1.150	0.7630	0.8275	0.6750	0.5538	0.5263	1.6732	0.8215	0.5270
1.100	0.8442	0.8835	0.7429	0.5857	0.5567	1.3453	0.7987	0.5577

Only the ratios where thermal energy is related are affected with the inclusion of heat losses in the module. Changes are less than 5% and the highest heat ratio change is at thermoneutral voltage where the heat ratio decreases 0.0324 and the highest electrolysis efficiency change is at 1.1 V.

3.2.2 Effects of setting the minimum temperature difference in the heat exchangers to 10 K

Setting the minimum temperature difference at 10 K decreases the amount of heat transfer in the heat exchangers. Thus, the recovery heat system becomes less efficient affecting thermal efficiency of the system. This can be seen in table 14, where power ratios are not affected by setting the minimum temperature but ratios where thermal energy is related.

The effects of considering 10 K as the minimum temperature difference in the system are more substantial than heat losses in the module.

Other aspect where the minimum temperature difference affects is the total heat exchanger area. Heat exchanger area decreases when the minimum temperature difference increases. The total heat exchanger area for the system operating at thermoneutral voltage without the limited temperature difference is 16,184,769 m^2; the area for the same system operating with the limited temperature difference is 452,757.3 m^2.

Table 14. Power ratios, heat ratio and electrolysis and fuel cell efficiency considering 10 K as the minimum temperature difference in the heat exchangers.

V_{ec}	r_p	r_c	r_t	r_t no HT-TES	r_t no TES	r_q	η_{ec}	η_{fc}
1.2843	0.5764	0.6968	0.5161	0.4672	0.4439	3.2123	0.8880	0.4445
1.2000	0.6886	0.7673	0.6121	0.5119	0.4869	1.9067	0.8309	0.4963
1.1500	0.7630	0.8139	0.6750	0.5377	0.5116	1.4698	0.8002	0.5270
1.1000	0.8442	0.8645	0.7429	0.5626	0.5357	1.1543	0.7714	0.5577

3.2.3 Effects of heat losses in the thermal energy storage

Heat losses from the thermal energy storage are unavoidable, thus it is very important to consider them in the simulation. Heat losses can be reduced with very high efficient insulation material. Insulation materials were described in the previous sections. Table 15 shows power ratios, heat ratio and electrolysis and fuel cell efficiencies considering heat losses in TES.

Only heat ratio and the power delivered by the Rankine cycle are affected by heat losses in the TES. Because the heat ratio is above 1 in all the voltages, the system is not affected in the performance directly. Heat losses in thermal energy storage could become a problem when heat ratios are close to 1.

Power ratio, when HT-TES is not considered, is the same as in table 14 for two reasons. First, heat losses in HT-TES do not exist and second, heat losses in the LT-TES are compensated by the excess of heat stored at low temperatures.

Table 15. Power ratios, heat ratio and electrolysis and fuel cell efficiency considering heat losses in TES

V_{ec}	r_p	r_c	r_t	r_t no HT-TES	r_t no TES	r_q	η_{ec}	η_{fc}
1.284	0.5764	0.6942	0.5161	0.4672	0.4439	3.0638	0.8880	0.4445
1.200	0.6886	0.7649	0.6121	0.5119	0.4869	1.8540	0.8309	0.4963
1.150	0.7630	0.8115	0.6750	0.5377	0.5116	1.4385	0.8002	0.5270
1.100	0.8442	0.8623	0.7429	0.5626	0.5357	1.1351	0.7714	0.5577

3.2.4 Effects of thermal energy quality

Until now, the energy quality of the heat recovery system has not been considered. Storing 1 kW of heat at 1000 K is not the same than storing the same 1 kW at 300 K. Thus, the analysis of thermal energy quality becomes important. Table 16 shows the effects of thermal energy quality in the system.

Table 16. Power ratios and heat ratios considering thermal energy quality

V_{ec}	r_p	r_c	$Q_{rec,LT}/Q_{req,LT}$	$Q_{rec,HT}/Q_{req,HT}$	r_t	r_{ct}
1.2843	0.5764	0.6403	5.3515	1.8555	0.5161	0.5733
1.2000	0.6886	0.7490	4.9015	0.9112	0.6013	0.6540
1.1500	0.7630	0.8216	4.6323	0.6463	0.6179	0.6653
1.1000	0.8442	0.9008	4.3608	0.4682	0.6331	0.6756

Power ratios decrease considerably when the energy quality is applied. The main reason for the decrease is that the excess of heat is at lower temperature but at high temperature storage the ratio is less than one, so more electric power is required to preheat the steam and the air. Unlike in thermoneutral voltage system, the effects of energy quality are very significant in the other systems. The ratio between the fuel cell power and the total electric power input decreases from 0.7429 to 0.6331.

3.2.5 Effects of temperature drop in the cell

So far, temperature in the cell during electrolysis has been kept constant at 1000 K. As it was mentioned before, when electrolysis process is performed with lower voltages than thermoneutral voltage,

temperature of the process decreases and an external heat input is required. Therefore, electrolysis efficiency decreases as it could see in figure 20, chapter 2.

Allowing a temperature drop of 100 K in the cell stack will reduce the extra thermal energy to heat the system. As a consequence, air heater (HE3) will use less energy and overall efficiency will increase. Figure 32 (a) shows the energy input distribution at constant temperature while figure 32 (b) shows it with a temperature drop of 100 K. Figure 33 shows the difference between the required energy in the air preheater in both cases.

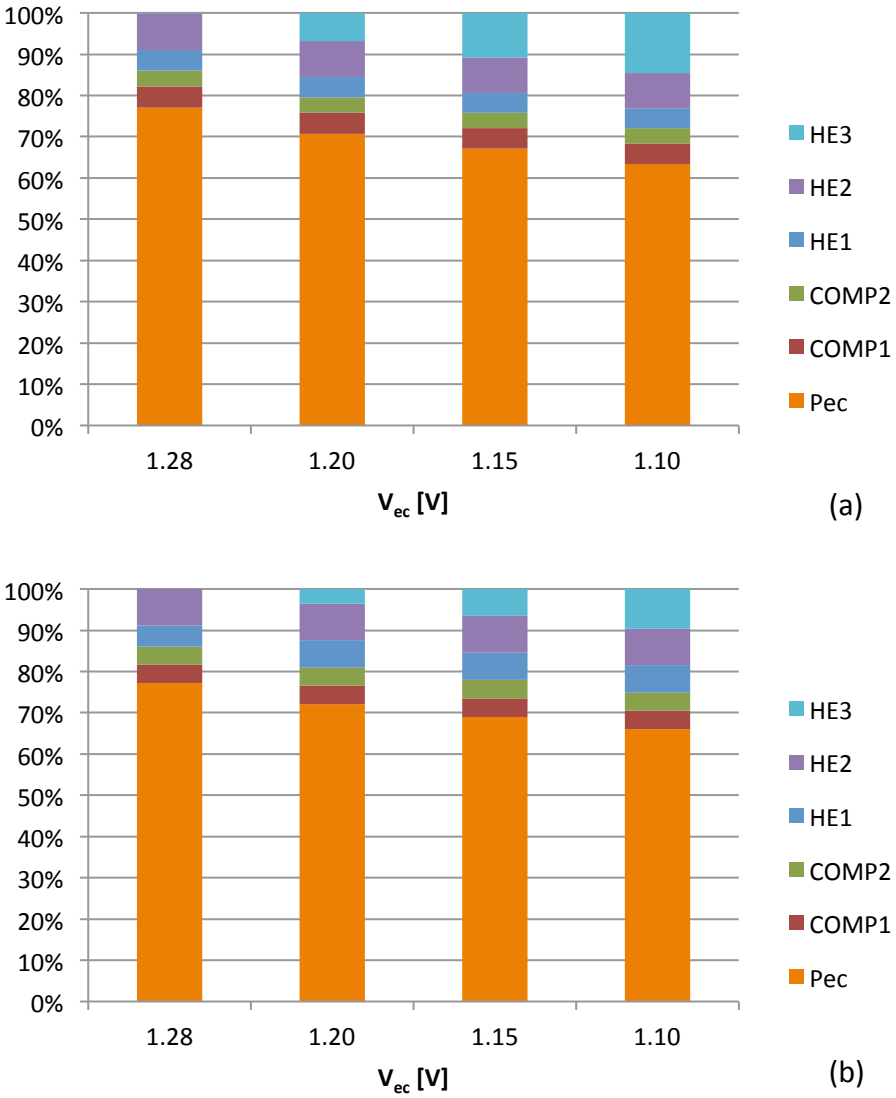

Fig.32. Energy input distribution for electrolysis process at different V_{ec}, a) Temperature constant in the cell, b) Temperature drop of 100 K.

In figure 32 a) and b), it is possible to observe a decrease on the energy used by the air preheater. At thermoneutral voltage, air preheater does not consume energy when temperature drops in the cell stack. A better observation can be done in figure 33, where the reduction of the energy consumed by the air preheater decreases around 30% of its value at 1.2, 1.15 and 1.10 voltages.

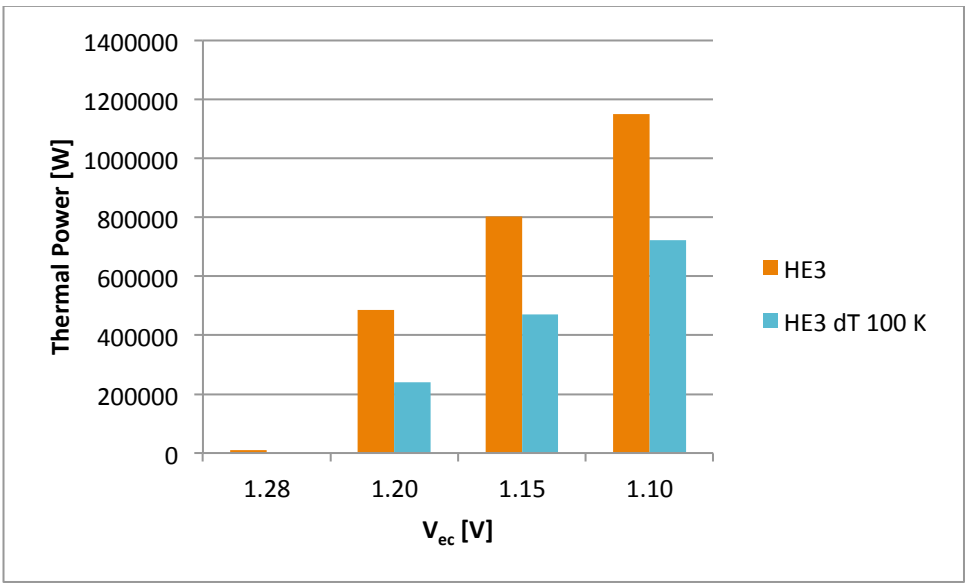

Fig. 33. Power consumptions of the air preheater with constant temperature and with a temperature drop of 100 K

Heat duty of air preheater is not the only parameter affected by the temperature drop. Heat ratios between the heat stored and the heat required and power ratios (r_t and r_{ct}) are affected. The temperature drop in the electrolysis process does not affect heat recovered from the fuel cell. However, heat required for electrolysis is highly affected when a temperature drop exists. When output temperature of the exhaust gases decreases, the energy recovered from the exhaust gases is less; as a consequence, the vaporizer requires a higher heat duty decreasing the heat ratio at low temperature. At higher temperature, the heat ratio increases because the reduction in energy consumption by the air preheater. Power ratios increases because required energy for electrolysis decreases. Power ratios in table 17 show an increase of 4% with power ratios in table 16, thus running the system with a temperature drop in the cell stack benefits the round cycle efficiency.

Table 17. Power ratios and heat ratios considering a temperature drop of 100 K

V_{ec}	r_p	r_c	$Q_{rec,LT}/Q_{req,LT}$	$Q_{rec,HT}/Q_{req,HT}$	r_t	r_{ct}
1.2843	0.5764	0.6414	5.2680	1.8840	0.5166	0.5749
1.2000	0.6886	0.7438	3.6749	1.1615	0.6289	0.6793
1.1500	0.7630	0.8162	3.4726	0.8334	0.6537	0.6992
1.1000	0.8442	0.8952	3.2686	0.6084	0.6772	0.7181

After analysing the first scenario and the contribution of every loss to the system, it is possible to determine what parameters should be modified to decrease losses and increase efficiency. The most significant losses are the energy required to compress hydrogen, around 10% of the total energy input. Heat quality is another parameter than can be modified in order to increase efficiency.

3.3 Scenario 2: Catalytic burner

In this scenario, a catalytic burner is added after the fuel cell in order to increase the amount of heat stored at high temperatures. Figure 34 shows the layout. Four different systems are evaluated operating at different voltages.

A special assumption for this scenario is the efficiency of the burner, which is considered as 100% efficient. All the hydrogen entering the burner is oxidised. H_2 enters the system at ambient temperature and atmospherics pressure through stream 1 and is preheated to the operating temperature. O_2 enters the system at ambient temperature and atmospherics pressure in stream 4 and is preheated to the operating temperature. In the same way, air enters the system through stream 7 at ambient temperature and atmospheric pressure, and then is preheated to the operating temperature. After reacting in the fuel cell, the remaining H_2 and O_2 are burnt; air is used to control burner temperature [25]. Steam is sent through stream 20 to preheat cold H_2, O_2 and air. Air is sent directly to the HT-TES through stream 14 to transfer part of the heat, after that, it is sent to preheat O_2 and cold air to the operating temperature. Finally, it is sent to the LT-TES where it will transfer all the remaining thermal energy.

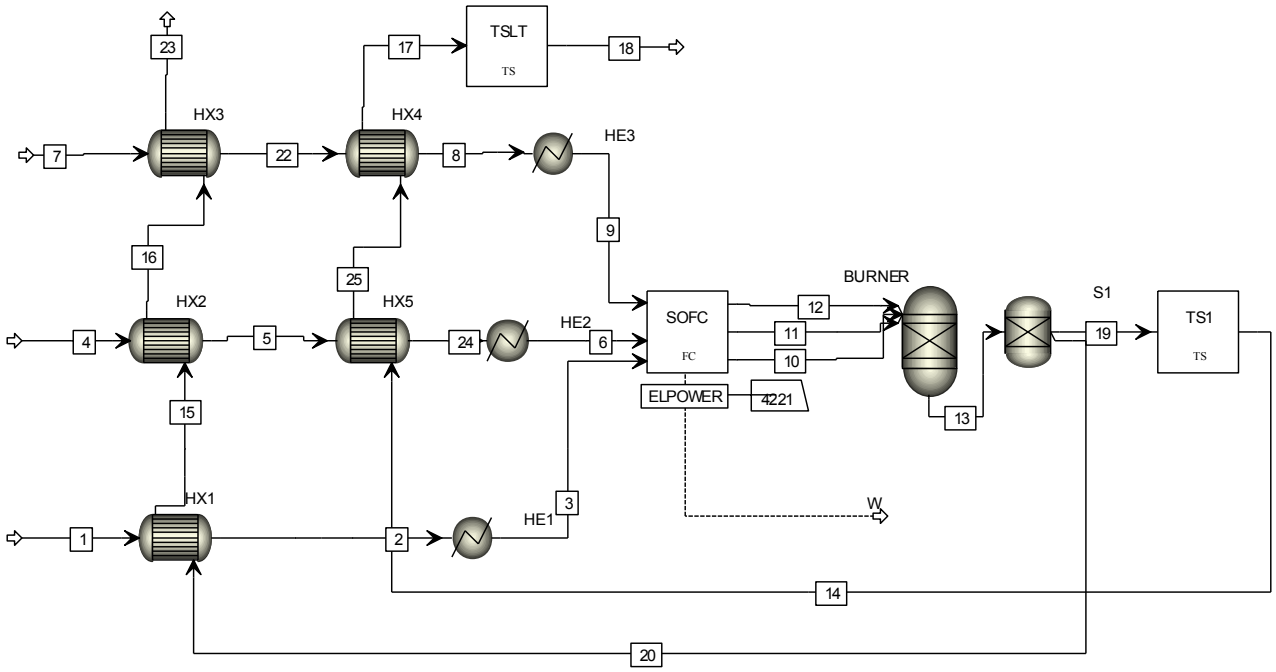

Fig. 34. Layout in Aspen plus™ of the fuel cell system including the afterburner

General conditions and characteristics are the same that those from scenario 1. Beside the addition of the burner, the other important aspect that was changed is H_2 flow. Scenario 1 considers hydrogen recirculation in the system, so the mass flow circulating the system is the hydrogen produced plus the hydrogen used for electrolysis, but for this scenario recirculation cannot be considered because of the burning process. Therefore, mass flow circulating the system is only the hydrogen produced by electrolysis.

Table 18. Power ratios and heat ratios considering a burner in the system

V_{ec}	r_p	r_c	$Q_{rec,LT}/Q_{req,LT}$	$Q_{rec,HT}/Q_{req,HT}$	r_t	r_{ct}	r_t no TES
1.2843	0.5342	0.6018	5.6856	1.9033	0.4784	0.5389	0.4635
1.2000	0.6286	0.6943	5.2420	1.0026	0.5591	0.6168	0.4909
1.1500	0.6912	0.7554	4.9805	0.7493	0.5737	0.6271	0.5065
1.1000	0.7594	0.8221	4.7210	0.5781	0.5873	0.6358	0.5217

The effects of the reduced hydrogen flow can be seen in table 18, in Scenario 1, fuel cell power ratio was 0.8442 and when the burner is added the ratio decreases to 0.7594. This is mainly caused by the reduction of hydrogen flow in the system. The ratio of heat stored at high temperature increases but it is not enough to compensate the electric power lost, thus the round cycle efficiency decreases from the previous scenario.

Adding a burner does not represent any advantage, even though high temperature heat ratio increases, total efficiencies decrease.

3.4 Scenario 3: Pressurized electrolysis

Hydrogen compression is the most demanding energy process after electrolysis and heating. It consumes about 10 per cent of the total energy input. Energy savings can be obtained if the compression of hydrogen is changed by pressurising water. Operating an electrolysis pressurized system could help to reduce the energy consumption.

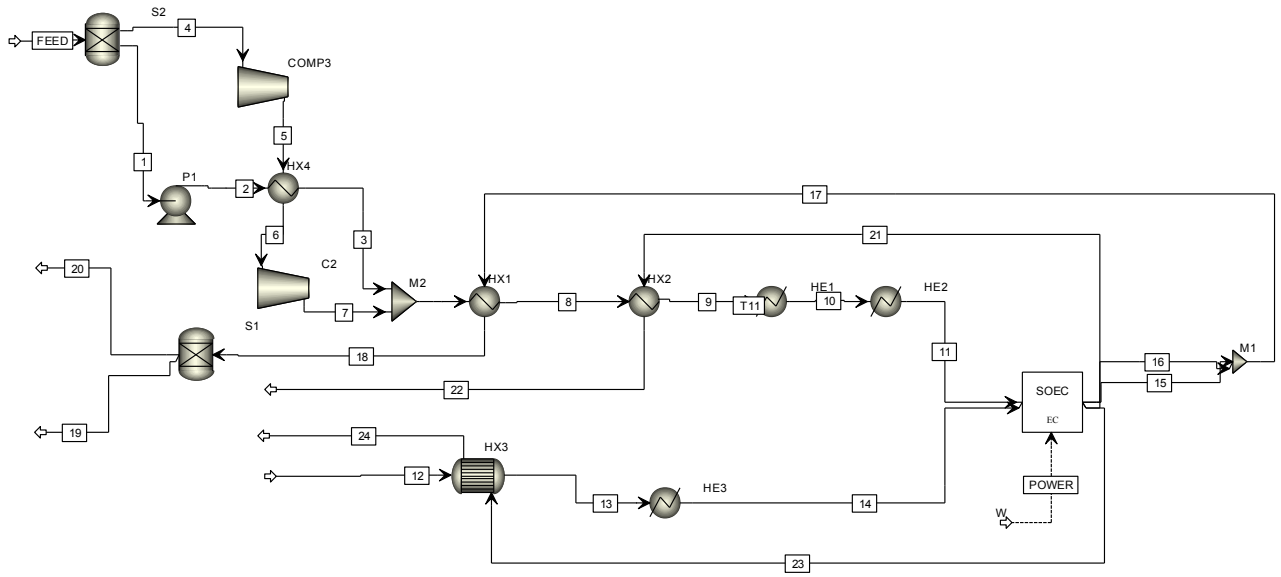

Fig. 35. Layout in Aspen plus^{TM} for pressurized solid oxide electrolysis cells

Different studies have suggested the use of pressurized solid oxide cells for electrolysis and have shown its benefits like reduction in the energy consumption for the compressors and reduction of ASR [19,43]. However, the effects of increasing pressure on the cell are beyond the scope of this work, values at 1 atm are considered to simulate this scenario.

Increasing water pressure will raise the temperature at which vaporizes; therefore, a different material for thermal energy storage is required. Vaporization temperature at 2 MPa is at 212.3 ^{o}C, thus Na/K/NO_3 (0.5/0.5) is used as the PCM, which melting temperature is at 220 ^{o}C. Some changes have to be done in the heat recovery system to store thermal energy at higher temperature. Figure 36 shows the changes done in the system.

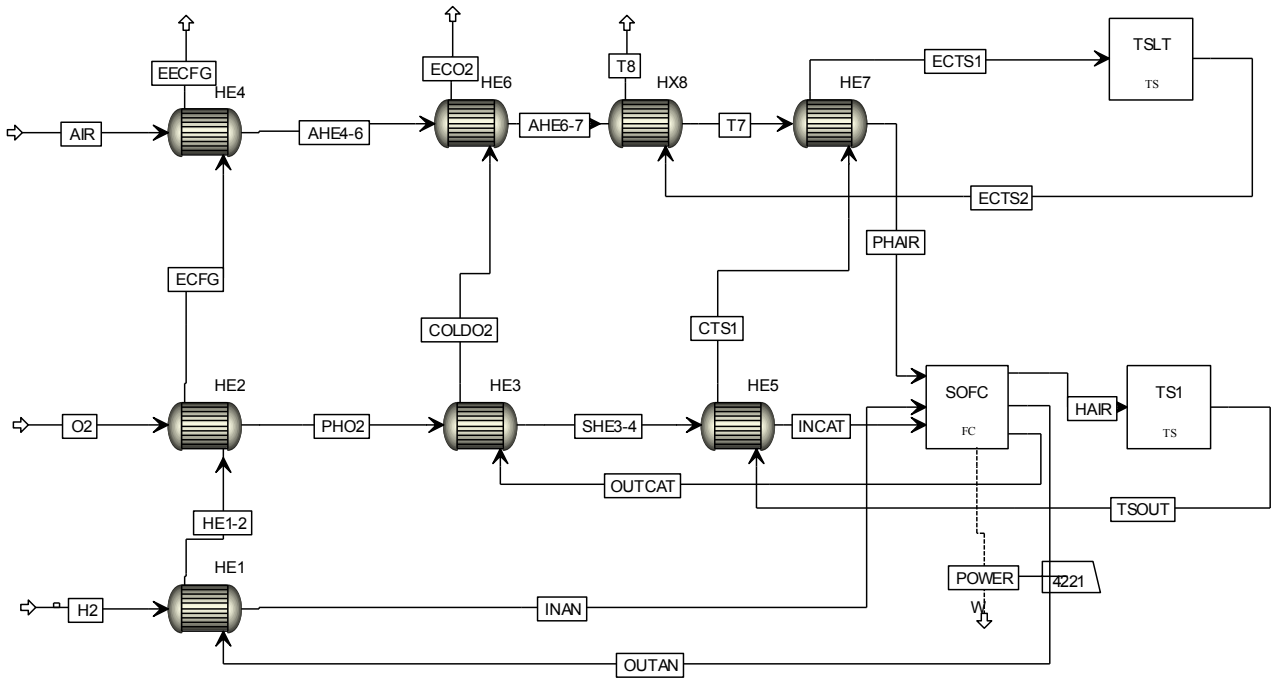

Fig. 36. Heat recovery system layout in Aspen plus^{TM} for pressurized solid oxide electrolysis cells

Table 19. Power ratios and heat ratios for pressurized solid oxide electrolysis cells

V_{ec}	r_p	r_c	$Q_{rec,LT}/Q_{req,LT}$	$Q_{rec,HT}/Q_{req,HT}$	r_t	r_{ct}	r_t no TES
1.2843	0.5764	0.6224	1.8032	2.1836	0.5730	0.6478	0.4798
1.2000	0.6886	0.7024	1.4279	1.0180	0.6844	0.6936	0.5368
1.1500	0.7630	0.7444	1.2038	0.7120	0.7041	0.7072	0.5647
1.1000	0.8441	0.7938	0.9781	0.5109	0.7187	0.7195	0.5920

Comparing results from table 16 and 19, it is possible to see an increment in power ratios. However, thermal energy ratios have decreased i.e. less thermal energy has been recovered and stored in the thermal energy storage. A decrement on thermal energy is compensated by the electric energy saved by

pressurising water instead of compressing hydrogen. However, TES make a great contribution to the power ratio, which increases from 0.4798 to 0.5730 at thermoneutral voltage and from 0.5920 to 0.7187 at 1.1 V.

3.4.1 Pressurised electrolysis with temperature drop in the cell stack

A temperature drop in the cell operating at atmospheric pressure increases the efficiency. Therefore, the same behaviour is expected operating pressurised electrolysis. In table 20, it is possible to see a decrease in the heat ratio at low temperature and an increase on the heat ratio at high temperature following the same pattern as electrolysis at atmospheric pressure. Furthermore, power ratios ($\mathbf{r_t}$ and $\mathbf{r_{ct}}$) show and increment of 5% as it was expected.

Table 20. Power ratios and heat ratios for pressurized solid oxide electrolysis cells with temperature drop

V_{ec}	r_p	r_c	$Q_{rec,LT}/Q_{req,LT}$	$Q_{rec,HT}/Q_{req,HT}$	r_t	r_{ct}	r_t no TES
1.2843	0.5764	0.6526	1.4671	2.2216	0.5730	0.6488	0.4812
1.2000	0.6886	0.6914	1.1326	1.2814	0.7168	0.6884	0.5444
1.1500	0.7630	0.7622	0.9620	0.8893	0.7406	0.7386	0.5769
1.1000	0.8441	0.8393	0.7904	0.6349	0.7629	0.7574	0.6092

In this scenario it can be clearly seen that the use of pressurised electrolysis increases the efficiency of the system up to 10% and thermal energy storage still contribute to raise the efficiency. Additionally, it shows the behaviour when a temperature drop exists.

3.5 Scenario 4: Energy from hydrogen expansion

The principle of compressed air energy storage can be applied to the hydrogen storage at high pressure. Scenario 4 intends to describe the previous system coupled with a compressed air energy storage system working with compressed hydrogen. The compressed air energy storage is based on the model described by Karellas et al. [17].

Hydrogen needs to be heated before entering the turbines. Heat required is supplied by the thermal energy storage and the exhaust gases (figure 21 stream T8) from the cell. When the heat required to raise hydrogen temperature is more than the energy contained in the exhaust gases and in the excess of heat stored, an electric heater raises hydrogen temperature. The total power generated by the system, P_{ca}, is considered as the sum of the supplied power by the fuel cell and the two turbines (TU1 and TU2)

The energy consumed to preheat hydrogen affects the heat ratio at thermoneutral voltage, which decreases from 1.4671 to 1.3797, while it does not have any effect at 1.2, 1.15 and 1.1 V. Thus, it can be concluded that thermal energy from the exhaust gases from the cell is enough to preheat hydrogen at all voltages except at thermoneutral voltage. However, an extra electric heater is not needed because the excess of heat stored at thermoneutral voltage is enough to supply the required energy to warm hydrogen.

Table 21. Power ratios and heat ratios for pressurized solid oxide electrolysis cells and compressed hydrogen

V_{ec}	r_p	r_c	$Q_{rec,LT}/Q_{req,LT}$	$Q_{rec,HT}/Q_{req,HT}$	r_t	r_{ct}	r_{ca}
1.2843	0.5764	0.6515	1.3797	2.1836	0.5730	0.6478	0.6041
1.2000	0.6886	0.6955	1.4279	1.0180	0.6844	0.6912	0.7177
1.1500	0.7630	0.7664	1.2038	0.7120	0.7041	0.7072	0.7363
1.1000	0.8442	0.8438	0.9781	0.5109	0.7187	0.7184	0.7498

When considering the energy from hydrogen expansion, power ratio increases from 0.7187 up to 0.7498 at 1.1 V and from 0.5730 up to 0.6041 at thermoneutral voltage. Even though, thermal ratio decreases at thermoneutral voltage, energy from hydrogen expansion has a similar contribution at all voltages. Comparing column r_{ct} and r_{ca} in table 21, it is possible to see that excess of heat applied to a Rankine cycle gives a better round cycle efficiency than hydrogen expansion system. Unlike thermoneutral voltage, hydrogen expansion system has a higher contribution than Rankine cycle at lower voltages.

3.6 Scenario 5: By-product Oxygen

So far, oxygen produced in electrolysis as by product is used to oxidize hydrogen in the cell. However, oxygen is a valuable by-product that is used in several industries. Moreover, energy consumption of oxygen is between 0.2 and 0.5 kW h/kgO_2 for big scale production and between 0.7 and 1 kW h/kgO_2 [18,19,45] for small production; theoretical value is 0.05 kW h/kgO_2 [45]. Therefore, considering a system, where oxygen can be stored, could generate significant energy savings. On the other hand, using air instead of oxygen to oxidize hydrogen drops the cell voltage and reduces power generation. Thus it is important to analyse the energy savings and power drops by storing oxygen.

From figure 36 and figure 38, it can be seen that heat recovery system becomes simpler since all the heat exchangers used to preheat oxygen can be removed. It is assumed a working pressure of 2 MPa and no pressure drops in the anode side in electrolysis are considered.

Table 22, 23 and 24 show the fuel cell performance operating with air and oxygen as oxidizer, respectively. As it was mentioned before, using air as oxidizer drops the voltage and power of the cell, whereas the heat recovered increases.

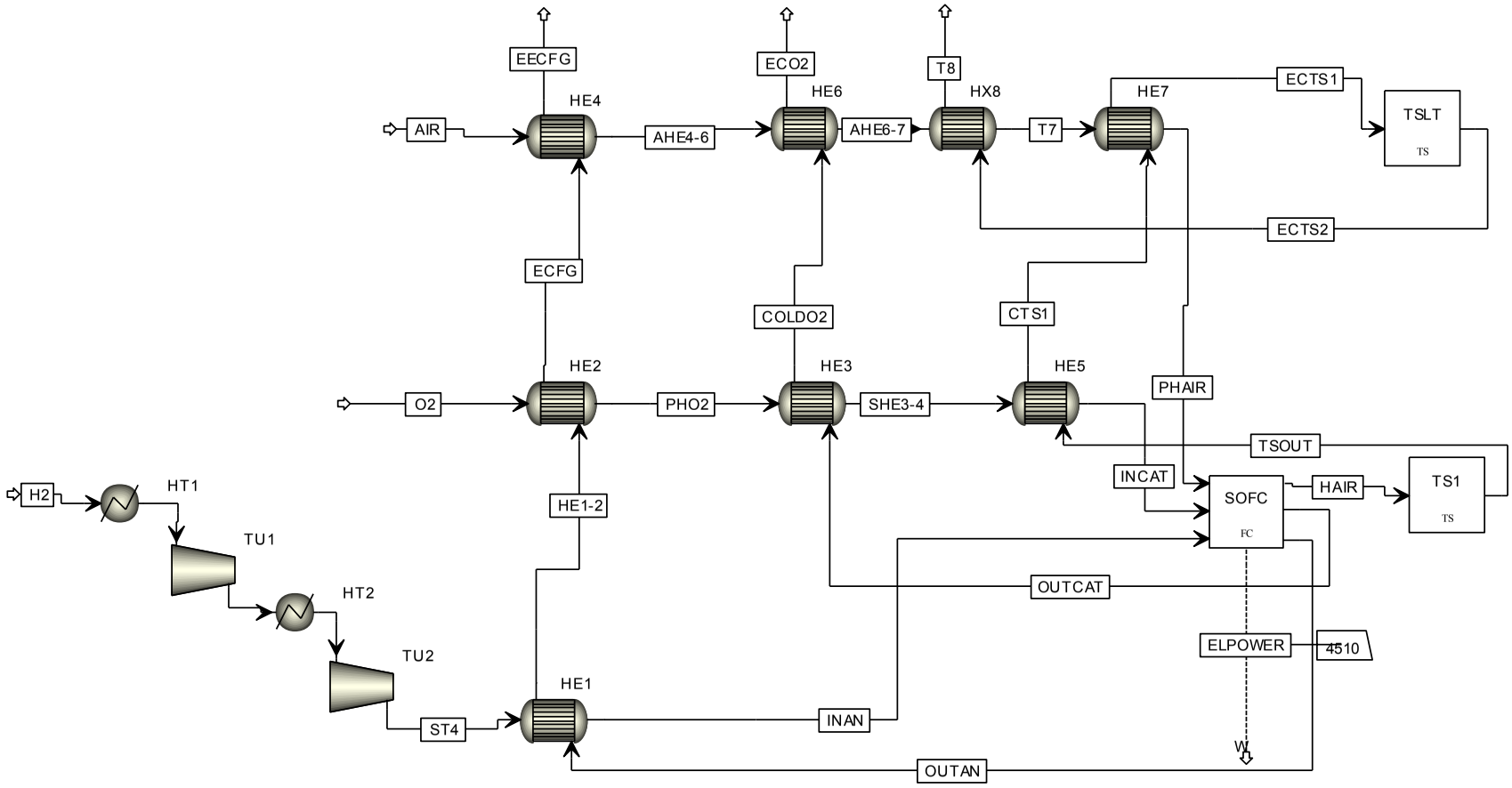

Fig. 37. Compressed hydrogen energy storage system layout in Aspen plus™

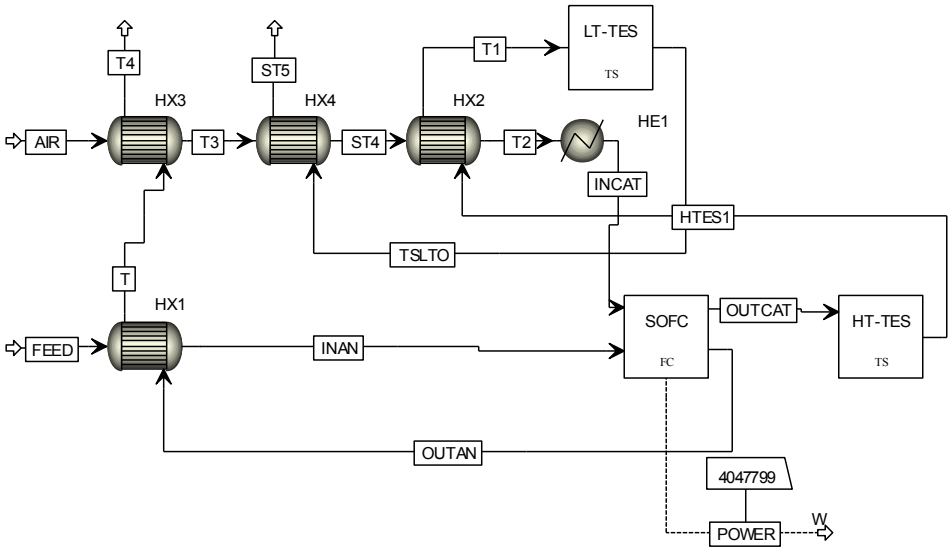

Fig. 38. Layout in Aspen plus™ for heat recovery system using air as oxidizer.

Table 22. Fuel cell performance using air as oxidizer

V_{ec} [V]	P_{fc} [kW]	V_{fc} [V]	I [a/cm^2]	HRLT [kW]	HR [kW]
1.28	2717.36	0.70	1.36	638.94	1209.44
1.20	3258.52	0.78	0.94	552.98	1098.04
1.15	3616.93	0.83	0.69	496.58	1023.73
1.10	4007.73	0.88	0.44	435.72	942.08

Table 23. Fuel cell performance using O_2 as oxidizer

V_{ec} [V]	P_{fc} [kW]	V_{fc} [V]	I [a/cm^2]	HRLT [kW]	HR [kW]
1.28	2881.75	0.73	1.36	617.86	1135.99
1.20	3443.10	0.82	0.94	522.96	1019.07
1.15	3815.05	0.87	0.69	459.69	941.01
1.10	4220.81	0.92	0.44	390.18	855.16

Table 24. Power ratios and heat ratios for pressurized solid oxide electrolysis cells using air as oxidizer

V_{ec}	r_p	r_c	$Q_{rec,LT}/Q_{req,LT}$	$Q_{rec,HT}/Q_{req,HT}$	r_t	r_{ct}
1.2843	0.5435	0.6250	1.3387	2.2808	0.5404	0.6214
1.2000	0.6517	0.6623	1.7746	1.0781	0.6581	0.6583
1.1500	0.7234	0.7284	1.3000	0.7621	0.6758	0.6805
1.1000	0.8015	0.8032	1.0919	0.5544	0.6921	0.6935

Although the ratio between the electric power released and the electric power for electrolysis at 1.1 V decreases from 0.84 to 0.80, the ratio between the electric power and the total electric power required decreases from 0.71 to 0.69. This is a consequence of the increase of the thermal energy recovered.

The required energy to produce O_2, which is between 0.1515 and 0.1571 kW h/kg O_2 is shown in table 25. The real energy cost of storing oxygen is assumed as the difference between the electric energy produced when oxygen is used as oxidant gas and the electric energy generated when air is used as oxidant gas, thus the energy per kilogram of oxygen is given by equation 56

$$E_{rO_2} = \frac{E_{fc,O_2} - E_{fc,air}}{m_{O_2}} \quad (56)$$

Where E_{O_2} is the energy per kilogram of oxygen, m_{o_2} is the oxygen produced in 12 hours [kg O_2], E_{fc,O_2} [kWh] is the total energy that could be produced using oxygen as oxidant in 12 hours and $E_{fc,air}$ is the total energy generated using air as oxidant in the fuel cell [kWh].

Table 25. Required energy for oxygen storage.

V_{ec} [V]	m_{O2} [kg O_2]	E_{rO2}[kW h/kg_{O2}]	E_r (in 12 h) [kW h]	E_r* [kW h]	E_r/E_r*
1.28	13944.77	0.1415	1972.70	6972.38	0.28
1.20	14924.04	0.1484	2214.90	7462.02	0.30
1.15	15572.91	0.1527	2377.34	7786.45	0.31
1.10	16280.77	0.1571	2556.90	8140.38	0.31

E_r* is the required energy used assuming 0.5 kW h/kg O_2 [45]

E_r represents 30% of E_r* that is the required energy to produce oxygen using conventional technologies assuming 0.5 kW h/kg O_2, thus oxygen as by-product represents around 70% energy savings justifying the cell design proposed in this work in order to keep oxygen purity.

3.7 Scenario 6: Asymmetric operation

The previous scenarios have been operated symmetrically (12 hours electrolysis cell – 12 hours fuel cell) producing and consuming hydrogen at the same rate. However, in energy markets where periods to produce or sell electricity are not even, an analysis of the system behaviour under different time of operation of both fuel cell and electrolysis cell is important.

The analysis is based on the reference system described in scenario 1. Electrolysis is operated for 12 hours and then hydrogen is consumed at different rates according to the fuel cell time of operation, which varies between 12 and 24 hours. The analysis is made at four different voltages.

Figure 39 shows the trend of the power ratio between the fuel cell and the electrolysis power at different voltages. The power ratios tend to increase as the time of operation increases, whereas the heat ratios decrease. The cause is a reduction of current density due the reduction of the consumption rate of hydrogen; the cells generate more electric power and less thermal power.

In order to avoid the use of external sources of heat, the time of operation of the fuel cell is limited by the ratio between the heat supplied by the fuel cell and the heat required for electrolysis, which has to be

higher than one. In figure 40, it is possible to observe the drop of the heat ratio at different voltages and times of operation. At 1.1 and 1.15 the time of operation cannot be longer than 13 an 14 hours. On the other hand, after 24 hours of operation, at 1.2 and 1.28 the heat ratios are still greater than 1, thus the time of operation can exceed the double of time of electrolysis operation at this voltages.

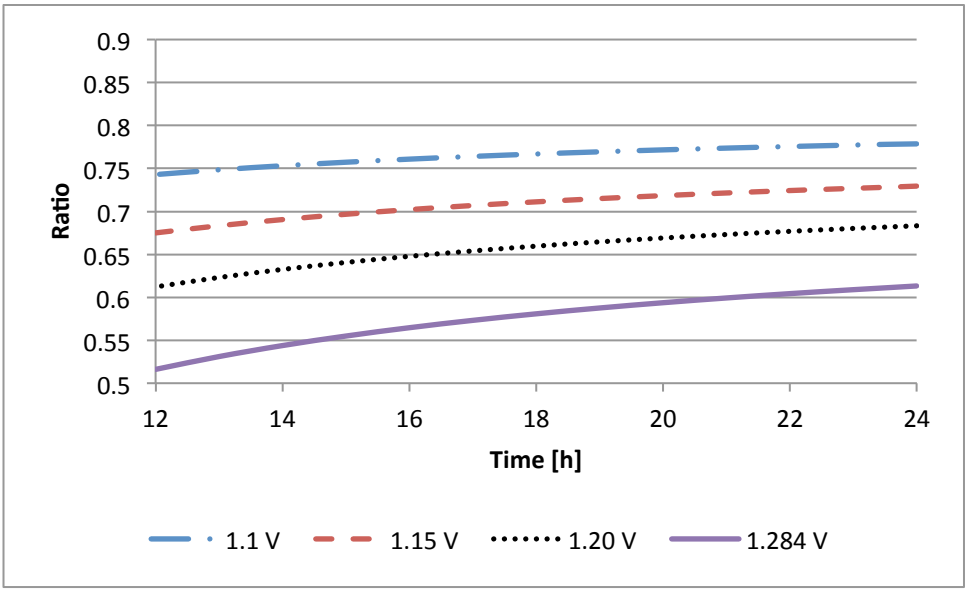

Fig. 39. r_t at different voltages and different times of operation

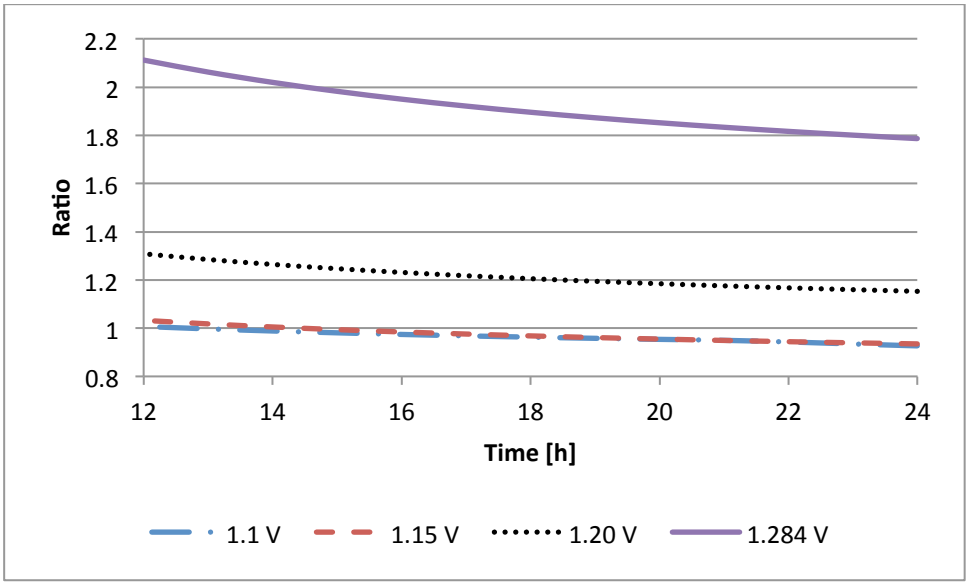

Fig. 40. r_q at different voltages and different times of operation

Different periods of operation can be applied to the system. These periods will depend on the requirements to meet. As mentioned before, one of the aims of storing energy and converted to electric power is to minimize the effects of electric power fluctuation. Figure 41 shows the wind production and net consumption in west part of Denmark on the 3rd of January 2013. From 2 am to 6 in the morning, wind

power production was higher than the net consumption. The next 18 hours consumption was higher than wind production. Following the same pattern, figure 42 shows the performance of the reference system.

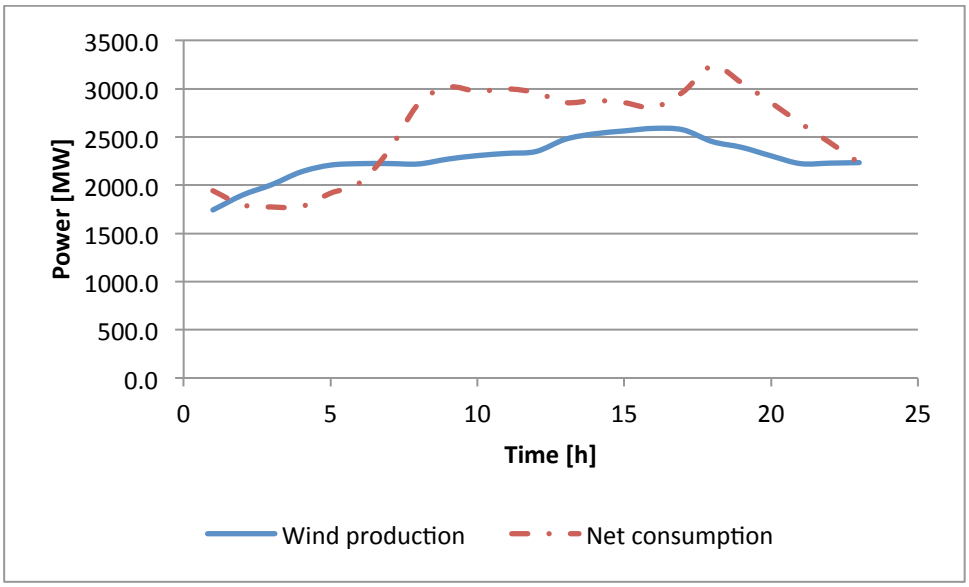

Fig. 41. Wind production and net consumption in west part of Denmark on the 3rd of January 2013

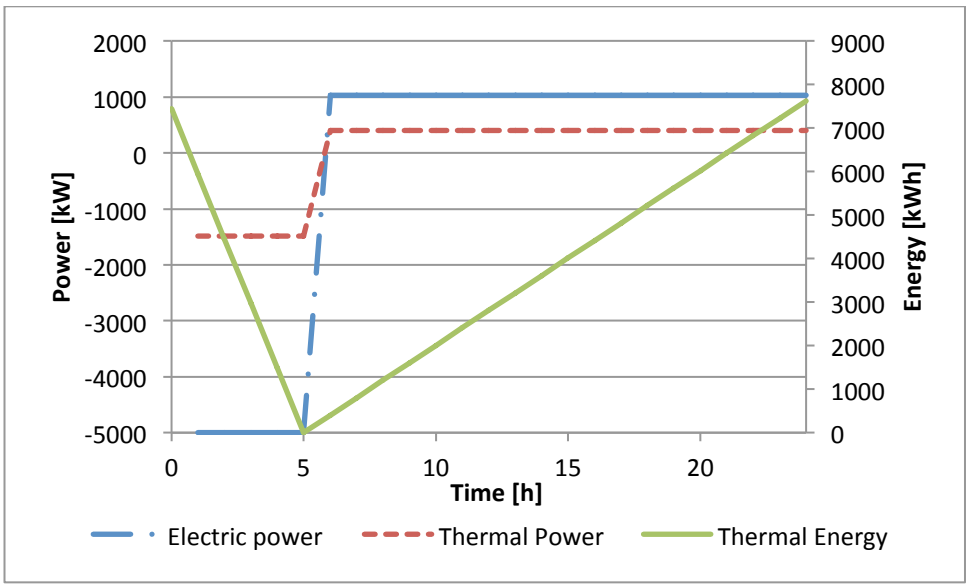

Fig. 42. Power and energy in 5 h electrolysis 19 h fuel cell at 1.2 V

In five hours, the supplied electric energy is 25 MWh and supplied thermal energy is 7.44 MWh for electrolysis. In 19 hours, the electric energy generated is 19.6 MWh and the thermal energy recovered is 7.6MWh. Power ratio at the end of 24 hours is 0.7838 and heat ratio is 1.0253. From table 12, it can be seen an increment on the power ratio of 0.0952 while heat ratio decreases 0.8307.

The last scenario shows the advantages of operating the system with electrolysis periods shorter than fuel cell periods. Extending fuel cell periods the cells operate with higher electric efficiency.

4 Conclusions and further work

4.1 Conclusions

Hydrogen storage and high temperature electrolysis are feasible options to deal with energy fluctuation, energy over production and energy shortcomings caused by the penetration of renewables energies. Efficiency of these technologies can be increased if they are combined with solid oxide cell and thermal energy storage. High temperature electrolysis is an attractive technology to couple with renewable energy sources like photovoltaic and wind power. On the other hand, hydrogen, as energy carrier, represents an alternative option with a lot of flexibility. It can be used directly in many applications like burners, fuel cells or used to generate other fuels like syngas or liquid fuels.

Phase change materials as thermal energy storage are a feasible option to store heat released by the fuel cell and use it for further electrolysis process. The wide range of PCM allows storing thermal energy at different temperatures, giving to the system more flexibility on the operating conditions.

The model in the present work shows similar results in electrolysis and fuel cell performance with previous studies. With the same electric input, the reference system produces 31 kg of H_2, while the model in the present work produces 33 and 34 kg of H_2 with similar efficiencies. Electrolysis system shows the highest efficiency at 1.284 V and 90% of steam utilization. Thermal energy stored represents 27.1 % of the total energy released by the fuel cell, which is less than the mentioned in the reference studies.

Electric power input affects directly the current density in the cell, thus the operating voltage of electrolysis. Heat ratio is sensible to the current density, air temperature at the inlet of the cell and the operating temperature threshold in the thermal storage. The best air temperature was found to be 973.15 K and the maximum heat ratio is when TES are cooled to ambient temperature.

Round cycle efficiency of the system is highly improved with the inclusion of a PCM. It could increase from 0.444 to 0.74 and when it is compared with similar systems with efficiencies around 0.29 represents an important progress. However, implementation of only LT-TES does not increase significantly the round cycle efficiency because the required energy to generate steam represents less than 10% of the total energy input. When a temperature drop is considered in the cell stack, the energy to generate steam increases around 5% and thermal energy required at high temperatures decreases at the same ratio. Therefore, it is still convenient to have HT-TES to store heat that could be used to preheat the cold streams to the operating temperature.

From different evaluated configurations, the system that considers a pressurized electrolysis process represents the most efficient system due the reduction in the energy consumed by the compressors. On the other hand, the system that considers a burner instead of recirculation system of hydrogen was the less efficient. Even though the high temperature heat ratio increased, power production decreases considerably.

Adding parallel systems that use excess of heat or hydrogen expansion to generate more electric power increases the round cycle efficiency between 2 to 10%, depending on the system. However, these systems should be evaluated economically in order to justify their implementation.

After analysing the use of oxygen or air as oxidizer in the cell, it can be concluded that storing oxygen can generate significant energy savings that compensate the power losses and represents a good alternative of oxygen as by-product.

Operation periods proved to be an important parameter that can easily be modify in order to increase efficiency. The same system working 12 hours as electrolysis at 1.2 V and 12 h as fuel cell showed a power ratio of 0.6886, whereas working 5 hours as electrolysis at 1.2 V and 19 h as fuel cell showed a power ratio of 0.7838 showing better heat management.

In general, a model capable to predict accurately and realistic the energy flows and efficiencies in different scenarios has been developed. It has shown the advantages of using solid oxide cells as electrolysis and fuel cells, adding thermal energy storages to recover heat produced by the fuel cell for further use in high temperature electrolysis. It has also shown the importance of the operation periods, moreover it has proved that the system described in the present work can be a feasible solution to deal with energy fluctuation, energy over production and energy shortcomings caused by the penetration of renewables energies because it shows higher efficiencies than current systems.

4.2 Further work

Many assumptions have been done in the present work and could lead to an over estimation of the results. For this reason, it is important to list some of the opportunity areas where a more detailed work could bring better results:

- The present work uses a constant value of ASR and does not take in consideration cell degradation for using the same cell as electrolysis and fuel cell. Therefore, a more detailed study of the effects of using the same solid oxide cell as electrolysis and fuel cell on the cell quality could improve results.
- Heat transfer across the cell boundaries exists but it is not considered in the present work. A detailed temperature and heat transfer profile inside the cell module will help to get better estimation of heat losses.
- Renewable energy sources do not behave as steady state system, so the adjustment of the present work to transient systems will increase the accuracy of the system.
- Some scenarios presented in this work can increase the efficiency but an economic evaluation of the systems will justify their implementation in the energy market.

References

[1] D. Connolly , H. Lund , B.V. Mathiesen , E. Pican , and M. Leahy , "The technical and economic implications of integrating fluctuating renewable energy using energy storage ," *Renewable Energy* , vol. 43, pp. 47-60 , 2012.

[2] Hamidreza Zareipour, Marc Beaudin, Anthony Schellenberglabe, and William Rosehart, "Energy storage for mitigating the variability of renewable electricity sources: An updated review," *Energy for Sustainable Development*, vol. 14, pp. 302-314, 2010.

[3] Haisheng Chen, Thang Ngoc Cong, and Wei Yang, "Progress in electrical energy storage system: A critical review," *Progress in Natural Science* , vol. 19, pp. 291–312, 2009.

[4] Susan M. Schoenung, "Characteristics and Technologies for Long-vs. Short-Term Energy Storage: A study by the DOE Energy Storage Systems Program." Sandia National Laboratories, Albuquerque, New Mexico, USA, SAND2001-0765, 2001.

[5] Mingyong Wang, Zhi Wang, Xuzhong Gong, and Zhancheng Guo, "The intensification technologies to water electrolysis for hydrogen production – A review," *Renewable and Sustainable Energy Reviews*, vol. 29 , pp. 573–588 , 2014.

[6] A Djafour et al., "Photovoltaic-assisted alkaline water electrolysis: Basic principles ," *International Journal of Hydrogen Energy*, vol. 36 , pp. 4117–4124, 2011.

[7] Frano Barbir , "PEM electrolysis for production of hydrogen from renewable energy sources ," *Solar energy*, vol. 78 , pp. 661–669 , 2005.

[8] R.J. Braun, W.L. Becker, M. Penev, and M. Melaina, "Production of FischereTropsch liquid fuels from high temperature solid oxide co-electrolysis units," *Energy*, vol. 47, pp. 99-115, 2012.

[9] Youngjoon Shin, Wonseok Park, Jonghwa Chang, and Jongkuen Park, "Evaluation of the high temperature electrolysis of steam to produce hydrogen," *International Journal of Hydrogen Energy*, vol. 32, pp. 1486 – 1491, 2007.

[10] Christine Mansilla, Jon Sigurvinsson, Andre´ Bontemps, Alain Mare´chal, and Francois Werkoff, "Heat management for hydrogen production by high temperature steam electrolysis," *Energy*, vol. 32, pp. 423–430, 2007.

[11] Floriane Petipas, Annabelle Brisse, and Chakib Bouallou, "Model-based behaviour of a high temperature electrolyser system operated at various loads," *Journal of Power Sources*, vol. 239, pp. 584-595, 2013.

[12] S.D. Sharma and Kazunobu Sagara, "Latent heat storage materials and systems: a review," *International Journal of Green Energy*, vol. 2, pp. 1–56, 2005.

[13] F. Handan Tezel and Daniel Dicaire, "Regeneration and efficiency characterization of hybrid adsorbent for thermal energy storage of excess and solar heat," *Renewable Energy*, vol. 36, pp. 986-992, 2011.

[14] Marc A. Rosen and Ali H. Abedin, "A Critical Review of Thermochemical Energy Storage Systems," *The Open Renewable Energy Journal*, vol. 4, pp. 42-46, 2011.

[15] K Agbossou, R. Chahine, and J. Hamelin, "Renewable energy systems based on hydrogen for remote applications," *Journal of Power Sources*, vol. 96, no. 1, pp. 168–172, 2001.

[16] Beatriz Escobar, José Hernández, and Romeli Barbosa, "Analytical model as a tool for the sizing of a hydrogen production system based on renewable energy: The Mexican Caribbean as a case of study," *Journal of Hydrogen Energy*, 2012.

[17] S. Karellas and N. Tzouganatos, "Comparison of the performance of compressed air and hydrogen energy storage systems: Karpathos island case study," *Renewable and Sustainable Energy Reviews*, vol. 29, pp. 865–882, 2014.

[18] Paolo Iora and Paolo Chiesa, "High efficiency process for the production of pure oxygen based on solid oxide fuel cell solid oxide electrolyzer technology," *Journal of Power Sources*, vol. 190, pp. 408–416, 2009.

[19] P. Iora, M.A.A. Taher, P. Chiesa, and N.P. Brandon, "A one dimensional solid oxide electrolyzer fuelcel lstack model and its application to the analysis of a high efficiency system for oxygen production," *Chemical Engineering Science*, vol. 20, pp. 293–305, 2012.

[20] EG&G Technical Services, Inc., *Fuel Cell Handbook*. Morgantown, West Virginia: U.S. Department of Energy, 2004.

[21] Nguyen Quang Minh and Takehiko Takahashi , *Science and Technology of Ceramic Fuel Cells*. Amsterdam: Elsevier, 1995.

[22] Domenico Ferrero, Andrea Lanzin, and Massimo Santarel, "A comparative assessment on hydrogen production from low- and high-temperature electrolysis," *International Journal of Hydrogen Energy*, no. 38, pp. 3523-3536, 2013.

[23] Xiongwen Zhanga, S.H. Chanb, Guojun Li, and H.K. Hob, "A review of integration strategies for solid oxide fuel cells," *Journal of Power Sources*, vol. 195, pp. 685–702, 2010.

[24] Vincenzo Liso, Yingru Zhao, Nigel Brandon, Mads Pagh Nielsen, and Søren Knudsen Kær, "Analysis of the impact of heat-to-power ratio for a SOFC based mCHP system for residential application," *International Journal of Hydrogen*, vol. 36, pp. 13715-13726, 2011.

[25] Pilar Lisbona, Alessandro Corradetti, Roberto Bove, and Piero Lunghi, "Analysis of a solid oxide fuel cell system for combined heat and power applications under non-nominal conditions," *Electrochimica Acta*, vol. 53, pp. 1920–1930, 2007.

[26] Patrick Lovera, Franck Blein, and Julien Vulliet. (2006, June) Association Algérienne de l'Hydrogène. [Online]. http://www.cder.dz/A2H2/Medias/Download/Proc%20PDF/PARALLEL%20SESSIONS/%5BS05%5D%20Production%20-%20Water%20Electrolysis/15-06-06/356.pdf

[27] Randall S. Gemmena, Mark C. Williams, and Kirk Gerdesc, "Degradation measurement and analysis for cells and stacks," *Journal of Power Sources* , vol. 184, pp. 251–259, 2008.

[28] James O'Brien, Xiaoyu Zhang, and Robert C. O'Brien, "Improved durability of SOEC stacks for high temperature electrolysis," *International Journal of Hydrogen Energy*, vol. 38, pp. 20-28, 2013.

[29] Yunus Çengel and Michael A. Boles, *Thermodynamics an engineering approach*.: McGraw Hill, 2000.

[30] Patrice Pinel, Cynthia A. Cruickshank, and Ian Beauso, "A review of available methods for seasonal storage of solar thermal energy in residential applications.," *Renewable and Sustainable Energy Reviews*, vol. 15, pp. 3341– 3359, 2011.

[31] Belén Zalba, José Ma. Marín, and Luisa F. Cabeza, "Review on thermal energy storage with phase change: materials, heat transfer analysis and applications," *Applied Thermal Engineering*, no. 23, pp. 251-283, 2003.

[32] Atul Sharma, Atul Tyagi, C.R. Chen, and D. Buddhi, "Review on thermal energy storage with phase change materials and applications," *Renewable and Sustainable Energy Reviews*, no. 13, pp. 318-345, 2009.

[33] Francis Agyenim, Neil Hewitt, and Philip Eames , "A review of materials, heat transfer and phase change problem formulation for latent heat thermal energy storage systems (LHTESS)," *Renewable and Sustainable Energy Reviews*, vol. 14, pp. 615–628, 2010.

[34] Pablo Dolado, Javier Mazo, Ana Lázaro, José María Marín, and Belén Zalba, "Experimental validation of a theoretical model: Uncertainty propagation analysis to a PCM-air thermal energy storage unit," *Energy and Buildings*, vol. 45, pp. 124–131, 2012.

[35] N. Gokon , D. Nakano, S. Inuta , and T. Kodama, "High-temperature carbonate/MgO composite materials as thermal storage media for double-walled solar reformer tubes," *Solar Energy*, vol. 82, pp. 1145–1153, 2008.

[36] Nobuyuki Gokon, Shin-ichi Inuta, Shingo Yamash, Tsuyoshi Hatamachic, and Tatsuya Kodama, "Double-walled reformer tubes using high-temperature thermal storage of molten-salt/MgO composite for solar cavity-type reformer," *International Journal of Hydrogen Energy*, vol. 34, pp. 7143 - 7154, 2009.

[37] D. Sánchez, A. Muñoz, and T. Sánchez, "An assessment on convective and radiative heat transfer modelling in tubular solid oxide fuel cells," *Journal of Power Sources*, vol. 169, no. 1, pp. 25-34, 2007.

[38] Yingru Zhao , Nilay Shah , and Nigel Brandon, "Comparison between two optimization strategies for solid oxide fuel cellegas turbine hybrid cycles," *International Journal of Hydrogen Energy*, vol. 36, pp. 10235-10246, 2011.

[39] Bureau of Energy Efficiency. Syllabus For Energy Manager/Auditors. [Online]. http://www.enercon.gov.pk/images/pdf/2ch5.pdf

[40] Tata D.N.Nandi, *Handbook on Refractories*. New Delhi: McGraw Hill, 1987.

[41] Sriram Gopalan, Mohsen Mosleh, Joseph J. Hartvigsen, and Robert D. McConnell, "Analysis of self-sustaining recuperative solid oxide electrolysis systems," *Journal of Power Sources*, vol. 185, pp. 1328–1333, 2008.

[42] Masoud Rokni, "Thermodynamic analysis of an integrated solid oxide fuel cell cycle with a rankine cycle," *Energy Conversion and Management*, vol. 51, pp. 2724–2732, 2010.

[43] Xiufu Sun et al., "Thermodynamic analysis of synthetic hydrocarbon fuel production in pressurized solid oxide electrolysis cells," *International Journal of Hydrogen Energy*, vol. 37, pp. 17101-17110, 2012.

[44] Jan H.S.J. Thijssen, "The impact of Scale-Up and production volume on SOFC Manufacturin Cost," National Energy Technology Laboratory, Redmond, Washington, USA, publication, 2007.

[45] Takeyoshi Kato, Mitsuhiro Kubota, Noriyuki Kobayashi, and Yasuo Suzuoki, "Effective utilization of by-product oxygen from electrolysis hydrogen production," *Energy*, vol. 30 , pp. 2580–2595, 2005.

Appendix A: Fortran code

A.1 Solid oxide electrolyser cell

The electrolysis submodel solves the energy balance and mass balance. When the electrolysis process is isothermal, air mass is calculated to balance the energy. When the process is not isothermal and variations of temperature exists, the model calculates the operational voltage at the output temperature T_{out} and iterates this calculation until the operating voltage is equal to the cell voltage. Figure 43 shows the flowchart for the electrolysis submodel.

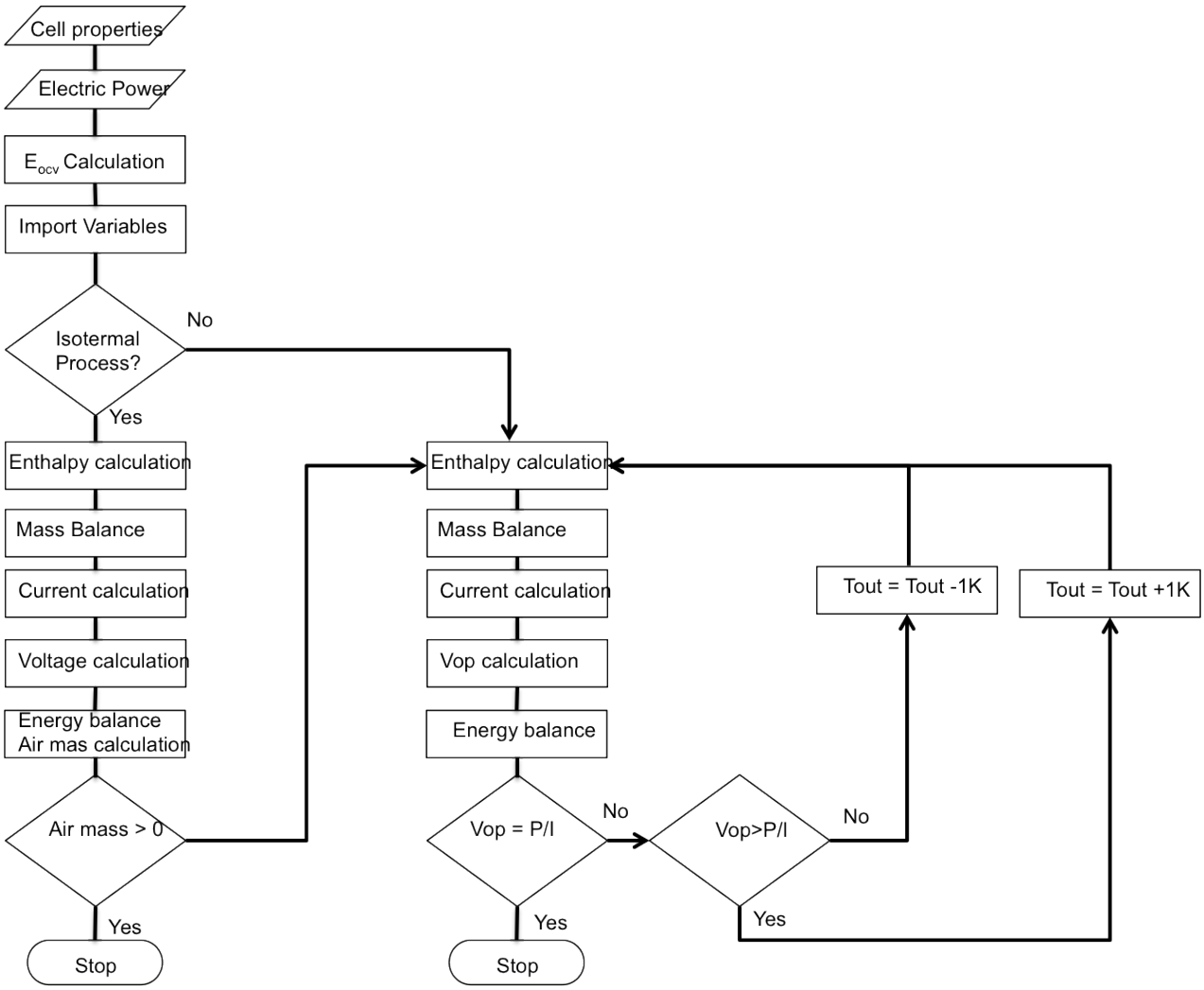

Fig. 43. Solid oxide electrolyser cell flow chart

Open circuit voltage and partial fraction of the components are calculated in Aspen plus™ interface. The calculation are done with the following FORTRAN code:

CALCULATOR C1

Defined Variable	Path
NH2O	Block-Var Block=SOEC Variable=REAL-VAR Sentence=REAL Element=15
NIH2O	Stream-Var Stream=FEED Substream=MIXED Variable=MOLE-FLOW Units=kmol/sec
SR	Block-Var Block=SOEC Variable=REAL-VAR Sentence=REAL Element=4
SU	Block-Var Block=SOEC Variable=REAL-VAR Sentence=REAL Element=1
X1H2	Mole-Frac Stream=FEED Substream=MIXED Component=HYDROGEN
X2H2	Mole-Frac Stream=CATHODE Substream=MIXED Component=HYDROGEN
XAH2	Local-Param
X1H2O	Mole-Frac Stream=FEED Substream=MIXED Component=WATER
X2H2O	Mole-Frac Stream=CATHODE Substream=MIXED Component=WATER
XAH2O	Local-Param
X1O2	Mole-Frac Stream=FEED Substream=MIXED Component=OXYGEN
X2O2	Mole-Frac Stream=O Substream=MIXED Component=OXYGEN
XAO2	Local-Param
T	Local-Param Physical type=Temperature- Units=K Initial value=1000
MFAIR	Block-Var Block=SOEC Variable=REAL-VAR Sentence=REAL Element=17
AIRIN	Stream-Var Stream=AIR Substream=MIXED Variable=MOLE-FLOW Units=kmol/sec
MODE	Block-Var Block=SOEC Variable=REAL-VAR Sentence=REAL Element=8
EN	Block-Var Block=SOEC Variable=REAL-VAR Sentence=REAL Element=9
TI	Stream-Var Stream=HFEED Substream=MIXED Variable=TEMP Units=K
TO	Stream-Var Stream=H2 Substream=MIXED Variable=TEMP Units=K
DG	Local-Param
EO	Local-Param

```
NIH2O=NH2O/SU
NIH2O = NIH2O/(1-SR
T=(TI+TO)/2
DG=244800-49.18*T-0.00272*T**2
EO = DG/(2*96485)

XAH2=(X1H2+X2H2)/2
XAH2O=(X1H2O+X2H2O)/2
XAO2=(X1O2+X2O2)/2
X=XAH2O/(XAH2*(XAO2**(0.5)))
EN=EO+(8.314*T*log(X)/(2*96485))

IF (MODE .EQ. 1) THEN
   AIRIN=MFAIR
END IF
```

Energy balance, mass balance, current and voltage calculations are done in a subroutine called by Aspen plus™ named SOEC.f

SOEC.f code

```
C$ #1 BY:Rafael Cuellar jun 2013
C
C    User Unit Operation Model (or Report) Subroutine for USER2
C
     SUBROUTINE SOEC (NMATI,  SIN,    NINFI,   SINFI,  NMATO,
    2                 SOUT,   NINFO,  SINFO,   IDSMI,  IDSII,
    3                 IDSMO,  IDSIO,  NTOT,    NSUBS,  IDXSUB,
    4                 ITYPE,  NINT,   INT,     NREAL,  REAL,
    5                 IDS,    NPO,    NBOPST,  NIWORK, IWORK,
    6                 NWORK,  WORK,   NSIZE,   SIZE,   INTSIZ,
    7                 LD   )
C
     IMPLICIT NONE
C
C    DECLARE VARIABLES USED IN DIMENSIONING
C
     INTEGER NMATI, NINFI, NMATO, NINFO, NTOT,
    +        NSUBS, NINT,  NPO,   NIWORK,NWORK,
    +        NSIZE
C
#include "ppexec_user.cmn"
#include "dms_plex.cmn"
     Real*8 B(1)
     Equivalence (B(1),IB(1))
C
C
C
#include "dms_ncomp.cmn"
C
C    THIS SUBROUTINE WILL SEPARATE WATER INTO THE SECOND OUTLET
C
C    FIRST COPY FIRST INLET TO FIRST OUTLET
C
C
C    DECLARE ARGUMENTS
C
     INTEGER IDSMI(2,NMATI),      IDSII(2,NINFI),
    +        IDSMO(2,NMATO),      IDSIO(2,NINFO),
    +        IDXSUB(NSUBS),ITYPE(NSUBS), INT(NINT),
```

```
     +       IDS(2,3),     NBOPST(6,NPO),
     +       IWORK(NIWORK),INTSIZ(NSIZE),NREAL, LD
      INTEGER KH2O
      REAL*8 SIN(NTOT,NMATI),     SINFI(NINFI),
     +      SOUT(NTOT,NMATO),    SINFO(NINFO),
     +      WORK(NWORK),  SIZE(NSIZE), REAL (NREAL)

C
C     DECLARE LOCAL VARIABLES
C
      INTEGER OFFSET, IERR, LDATA, KDIAG, IDX(10), NCP,
     +       INDEX, LMW, IFAIL, KBASE, KH, KER, C, SN
      REAL*8  SU, TOUT, AR, SR, AS, NC, HFOUT(NMATO), X(10), FLOW,
     +       HMXI(NMATO), DHMX, QS, MF, HFIN(NMATO), P, PHIO(NMATO),
     +       HO(NCOMP_NCC),SO(NMATO), GO(NMATO), VO(NMATO),DPHI, DH,
     +       DS,DG,DV, HA(NCOMP_NCC), V, MFH2OI, MFAIR, HH2I, HH2O,
     +       HH2OI, HH2OO, HO2I, HO2O, HAIRI, HAIRO, F, ASR, TA, QL,En,
     +       J, Vop, GC, MFH2I, MODE, I, E


C     DECLARE FUNCTIONS

      INTEGER USRUTL_GET_REAL_PARAM,  ! These functions allow access to real
     +       USRUTL_GET_INT_PARAM,   ! and integer parameters using named
     +       USRUTL_SET_REAL_PARAM   ! references, and to write results data
                                     ! to Aspen Plus.
      INTEGER DMS_IFCMNC  !Determines offset to universal constant data.

      REAL*8  DLOG        !Standard Fortran function.

C
C     BEGIN EXECUTABLE CODE
C     Get configured REAL variables from Aspen Plus REAL PARAMETERS

      IFAIL = 0
      INDEX = 0
      SU = REAL(1)
      TOUT = REAL(2)
      ASR = REAL(3)
      SR = REAL(4)
      AS = REAL(5)
      NC = REAL(6)
      QL = REAL(7)
```

```
      MODE = REAL(8)        !0 TO CALCULATE TEMPERATURE IN AN ADIABATIC SYSTEM
                            !1 TO CALCULATE THE HEAT REQUIRED IN AN ISOTHERMAL SYSTEM

      P = SINFI(1)          !ELECTRIC POWER INPUT [W
      F = 96485             !FARADAY'S CONSTANT
      E=REAL(9)
      IF (E .GT. 1.5) THEN
        E=0.998
      END IF

      IF (E .LT. 0.8) THEN
        E=0.998
      END IF
      En = E            !Nernst Voltage, Open circuit Voltage

C     Calculate Enthalpy IN

      IF (MODE .EQ. 0) THEN
      DO 1 GC = 1, 20000
        IF (SIN(2,1) .EQ. 0) THEN
          SIN(2,1) = 0.00001
          SIN(NCOMP_NCC+2,1)=1000
          SIN(NCOMP_NCC+3,1)=101325
        END IF

      DO 10 C=1,NMATI
        CALL SHS_CPACK      (SIN(1,C), NCP, IDX, X, FLOW)
        KDIAG = 4
        KBASE = 1
        KH = 1


        CALL PPMON_ENTHV    (SIN(NCOMP_NCC+2,C),SIN(NCOMP_NCC+3,C), X,
     +                  NCP, IDX, NBOPST, KDIAG, KBASE, KH,
     +                  HMXI(C), DHMX,KER)


10    CONTINUE

      HH2OI = HMXI(1)           !ENTHALPY [J/KMOL]
      HAIRI = HMXI(2)           !ENTHALPY [J/KMOL]
      MFH2OI = SIN(NCOMP_NC+1,1)  !MOLE FLOW [KMOL/SEC]
```

```
      MFAIR = SIN(NCOMP_NC+1,2)  !MOLE FLOW [KMOL/SEC]

C     MODEL REACTIONS

      SOUT(1,1) = SIN(2,1)*SU+SIN(1,1)
      SOUT(2,2) = SIN(2,1)*(1-SU)
      SOUT(1,3) = 0
      SOUT(2,3) = 0
      SOUT(3,3) = 0.5*SIN(2,1)*SU
      SOUT(3,4) = SIN(3,2)
      SOUT(4,4) = SIN(4,2)

C     FILL SOUT ARRAY

        DO 200 SN = 1, NMATO
           SOUT(NCOMP_NCC+3,SN) = SIN(NCOMP_NCC+3,SN)
           SOUT(NCOMP_NCC+2,SN)= TOUT
200        CONTINUE

C     ENTHALPY OUT CALCULATIONS [J/KMOL]

DO 400 C=1,NCOMP_NCC
           CALL SHS_CPACK      (SOUT(1,C), NCP, IDX, X, FLOW)
           KDIAG = 4
           KBASE = 1

        CALL PPMON_ENTHV    (SOUT(NCOMP_NCC+2,C),SOUT(NCOMP_NCC+3,C),
     +                  X, NCP, IDX, NBOPST, KDIAG, KBASE, KH,
     +                  HO(C), DHMX,KER)

           HA(C)=HO(C)

400        CONTINUE
      HH2O = HO(1)    !ENTHALPY OUT [J/KMOL]
      HH2OO = HO(2)   !ENTHALPY OUT [J/KMOL]
      HO2O = HO(3)    !ENTHALPY OUT [J/KMOL]
      HAIRO = HO(4)   !ENTHALPY OUT [J/KMOL]
C     ENERGY BALANCE AND STEAM INPUT CALCULATION

      J=(-En/(2*ASR))+((P/NC)/(AS*ASR)+(EN/(2*ASR))**2)**(0.5)
      TA=(1+SR/(SU*(1-SR)))*HH2O+0.5*HO2O+(1-SU)*(HH2OO/SU)
      TA=TA-(HH2OI*(1/(SU*(1-SR))))
      MFH2I = (P+MFAIR*HAIRI-MFAIR*HAIRO-QL)
```

```
      MFH2I = MFH2I/TA

C     VOLTAGE CALCULATION

      I =2*F*MFH2I*1000
      V = P/I
      Vop = En + J*ASR

      IF (Vop .LT. V) THEN
        IF (V-Vop .GT. 0.0001 ) THEN
        TOUT = TOUT-0.1
        END IF
        IF (V-Vop .LE. 0.0001) EXIT
      END IF

      IF (Vop .GT. V) THEN
        IF (Vop-V .GT. 0.0001) THEN
        TOUT = TOUT+0.1
        END IF
        IF (Vop-V .LE. 0.0001) EXIT
      END IF

1     CONTINUE

C     SETTING VALUES AS OUTPUT PARAMETERS

      REAL(10) = TA
      REAL(11) = TOUT
      REAL(12) = GC
      REAL(13) = J
      REAL(14) = Vop
      REAL(15) = MFH2I
      REAL(16) = V
END IF

C     CALCULATING THE HEAT INPUT



      IF (MODE .EQ. 1) THEN
        IF (SIN(2,1) .EQ. 0) THEN
          SIN(2,1) = 0.00001
          SIN(NCOMP_NCC+2,1)=1000
```

```
          SIN(NCOMP_NCC+3,1)=101325
        END IF

      DO 101 C=1,NMATI
        CALL SHS_CPACK      (SIN(1,C), NCP, IDX, X, FLOW)
        KDIAG = 4
        KBASE = 1
        KH = 1

        CALL PPMON_ENTHV    (SIN(NCOMP_NCC+2,C),SIN(NCOMP_NCC+3,C), X,
     +                  NCP, IDX, NBOPST, KDIAG, KBASE, KH,
     +                  HMXI(C), DHMX,KER)

101    CONTINUE

      HH2OI = HMXI(1)           !ENTHALPY [J/KMOL]
      HAIRI = HMXI(2)           !ENTHALPY [J/KMOL]
      MFH2OI = SIN(NCOMP_NC+1,1)  !MOLE FLOW [KMOL/SEC]
      MFAIR = SIN(NCOMP_NC+1,2)  !MOLE FLOW [KMOL/SEC]

C     MODEL REACTIONS

      SOUT(1,1) = SIN(2,1)*SU+SIN(1,1)
      SOUT(2,2) = SIN(2,1)*(1-SU)
      SOUT(1,3) = 0
      SOUT(2,3) = 0
      SOUT(3,3) = 0.5*SIN(2,1)*SU
      SOUT(3,4) = SIN(3,2)
      SOUT(4,4) = SIN(4,2)

C     FILL SOUT ARRAY

        DO 2001 SN = 1, NMATO
           SOUT(NCOMP_NCC+3,SN) = SIN(NCOMP_NCC+3,1)
           SOUT(NCOMP_NCC+2,SN)= TOUT
2001       CONTINUE
      SOUT(NCOMP_NCC+3,4) = SIN(NCOMP_NCC+3,2)
C     ENTHALPY OUT CALCULATIONS [J/KMOL]

        DO 4001 C=1,NCOMP_NCC
          CALL SHS_CPACK      (SOUT(1,C), NCP, IDX, X, FLOW)
          KDIAG = 4
          KBASE = 1
```

```
      CALL PPMON_ENTHV    (SOUT(NCOMP_NCC+2,C),SOUT(NCOMP_NCC+3,C),
     +                  X, NCP, IDX, NBOPST, KDIAG, KBASE, KH,
     +                  HO(C), DHMX,KER)


        HA(C)=HO(C)

4001     CONTINUE
    HH2O = HO(1)    !ENTHALPY OUT [J/KMOL]
    HH2OO = HO(2)   !ENTHALPY OUT [J/KMOL]
    HO2O = HO(3)    !ENTHALPY OUT [J/KMOL]
    HAIRO = HO(4)   !ENTHALPY OUT [J/KMOL]

C    ENERGY BALANCE AND STEAM HEAT INPUT CALCULATION

    J=(-En/(2*ASR))+((P/NC)/(AS*ASR)+(EN/(2*ASR))**2)**(0.5)
    MFH2I=J*NC*AS/(2*F*1000)

    TA=(1+SR/(SU*(1-SR)))*HH2O+0.5*HO2O+(1-SU)*(HH2OO/SU)
    TA=TA-(HH2OI*(1/(SU*(1-SR))))

    MFAIR = P-MFH2I*TA-QL
    MFAIR = MFAIR/(-HAIRI+HAIRO)

C    CALCULATING CELL VOLTAGE
    TA = NC*AS
    I =2*F*MFH2I*1000
    V = P/I
    Vop = En + J*ASR

    IF (MFAIR .LE. 0) THEN

      DO 500 GC = 1,10000
      MFAIR = 0.0000001

          DO 300 SN = 1, NMATO
            SOUT(NCOMP_NCC+3,SN) = SIN(NCOMP_NCC+3,SN)
            SOUT(NCOMP_NCC+2,SN)= TOUT
300         CONTINUE

          DO 600 C=1,NCOMP_NCC
```

```
                CALL SHS_CPACK    (SOUT(1,C), NCP, IDX, X, FLOW)

                KDIAG = 4
                KBASE = 1


      CALL PPMON_ENTHV    (SOUT(NCOMP_NCC+2,C),SOUT(NCOMP_NCC+3,C),
     +                  X, NCP, IDX, NBOPST, KDIAG, KBASE, KH,
     +                  HO(C), DHMX,KER)


               HA(C)=HO(C)

600            CONTINUE

                  HH2O = HO(1)    !ENTHALPY OUT [J/KMOL]
                  HH2OO = HO(2)   !ENTHALPY OUT [J/KMOL]
                  HO2O = HO(3)    !ENTHALPY OUT [J/KMOL]
                  HAIRO = HO(4)   !ENTHALPY OUT [J/KMOL]

      J=(-En/(2*ASR))+((P/NC)/(AS*ASR)+(EN/(2*ASR))**2)**(0.5)
      TA=(1+SR/(SU*(1-SR)))*HH2O+0.5*HO2O+(1-SU)*(HH2OO/SU)
      TA=TA-(HH2OI*(1/(SU*(1-SR))))
      MFH2I = (P+MFAIR*HAIRI-MFAIR*HAIRO-QL)
      MFH2I = MFH2I/TA

C     VOLTAGE CALCULATION
      I =2*F*MFH2I*1000
      V = P/I
      Vop = En + J*ASR

      IF (Vop .LT. V) THEN
        IF (V-Vop .GT. 0.0001 ) THEN
        TOUT = TOUT-0.1
        END IF
        IF (V-Vop .LE. 0.0001) EXIT
      END IF

      IF (Vop .GT. V) THEN
        IF (Vop-V .GT. 0.0001) THEN
        TOUT = TOUT+0.1
        END IF
        IF (Vop-V .LE. 0.0001) EXIT
```

```
    END IF

500   CONTINUE
    END IF

C     SETTING VALUES AS OUTPUT PARAMETERS

    REAL(10) = HH2OI
    REAL(11) = TOUT
    REAL(12) = TA
    REAL(13) = J
    REAL(14) = Vop
    REAL(15) = MFH2I
    REAL(16) = V
    REAL(17)= MFAIR

    END IF
    END
```

A.2 Solid Oxide Fuel Cell FORTRAN code

Solid oxide fuel cell subroutine only is used to make the calculation of the products based on the reactants input. Energy balance is done in Aspen plus™ with the following instructions:

Defined Variable	Path
HINAN	Stream-Var Stream=INAN Substream=MIXED Variable=MOLE-ENTHALP Units=J/kmol
HINCAT	Stream-Var Stream=INCAT Substream=MIXED Variable=MOLE-ENTHALP Units=J/kmol
HOUTCAT	Stream-Var Stream=OUTCAT Substream=MIXED Variable=MOLE-ENTHALP Units=J/kmol
HOUTAN	Stream-Var Stream=OUTAN Substream=MIXED Variable=MOLE-ENTHALP Units=J/kmol
EP	Work-Power Stream=ELPOWER Units=Watt
NFINAN	Mole-Flow Stream=INAN Substream=MIXED Component=HYDROGEN Units=kmol/sec
NFINCAT	Mole-Flow Stream=INCAT Substream=MIXED Component=OXYGEN Units=kmol/sec
NFOANH2O	Mole-Flow Stream=OUTAN Substream=MIXED Component=WATER Units=kmol/sec
NFOANH2	Mole-Flow Stream=OUTAN Substream=MIXED Component=HYDROGEN Units=kmol/sec
NFOCATO2	Mole-Flow Stream=OUTCAT Substream=MIXED Component=OXYGEN Units=kmol/sec
NFOANT	Parameter Parameter no.=3 Physical type=Mole-Flow- Units=kmol/sec
IFC	Block-Var Block=SOFC Variable=REAL-VAR Sentence=REAL Element=10
PFC	Block-Var Block=SOFC Variable=REAL-VAR Sentence=REAL Element=9
TINPUT	Stream-Var Stream=INAN Substream=MIXED Variable=TEMP Units=K
TOUTPUT	Stream-Var Stream=OUTAN Substream=MIXED Variable=TEMP Units=K

O2INPUT	Mole-Flow Stream=O2 Substream=MIXED Component=OXYGEN Units=kmol/sec
HFINAN	Parameter Parameter no.=7 Physical type=Enthalpy-Flo- Units=J/sec
HFOUTAN	Parameter Parameter no.=8 Physical type=Enthalpy-Flo- Units=J/sec
O2USED	Block-Var Block=SOFC Variable=REAL-VAR Sentence=REAL Element=3
EN	Block-Var Block=SOFC Variable=REAL-VAR Sentence=REAL Element=1
HAIRIN	Stream-Var Stream=PHAIR Substream=MIXED Variable=MOLE-ENTHALP Units=J/kmol
HAIROUT	Stream-Var Stream=HAIR Substream=MIXED Variable=MOLE-ENTHALP Units=J/kmol
NFAIRIN	Stream-Var Stream=AIR Substream=MIXED Variable=MOLE-FLOW Units=kmol/sec
UF	Block-Var Block=SOFC Variable=REAL-VAR Sentence=REAL Element=2
HL	Block-Var Block=SOFC Variable=REAL-VAR Sentence=REAL Element=4
ASR	Block-Var Block=SOFC Variable=REAL-VAR Sentence=REAL Element=5
AS	Block-Var Block=SOFC Variable=REAL-VAR Sentence=REAL Element=6
NC	Block-Var Block=SOFC Variable=REAL-VAR Sentence=REAL Element=7
V	Block-Var Block=SOFC Variable=REAL-VAR Sentence=REAL Element=8
CD	Block-Var Block=SOFC Variable=REAL-VAR Sentence=REAL Element=11
X1H2	Mole-Frac Stream=INAN Substream=MIXED Component=HYDROGEN
X2H2	Mole-Frac Stream=OUTAN Substream=MIXED Component=HYDROGEN
XAH2	Local-Param
X1H2O	Mole-Frac Stream=INAN Substream=MIXED Component=WATER
X2H2O	Mole-Frac Stream=OUTAN Substream=MIXED Component=WATER
XAH2O	Local-Param
X1O2	Mole-Frac Stream=INCAT Substream=MIXED Component=OXYGEN
X2O2	Mole-Frac Stream=OUTCAT Substream=MIXED Component=OXYGEN
XAO2	Local-Param
X	Local-Param
T	Local-Param Physical type=Temperature-

```
NFOANT=NFOANH2O+NFOANH2

IFC = 2*96485.33*UF*NFINAN*1000
CD = IFC/(AS*NC)
T = (TINPUT+TOUTPUT)/2
XAH2=(X1H2+X2H2)/2
XAH2O=(X1H2O+X2H2O)/2
XAO2=(X1O2+X2O2)/2
if (uf .eq. 1) then
XAO2=(X1O2+0)/2
end if

X=(XAH2*(XAO2**(0.5)))/(XAH2O)
EN=0.998+(8.314*T*log(X)/(2*96485))
V = EN - CD*ASR
PFC = ifc*V
```

```
    EP = PFC
    Tin = Tinput/1000
    to = toutput/1000

    HFINAN=NFINAN*HINAN
    HFOUTAN=NFOANT*HOUTAN
    O2USED=UF*NFINAN/2
    O2INPUT= O2USED/UF+0.000000001

    NFAIRIN=PFC-HFINAN+HFOUTAN-HINCAT*O2INPUT+HL
    NFAIRIN = NFAIRIN+HOUTCAT*(O2INPUT-O2USED)
    NFAIRIN=NFAIRIN/(HAIRIN-HAIROUT)
```

The mass balance is done in a subroutine named SOFC.f that is called by Aspen plus™.

SOFC.f code

```
C$ #1 BY: Rafael Cuellar June 2013
C     This suboroutine is only the mass balance generation inside the cell
C     User Unit Operation Model (or Report) Subroutine for USER2
C
      SUBROUTINE SOFC (NMATI,  SIN,    NINFI,   SINFI,  NMATO,
     2                 SOUT,   NINFO,  SINFO,   IDSMI,  IDSII,
     3                 IDSMO,  IDSIO,  NTOT,    NSUBS,  IDXSUB,
     4                 ITYPE,  NINT,   INT,     NREAL,  REAL,
     5                 IDS,    NPO,    NBOPST,  NIWORK, IWORK,
     6                 NWORK,  WORK,   NSIZE,   SIZE,   INTSIZ,
     7                 LD   )
C
      IMPLICIT NONE
C
C     DECLARE VARIABLES USED IN DIMENSIONING
C
      INTEGER NMATI, NINFI, NMATO, NINFO, NTOT,
     +        NSUBS, NINT,  NPO,   NIWORK,NWORK,
     +        NSIZE
C
#include "ppexec_user.cmn"
#include "dms_plex.cmn"
      Real*8 B(1)
      Equivalence (B(1),IB(1))
C
C
```

```
C
#include "dms_ncomp.cmn"
C
C
C
C     DECLARE ARGUMENTS
C
      INTEGER IDSMI(2,NMATI),      IDSII(2,NINFI),
     +        IDSMO(2,NMATO),      IDSIO(2,NINFO),
     +        IDXSUB(NSUBS),ITYPE(NSUBS), INT(NINT),
     +        IDS(2,3),     NBOPST(6,NPO),
     +        IWORK(NIWORK),INTSIZ(NSIZE),NREAL, LD
      INTEGER KH2O
      REAL*8 SIN(NTOT,NMATI),     SINFI(NINFI),
     +       SOUT(NTOT,NMATO),    SINFO(NINFO),
     +       WORK(NWORK),  SIZE(NSIZE), REAL (NREAL)
C
C     DECLARE LOCAL VARIABLES
C
      INTEGER OFFSET, IERR, LDATA, KDIAG, IDX(10), NCP, I, J,
     +        INDEX, LMW, IFAIL, KBASE, KH, KER, C, SN
      REAL*8  HFG, UF, CPS, TI, TM, TF, M, HFOUT(NMATO), X(10), FLOW,
     +        HMX(NMATO), DHMX, QS, MF, HFIN(NMATO)
C     DECLARE FUNCTIONS

      INTEGER USRUTL_GET_REAL_PARAM,  ! These functions allow access to real
     +        USRUTL_GET_INT_PARAM,   ! and integer parameters using named
     +        USRUTL_SET_REAL_PARAM   ! references, and to write results data
                                      ! to Aspen Plus.
      INTEGER DMS_IFCMNC  !Determines offset to universal constant data.

      REAL*8  DLOG        !Standard Fortran function.
C
C     BEGIN EXECUTABLE CODE
C     Get configured REAL variables from Aspen Plus REAL PARAMETERS
      IFAIL = 0
      INDEX = 0

      UF = REAL(2)

C     SETTING VALUES AS OUTPUT PARAMETERS
!1 --> CATHODE, 2 -->ANODE
```

```
      SOUT(3,1)= SIN(3,1)-SIN(2,2)*UF*0.5
      SOUT(2,2)=SIN(2,2)*(1-UF)
      SOUT(1,2)=SIN(2,2)*UF
      SOUT(4,1)=SIN(4,1)
      SOUT(3,2)=SIN(3,2)

      RETURN
      END
```

A.3 Thermal Energy Storage FORTRAN code

The calculations for the thermal energy storage values were done in a subroutine named TSCALC.f which is called by Aspen plus™.

TSCALC.f code

```
C$ #1 BY: Rafael Cuellar June 2013
C     Thermal Energy Storage
C     User Unit Operation Model (or Report) Subroutine for USER2
C
      SUBROUTINE TSCALC (NMATI,  SIN,    NINFI,   SINFI,  NMATO,
     2                   SOUT,   NINFO,  SINFO,   IDSMI,  IDSII,
     3                   IDSMO,  IDSIO,  NTOT,    NSUBS,  IDXSUB,
     4                   ITYPE,  NINT,   INT,     NREAL,  REAL,
     5                   IDS,    NPO,    NBOPST,  NIWORK, IWORK,
     6                   NWORK,  WORK,   NSIZE,   SIZE,   INTSIZ,
     7                   LD   )
C
      IMPLICIT NONE
C
C     DECLARE VARIABLES USED IN DIMENSIONING
C
      INTEGER NMATI, NINFI, NMATO, NINFO, NTOT,
     +        NSUBS, NINT,  NPO,   NIWORK,NWORK,
     +        NSIZE
C
#include "ppexec_user.cmn"
#include "shs_stwork.cmn"
#include "dms_plex.cmn"

      Real*8 B(1)
      Equivalence (B(1),IB(1))
```

```
C
C
C
#include "dms_ncomp.cmn"
C
C
C
C    DECLARE ARGUMENTS
C
     INTEGER IDSMI(2,NMATI),      IDSII(2,NINFI),
    +       IDSMO(2,NMATO),      IDSIO(2,NINFO),
    +       IDXSUB(NSUBS),ITYPE(NSUBS), INT(NINT),
    +       IDS(2,3),     NBOPST(6,NPO),
    +       IWORK(NIWORK),INTSIZ(NSIZE),NREAL, LD
     INTEGER KH2O, IRETN(6)
     REAL*8 SIN(NTOT,NMATI),     SINFI(NINFI),
    +      SOUT(NTOT,NMATO),    SINFO(NINFO),
    +      WORK(NWORK),  SIZE(NSIZE), REAL (NREAL)
C
C    DECLARE LOCAL VARIABLES
C
     INTEGER OFFSET, IERR, LDATA, KDIAG, IDX(10), NCP, I, J,
    +       INDEX, LMW, IFAIL, KBASE, KH, KER, C, SN, LCFLAG,
    +       NPROP, NPHASE,NRESULT
     REAL*8  HFG, CPL, CPS, TI,TO,TM, TF, M, HFOUT(NMATO), X(10), FLOW,
    +       HMX(NMATO), DHMX, QS, MF, HFIN(NMATO), HMX2(NMATO)

     CHARACTER*5 PROPS
     CHARACTER*6 PHASES

C    DECLARE FUNCTIONS

     INTEGER USRUTL_GET_REAL_PARAM,  ! These functions allow access to real
    +       USRUTL_GET_INT_PARAM,   ! and integer parameters using named
    +       USRUTL_SET_REAL_PARAM   ! references, and to write results data
                                    ! to Aspen Plus.
     INTEGER DMS_IFCMNC  !Determines offset to universal constant data.

     REAL*8  DLOG       !Standard Fortran function.
C
C    BEGIN EXECUTABLE CODE
C    Get configured REAL variables from Aspen Plus REAL PARAMETERS
     IFAIL = 0
```

```
      INDEX = 0
      HFG = REAL(1)              !LATENT HEAT

      CPL = REAL(2)              !SPECIFIC HEAT LIQUID

      CPS = REAL(3)              !SPECIFIC HEAT SOLID

      TI = REAL(4)               !INITIAL TEMPERATURE

      TM = REAL(5)               !METING TEMPERATURE

      TO = REAL (6)              !AIR OUTPUT TEMPERATURE

      M = REAL(7)                !PCM MASS

      QS=0


C     Calculate Enthalpy out

     DO 10 C=1,NMATI

        CALL SHS_CPACK      (SIN(1,C), NCP, IDX, X, FLOW)
        KDIAG = 4
        KBASE = 1
        KH = 1

        CALL PPMON_ENTHV    (REAL(6), SIN(NCOMP_NCC+3,C), X, NCP, IDX,
     +                  NBOPST, KDIAG, KBASE, KH, HMX(C), DHMX,
     +                  KER)


C     MODEL EQUATIONS

      HFOUT(C) = HMX(C)*SIN(NCOMP_NCC+1,C)
      HFIN(C)=SIN(NCOMP_NCC+4,C)*SIN(NCOMP_NCC+9,C)*SIN(NCOMP_NCC+1,C)
      QS=QS+HFOUT(C)-HFIN(C)
10    CONTINUE

      QS = -QS/1000

      IF (TI .LE. TM) THEN
         TF = QS/(M*CPS) + TI
```

```
      MF = 0
      IF (TF .GT. TM) THEN
        MF = (QS -M*CPS*(TM -TI))/(M*HFG)
        TF = TM
        IF (MF .GT. 1) THEN
          TF = ((QS - M*CPS*(TM-TI) - M*HFG)/M*CPL) + TM
          MF = 1
        END IF
      END IF
    END IF

    IF (TI .GT. TM) THEN
      TF = (QS/CPL)+TI
    END IF


C     FILL SOUT ARRAY

    DO 100 C=1,NCOMP_NCC
      DO 200 SN = 1, NMATO
        SOUT(C,SN) = SIN(C,SN)
         SOUT(NCOMP_NCC+3,SN) = SIN(NCOMP_NCC+3,SN)
         SOUT(NCOMP_NCC+2,SN)= REAL (6)


200       CONTINUE
100    CONTINUE

C     SETTING VALUES AS OUTPUT PARAMETERS

    REAL(8) = HMX2(NMATI)              !CONTROL VARIABLE
    REAL(9) = HMX(NMATI)               !CONTROL VARIABLE
    REAL(10) = HFOUT(NMATI)            !CONTROL VARIABLE
    REAL(11) = MF                      !MASS FRACTION
    REAL(12) = QS                      !THERMAL POWER
    RETURN
    END
```